Mara Kandeva-Ivanova
Aleksandar Vencl
Dimitar Karastoyanov

Advanced Tribological Coatings For Heavy-Duty Applications: Case Studies

Prof. Marin Drinov Publishing House of Bulgarian Academy of Sciences

BULGARIAN ACADEMY OF SCIENCES

INSTITUTE OF INFORMATION AND COMMUNICATION TECHNOLOGIES

Mara Kandeva-Ivanova
Aleksandar Vencl
Dimitar Karastoyanov

Advanced Tribological Coatings For Heavy-Duty Applications: Case Studies

Sofia • 2016

Prof. Marin Drinov Publishing House of Bulgarian Academy of Sciences

ISBN 978-954-322-858-4

CONTENTS

PREFACE 7

Chapter 1
INTRODUCTION 9
1.1. Surface engineering 9
1.2. Overview of applied coating deposition processes 12
1.2.1. Electroless plating 14
1.2.2. Hardfacing 16
1.2.3. Thermal spraying 20
1.3. Principles of abrasive and erosive wear 24
1.3.1. Abrasive wear 26
1.3.2. Erosive wear 31
References to Chapter 1 35

Chapter 2
ELECTROLESS NICKEL COMPOSITE COATINGS WITH NANOPARTICLES 38
2.1. Introduction 38
2.2. Materials 43
2.2.1. Nickel coatings with diamond (D) nanoparticles 43
2.2.2. Nickel coatings with silicon carbide (SiC) nanoparticles 44
2.2.3. Nickel coatings with boron nitride (BN) nanoparticles 45
2.3. Experimental details 46
2.3.1. Abrasive wear testing 46
2.3.2. Erosive wear testing 48
2.4. Results and discussion 50
2.4.1. Nickel coatings with diamond (D) nanoparticles 50
2.4.2. Nickel coatings with silicon carbide (SiC) nanoparticles 62
2.4.3. Nickel coatings with boron nitride (BN) nanoparticles 68
2.5. Conclusions 76
References to Chapter 2 78

Chapter 3
FERROUS-BASED COATINGS HARDFACED BY GAS METAL ARC WELDING (GMAW) 81
3.1. Introduction 81
3.2. Materials 83

3.2.1. Chemical compositions 83
3.2.2. Optimisation of the deposition parameters and deposition conditions 85
3.2.3. Microstructures and hardness 88
3.3. Experimental details 89
3.3.1. Abrasive wear testing 90
3.3.2. Vibro-abrasive wear testing 92
3.4. Results and discussion 95
3.4.1. Abrasive wear testing 95
3.4.2. Vibro-abrasive wear testing 102
3.5. Conclusions 107
References to Chapter 3 108

Chapter 4
HIGH VELOCITY OXYGEN FUEL (HVOF) SUPERALLOY COATINGS 111
4.1. Introduction 111
4.2. Optimisation of the deposition parameters 114
4.2.1. Materials 114
4.2.2. Experimental details 116
4.2.3. Results and discussion 118
4.3. Abrasive wear testing 124
4.3.1. Materials and deposition conditions 124
4.3.2. Microstructure, thickness, roughness and hardness characteristics 127
4.3.3. Experimental details 129
4.3.4. Results and discussion 130
4.4. Erosive wear testing 137
4.4.1. Materials and deposition conditions 137
4.4.2. Thickness and hardness characteristics 138
4.4.3. Experimental details 139
4.4.4. Results and discussion 140
4.5. Conclusions 144
References to Chapter 4 145

PREFACE

Energy conservation and environmental protection are the main objectives of scientific and engineering activities in the last decade and at the same time initiators of many researches and inventions. In doing so, it can be concluded that the various tribological systems are especially important in achieving rational use of energy. It is estimated that over 30% of the total energy produced in the world is spent for overcoming friction. In addition to direct energy savings by reducing friction, research in the field of tribology can contribute to the reduction of energy and usage of raw materials, by improving the tribological characteristics of the materials used in production of various machine elements. This is particularly related to the improvement of the wear resistance of materials, since wear losses are very high and wear represent the most common cause of failure in machines and equipment. It is estimated that over 30% of all failures in main machine elements are direct consequence of wear, and more than 50% are tribologically caused (poor maintenance and control).

By reducing wear, longer lives of machines are achieved and hence lower maintenance costs. The estimated costs of abrasive wear, as one of the most common types of wear, are between 1 and 4 % of the gross national product of the developed countries. Tribomaterials, as the subdiscipline of tribology, includes tribological studies of the existing materials and development of new materials with enhanced tribological characteristics. The wear resistance of some material in particular application depends on its chemical composition, structure and physical-mechanical characteristics, and selection of appropriate tribomaterial is a challenging task. In solving wear problems there are three main trends present nowadays, namely:

Development and application of new tribomaterials with enhanced tribological characteristics, including the development of lubricants:

- Development and application of new technologies of production which give qualitatively new properties of conventional materials;
- Development and application of new tribological coatings and surface modifications.

The monograph “Advanced Tribological Coatings for Heavy-Duty Applications: Case Studies” reflects the last trend in solving wear problems. It presents a summary of the researches conducted by the authors in the past few years, concerning the tribological coatings designed for different heavy-duty applications, with various coating materials, and deposited by different techniques. The

investigations were provoked by practical tasks assigned by companies in various industrial branches such as, improvement of the resource of calender shafts for sheet forming, screw worm conveyors, conveyor belt rollers, pumps, excavator bucket teeth and other equipment for heavy-duty applications under the impact loads and high temperatures and pressures, in abrasive, erosive and corrosive environment.

The book is structured in four chapters, from which the Chapter 1 covers the introduction remarks about the surface engineering, applied coating deposition techniques, coating properties and principles of abrasive and erosive wear. Other chapters are classified according to the used coating deposition process. Chapter 2 considers electroless nickel coatings with different nanoparticles (diamond, SiC and BN) addition. The application of these coatings is related to the possibilities for replacement of non-ecological chromium coating and to the improvement of the wear resistance of working shafts (calenders) involved in the production of sheet-formed and foliate materials, such as paper, cardboard, leather, etc. In Chapter 3, gas metal arc welding (GMAW) technique was used for hardfacing of different ferrous-based coatings. Primarily, these coatings are used as solutions for the regeneration of equipment used in road construction, agricultural and mining industry. Chapter 4 considers various superalloy coatings deposited with high velocity oxygen fuel (HVOF) spraying process. The investigated application of these coatings was as improvement of the wear resistance of equipment used in road construction, agricultural, mining and other industries.

The investigations presented in this monograph are product of the common work of the teams in two universities and one institute, i.e. Tribology Centre at the Faculty of Industrial Technology of the Technical University of Sofia headed by Assoc. Prof. Dr. Mara Kandeva; Tribology Laboratory at the Faculty of Mechanical Engineering of the University of Belgrade, headed by Assoc. Prof. Dr. Aleksandar Vencl; and Department “Embedded Intelligent Technologies” of the Institute of Information and Communication Technologies at the Bulgarian Academy of Sciences, headed by Prof. Dr. Dimitar Karastoyanov. The results of these investigations have been presented and published in numerous publications of the international conferences and scientific journals, and this monograph intends to consolidate and present them in a single volume.

The innovation results and solutions, as well as the publishing of this monograph have been done with the financial support from the FP7-REGPOT project 316087: Advanced Computing for Innovation (AComIn) of the Institute of Information and Communication Technologies headed by Prof. Galya Angelova, DSc together with the application and usage of the unique contemporary research equipment from the Laboratory of the Project SmartLab headed by Prof. Dr. Dimitar Karastoyanov.

Sofia, January 2016 The authors

Chapter 1
INTRODUCTION

1.1. Surface engineering

Surface engineering is the sub-discipline of tribology which deals with the surface of solids. Solids are composed of a bulk material covered (bounded) by a surface. The surface interacts with the surrounding environment. This interaction can degrade the surface over time. Degradation of the surface over time can be caused by wear, corrosion and creep. Surface engineering involves altering (changing) the properties of the surface in order to reduce the degradation over time, i.e. to extend the service life. Surface engineering is also applied in order to improve the performance (providing low- or high-friction contacts with other materials, serving as electronic circuit elements, etc.), and enhance the appearance of materials used for engineering components.

Although the surface normally cannot be made totally independent from the bulk, the demands on surface and bulk properties are often quite different. For example, in the case of a turbine blade for a high-performance jet engine, the bulk of the material must have sufficient creep resistance and fatigue strength at the service temperature to provide an acceptably safe service life. The surface of the material, on the other hand, must possess sufficient resistance to oxidation and hot corrosion under the conditions of service to achieve that same component life. In many instances, it is either more economical or absolutely necessary to select a material with the required bulk properties and specifically engineer the surface to create the required interface with the environment, rather than to find one material that has both the bulk and surface properties required to do the job [1].

The purpose of the formed protective surface layer is to protect the surface of the material from simple or complex load to which the material is not suitable. The basic and most common functions of protective layers are: increase of wear resistance; increase of corrosion resistance; increase of high-temperature resistance; oxidation protection (e.g. thermal barrier coatings); prevent the diffusion between layers, etc. Besides protective, there are other layers applied with the same processes but with different purpose, i.e. to: reduce the coefficient of friction (solid lubricants); repair the worn-out parts; increase the electrical and/or thermal conductivity or resistivity;

increase/decrease reflection, absorption, etc. (in optics); enhance the appearance (decorative layers), and so on.

A useful definition of the term surface engineering is: "treatment of the surface and near-surface regions of a material to allow the surface to perform functions that are distinct from those functions demanded from the bulk of the material" [1]. There are two distinct groups of surface treatments: surface modification techniques and coating deposition techniques. Surface modifications comprise all actions that significantly change the characteristics of the surface and near-surface layers (superficial layers) of materials used for engineering components, without adding any new material. There are surface modification by diffusion (changing the chemical composition of the surface layer) and surface modification by transformation (changing the structure of the surface layer). Coating deposition implies that additional material is applied on the surface of the base material (substrate). This additional material is usually different from the substrate, and deposited in one or more layers to obtain desired properties or dimensions. Coatings may be applied as liquids, gases or solids.

Surface engineering techniques are being used in the automotive, aerospace, missile, power, electronic, biomedical, textile, petroleum, petrochemical, chemical, steel, power, cement, machine tools, and construction industries. In 1995, surface engineering was a 10 billion GBP market in the UK. Coatings, to make surface life resistant to wear and corrosion, were approximately half the market. It is estimated that loss due to wear and corrosion in the USA is approximately 500 billion USD. In the USA, there are around 9524 establishments (including automotive, aircraft, power, and construction industries) who depend on engineered surfaces with support from 23,466 industries. There are around 65 academic institutions worldwide engaged in surface engineering research and education [2].

There are many different surface engineering techniques that have grown from laboratory conditions into commercial technologies. The classification of surface modification and coating deposition techniques could be done on several different ways. One of the classifications is mainly according to the type of energy used in the process (thermal, mechanical, thermo-mechanical, chemical, electro-chemical and thermo-chemical), as shown in **Fig. 1.1**.

The selection of appropriate surface modification or coating deposition technique for an engineering component can be made only when all significant parameters are known. In selecting appropriate technique for tribological coatings, the first requirement is to identify the dominant type of wear, as well as other types of wear. After that appropriate material is selected, and based on that suitable surface modification or coating deposition technique.

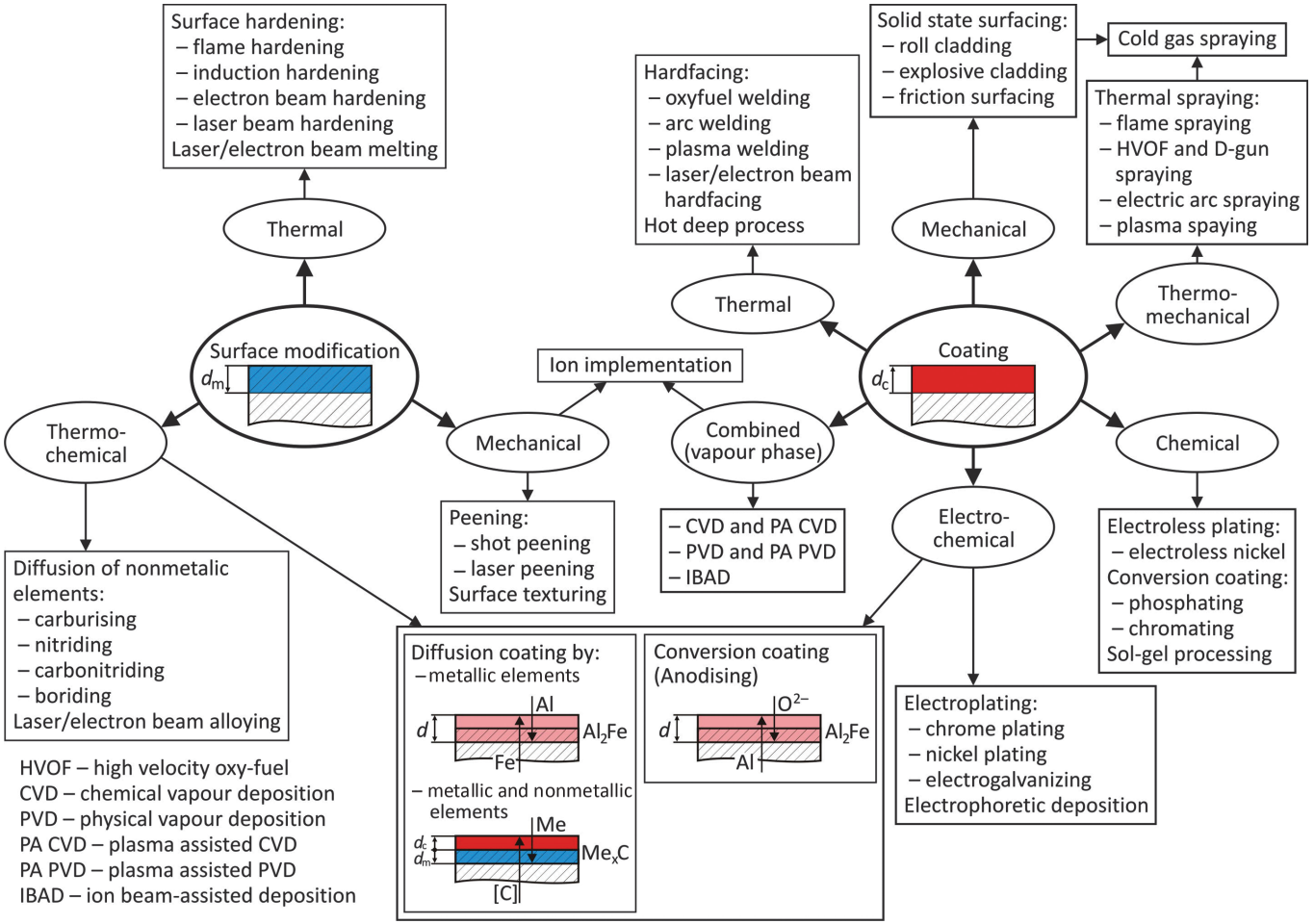

Fig. 1.1. Overview of main surface engineering (surface modification and coating deposition) techniques; adapted from [3]

Another approach is that, after identifying dominant wear type, first select appropriate technique, and based on that suitable material. Both approaches are valid since, for a particular application, two different combinations of material/technique can provide equally good results.

1.2. Overview of applied coating deposition processes

According to the ASM Handbooks coating is: "a relatively thin layer (less than 1 mm) of material applied by surfacing for the purpose of corrosion prevention, resistance to high-temperature scaling, wear resistance, lubrication, or other purposes", while the term surfacing is defined as: "deposition of filler metal (material) on a base metal (substrate) to obtain desired properties or dimensions". In other words, surfacing represent all the techniques for the coatings deposition [1].

Another classification of the coating deposition techniques is according to the physical state of the material to be coated. It divides the techniques into the following four categories: gaseous state processes; solution state processes; molten or semi-molten state processes; and solid state processes (**Fig. 1.2**).

In addition to the classifications shown in **Figs. 1.1** and **1.2**, tribological coatings can be classified according to the purpose (functional classification) as:

1. Repair or build-up coatings (similar materials) – material is deposited to achieve the required dimensions of the component, i.e. to restore its original/working dimensions;

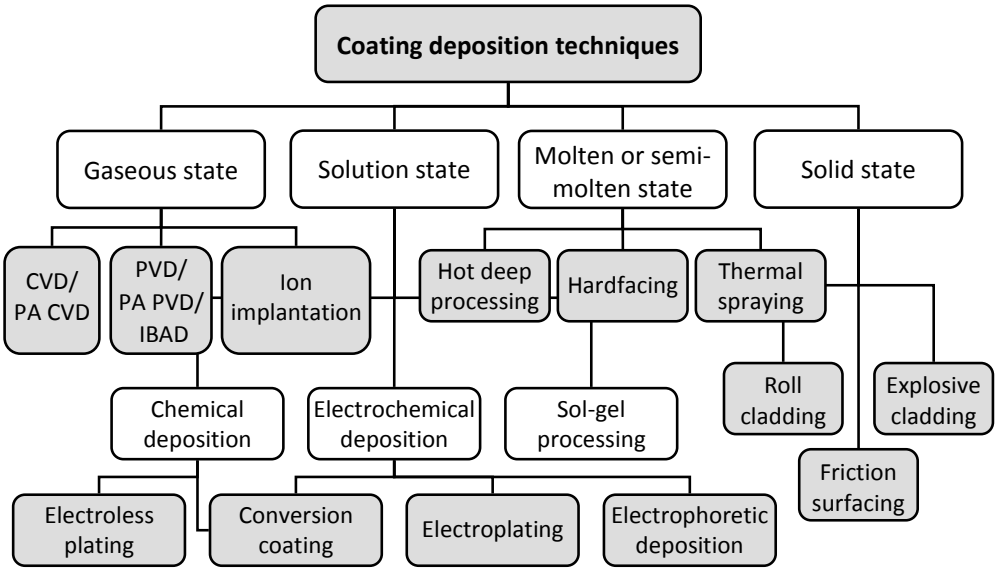

Fig. 1.2. Classification of the main coating deposition techniques

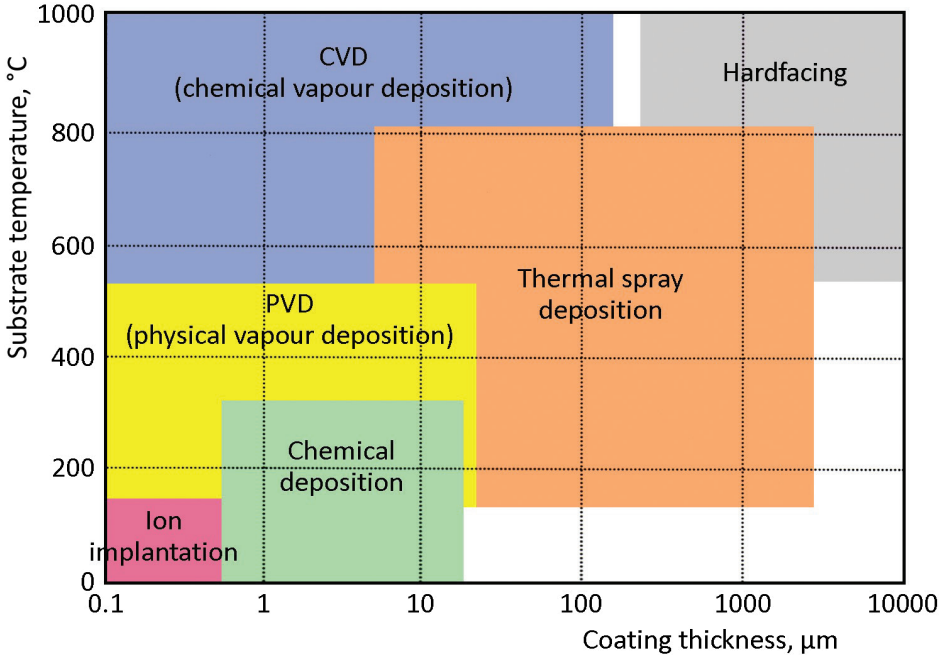

Fig. 1.3. Comparison of most used coating processes by the possible coating thickness and substrate temperature during deposition [5] (Reproduced by permission of Oerlikon Metco)

2. Coatings for obtaining/improving certain characteristics (dissimilar materials) – material is deposited to achieve wear reduction or to control combinations of wear, corrosion and oxidation;

3. Bonding or bond coatings (very dissimilar materials) – material is an intermediate layer deposited between the substrate and protective coating to provide metallurgical compatibility.

Two important parameters for the choice of coating processes are the thickness of the coatings that can be achieved and the substrate temperature during the process. Typical coating thicknesses vary from 0.1 mm to 10 mm, and the substrate temperatures vary from room temperature up to 1000 °C (**Fig. 1.3**). In general, thick coatings are desirable for longer life, but in some applications thin coatings are more desirable for the following reasons [4]:

- thin coatings accurately reproduce the substrate topography, removing the need for finishing (grinding);
- they tolerate better thermal expansion mismatches with the substrate;
- they do not change the mechanical properties of the substrate (important in thin substrates);
- when the substrates are flexible, they can bend freely without cracking.

Table 1.1. Comparative typical characteristics of applied coating deposition processes [6-8]

	Deposition process		
Characteristic	Electroless plating	Hardfacing	Thermal spraying
Deposition rate	1 - 30 µm/h	0.5 - 50 kg/h	0.1 -10 kg/h
Thickness	1 - 100 µm	1 - 10 mm	20 - 1000 µm
Substrate temperature	25 - 100 °C	500 -1200 °C	100 - 800 °C
Substrate material	Certain limitations	Mostly steels	Almost any material
Coating material	Metals, alloys, and composites	Mostly metals and alloys	Almost any material
Component (substrate) size	Limited by solution bath	May be limited by chamber size	May be limited by chamber size
Pretreatment	Chemical cleaning	Chemical cleaning	Roughening and chemical cleaning
Post-treatment	None/thermal treatment	None	None/substrate stress relief
Uniformity of coating	Good	Variable	Variable
Coating geometry	Omnidirectional	Line of sight	Line of sight
Bonding mechanism	Chemical	Metallurgical	Mechanical

Other important parameters for the coating processes choice are the hardness of the coating, working temperature transmitted to the coating material, deposition rate and price, possible component (substrate) size and simplicity of the process, pretreatment and post-treatment, uniformity of coating and thickness control, coating bonding mechanism, etc. The characteristics of the obtained coating depend very much on these parameters, i.e. on the applied deposition processes. Usually there are big differences in the types and character of the coating, for example in compositions and morphologies. Some typical characteristics of three coating deposition processes used and presented in this book are shown in **Table 1.1**.

1.2.1. Electroless plating

Electroless plating is a coating deposition process in which mainly chemical energy is applied for deposition of the material (**Fig. 1.1**). Together with electroplating, it is the main coating deposition process in solution state processes category (**Fig. 1.2**). The solutions used are usually aqueous, and

deposits can be produced on metallic or nonmetallic substrates. Solution state processes may be divided into the categories of chemical and electrochemical, but this division may not be straightforward since some reactions which appear to be purely chemical may in fact be electrochemical. One of the benefits of the solution processes is that they have no upper limit on thickness [6].

Electroless plating is a chemical deposition process that involves several simultaneous reactions in an aqueous solution, which occur without the use of external direct current source. In contrast to electroplating, it uses only one electrode (substrate) and instead of an anode, the metal is supplied by the metal salt. However, the solution for the electroless process needs to contain a reducing agent. The process will continue until either the metal ions in solution are depleted or the reducing agent is depleted. The process produces coatings of uniform thickness on irregularly shaped parts, provided the plating solution circulates freely over their surfaces.

Pretreatment for the electroless plating differs if the substrate is metallic or nonmetallic, and specific procedures are required for each type of substrate. Metallic substrates need to be cleaned from the contaminants (soil, dirt, corrosion products, oxides, tarnish, and others) by a series of chemicals. This is important because the adhesive bond strength between the metal substrate and the coating very much depend on this. In some cases, mechanical surface treatments, such as shot peening or sandblasting, are used in surface finishing prior to chemical treatment. Electroless plating, as an autocatalytic chemical reduction process initiated by the substrate, during surface cleaning requires the highest degree of care and control of all metal finishing procedures. Even naturally active (catalytic) surfaces can become passive when contaminated by foreign residues or oxide layers. Nonmetallic substrates lack catalytic properties and therefore require activating treatments that will render them catalytic. In general, this activation is done by seeding the surface with a catalytically active metal [9].

Beside advantages like needlessness of external direct current source and coating thickness uniformity on irregularly shaped parts, the downside is that the plating process is usually slower than e.g. electroplating, and cannot create such thick coatings of metal. In addition, pretreatment is necessary, since failure to clean contaminants result in poor adhesion of the coating. Lifespan of chemicals is limited and waste treatment cost is high due to the speedy chemical renewal.

The most common electroless plating method is electroless nickel plating, although copper, silver, gold, cobalt, palladium and chrome coatings can also be deposited [10]. It is an increasingly important coating technology, and

significant advantage of the electroless nickel process is that it can be used in conjunction with fine grade particles to produce composite coatings. Examples of materials used to reinforce the coatings in this way are SiC, WC, CrC, Al_2O_3, or diamond, as well as, solid lubricant particles, such as graphite, PTFE or calcium fluoride [6].

1.2.2. Hardfacing

Hardfacing represents a group of techniques for the coating deposition in which mainly thermal energy is applied for deposition of the material (**Fig. 1.1**). Together with thermal spraying, it is the main coating deposition process in molten and semi-molten state processes category (**Fig. 1.2**). Hardfacing could be defined as "coating deposition process in which a wear resistant, usually harder, material is deposited on the surface of a component by some of the welding techniques" [11]. Hardfaced coatings are sometimes referred to as weld-overlay or welded coatings. Also, in some literature they are classified as cladding coatings. The main purpose of the cladding coatings is to provide corrosion resistance, but since corrosion and wear process often "work" together clear distinguishing cannot be made. Corrosion and/or high-temperatures may accelerate wear (pitting corrosion, fretting corrosion, erosion corrosion, cavitation corrosion, etc.), so the hardfacing material should be corrosion resistant as well.

In most cases, hardfacing is used for controlling abrasive and erosive wear, like in mining, crushing and grinding, and agriculture industries (buckets, bucket teeth, mill hammers, ball mills, digging tools, conveyer screws, etc.). Hardfacing is also used to control combinations of wear and corrosion, as encountered by mud seals, plows, knives in the food processing industry, pumps handling corrosive liquids, or slurries. Typical base metal components that are cladded include the internal surfaces of carbon and low-alloy steel pressure vessels, paper digesters, urea reactors, tubesheets, nuclear reactor containment vessels, and hydrocrackers [12].

The use of a welding technique to deposit a coating is nearly as old as the use of welding to produce a joint. The process is practically the same, yet the purpose is different. Although the techniques are the same in most cases, special considerations are necessary for weld overlaying that are not required for welding a joint. Included in these considerations are the following:

- The chemical composition and mechanical properties of the surfacing material usually are quite different from those of the base material on which it is deposited;
- A relatively large area of base material is usually covered in surfacing, and the smallest possible amount of surfacing material is desired due to the

economic reason. As a result, there is frequently very large gradient in chemical composition and mechanical properties across the fusion line between the base material and the coating.

Both of these characteristics are closely connected with percentage of dilution, which should be as low as possible (but not too low). Most of the processes used to produce a hardfacing coating are based on fusion-welding techniques which were originally designed to weld joints. These processes involve melting of the some substrate (base) material so as to achieve a metallurgical bond between the coating and the base material. Indeed it is this melting of the substrate material that is one of the major differences between hardfacing and thermal spraying. This melting process means that the resultant alloy that solidifies (coating) is a mixture of the surfacing material and the base material. The composition of this alloy is defined by the percentage of dilution. The percentage of dilution equals the amount of base material melted (B) divided by the sum of surfacing material added and base material melted (A + B), the quotient of which is multiplied by 100 (**Fig. 1.4**). In other words, e.g. a dilution of 10% means that the coating contains 10% base material and 90% surfacing material [12]. Therefore, the main bonding mechanism between coating and substrate is diffusion, i.e. metallurgical bonding.

Probably the most outstanding difference between welding a joint and depositing a weld overlay is in the percentage of dilution, which is much more important in weld overlay surfacing. Dilution causes the chemical composition and structure of the deposit to be not the same as those of the welding consumable used to produce it. It also influence the required surface properties (especially hardness), and usually more than one layer is deposited to obtain required hardness. With each layer the influence of the base material is lower. The prediction of the microstructures and properties for the auste-

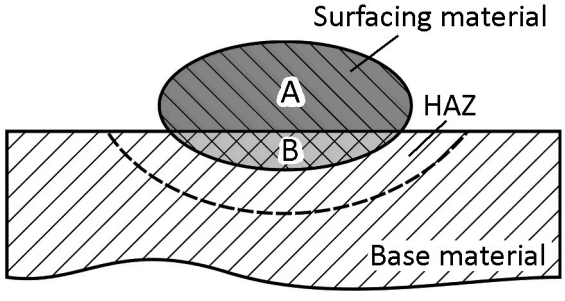

$$\text{Dilution} = \frac{B}{A+B} \times 100, \%$$

Fig. 1.4. Dilution of the surfacing material

nitic stainless steels is for example well studied and different microstructure prediction diagrams are used for that purpose, e.g. Schaeffler diagram, De-Long diagram, etc. [12].

Control of dilution plays an important part in the economics of the hardfacing process. A value between 10 and 15% is generally considered optimum. A dilution greater than 15% causes greater deterioration of the chemical composition and characteristics of the surfacing material, and it is necessary to apply more layers to obtain the required characteristics, which in turn raises the cost of the whole process. Unfortunately, most welding processes have considerably greater dilution [12]. On the other hand, a dilution smaller than 15% increases the risk of poor metallurgical bond between the coating and the substrate. These errors in bonding are very common for the dilution value below 5%. The dilution depends on the used base and surfacing material, on the selected welding process and on the chosen hardfacing parameters. Although each process has an expected dilution factor, experimenting with the hardfacing parameters can minimise dilution.

Pretreatment for the hardfacing includes: cleaning of the surface from oxides, rust, grease and oils, paint and other contaminants by various mechanical and chemical manners; shaping of the substrate is sometimes necessary to eliminate potential localised stress concentration and places where it is difficult to deposit a coating (sharp corners and edges); preheating of the substrate in order to prevent the occurrence of cracks in the coating and HAZ (heat affected zone).

Various welding techniques can be used to deposit a coating by hardfacing (**Fig. 1.5**), and each of them has some advantages and disadvantages. In addition, many hardfacing parameters must be considered when attempting to optimize a particular technique for a given application. The most widely used techniques, according to their popularity, are: flux cored arc welding (FCAW); gas metal arc welding (GMAW); shielded metal arc welding (SMAW); submerged arc welding (SAW); gas tungsten arc welding (GTAW); oxyfuel gas welding (OFW); plasma transferred arc welding (PTAW); laser harfacing, etc. [13].

Hardfacing material selection depends on its metallurgical compatibility with the substrate material. For example, alloys that form brittle intermetallic phases with the substrate are undesirable. Therefore, the available choice of coating materials is moderate. Since the number of materials suitable for hardfacing is limited, and most of them have been in service for a long time, majority of them are standardised [14]. The iron-based martensitic and austenitic alloys materials prevail (martensitic alloys hardens upon cooling, and austenitic alloys are soft after deposition and hardens after work-hardening).

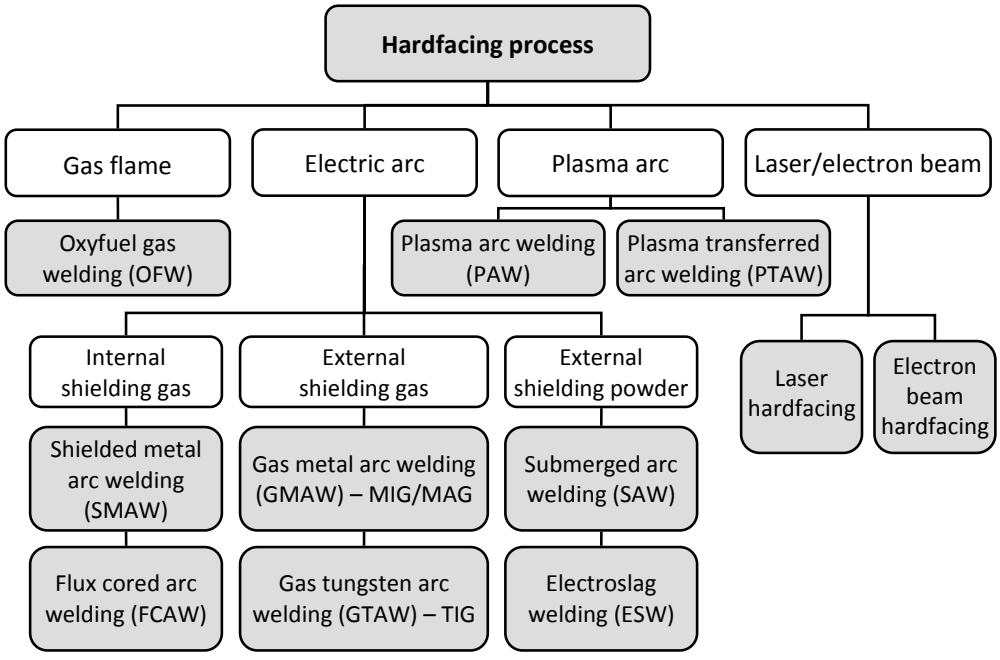

Fig. 1.5. Types of hardfacing processes (names of the techniques are shown as shaded)

There are also metal carbides (Cr and W) which contain large amounts of carbides in a soft, tough matrix, and some of the Ni, Co, Cu, Al and Cr alloys. The primary application of these materials is in severe mechanical wear conditions, although they often also have high corrosion resistance, and can be used when tribochemical wear is dominant type of wear (tribological components working in corrosive environment).

The choice of the substrate materials that can be hardfaced is also moderate. Hardfacing is mostly applied to carbon and low-alloy steels with C < 1%, high-carbon alloys with C > 1% (in this case a buffer layer may be required), stainless steels, manganese steels, cast irons, nickel-base alloys and copper-base alloys.

Compared to the other coating deposition processes, hardfacing has certain advantages and disadvantages. The advantages are, first of all, very good bonding between coating and substrate (metallurgical bond), and the possibility of depositing thick coating relatively quickly. In addition, the substrate generally does not require special preparation. Most hardfacing techniques are in service for a long time and relatively easy to apply. Disadvantages are that the coatings characteristics are not uniform and equal on the surface and below the surface (dilution influence) and that the coating

thickness control is poor. Then, there is a limited selection of the coating material (mainly steel and metal carbides), as well as the material basis (also mainly steels and some cast irons, Ni and Cu alloys). In addition, deposited coatings have high roughness and large deformations of the substrate are possible. For some components, e.g. bulldozer blades, a perfectly smooth surface is not required whereas, for gear wheels or valve seats, machining of the deposit is essential.

1.2.3. Thermal spraying

Thermal spraying represents a group of techniques for the coating deposition in which both, thermal and mechanical energy is applied for deposition of the material (**Fig. 1.1**). Together with hardfacing, it is the main coating deposition process in molten and semi-molten state processes category (**Fig. 1.2**). During the thermal spraying process, a coating feedstock material is melted or semi-melted and propelled, as individual particles or droplets, onto a cleaned and prepared substrate surface where it solidifies and adheres to surface, forming a solid layer (coating). Principle of thermal spraying coating deposition is shown in **Fig. 1.6**.

In thermal spraying process thermal energy is used to heat a feedstock material, which change its physical state from solid to molten or semi-molten state. The thermal spray gun generates the necessary heat by using combustible gases or an electric arc. Process gases provide the mechanical energy which is used to accelerate and spray particles or droplets of the melted or semi-melted feedstock material. The particles impact the surface at high

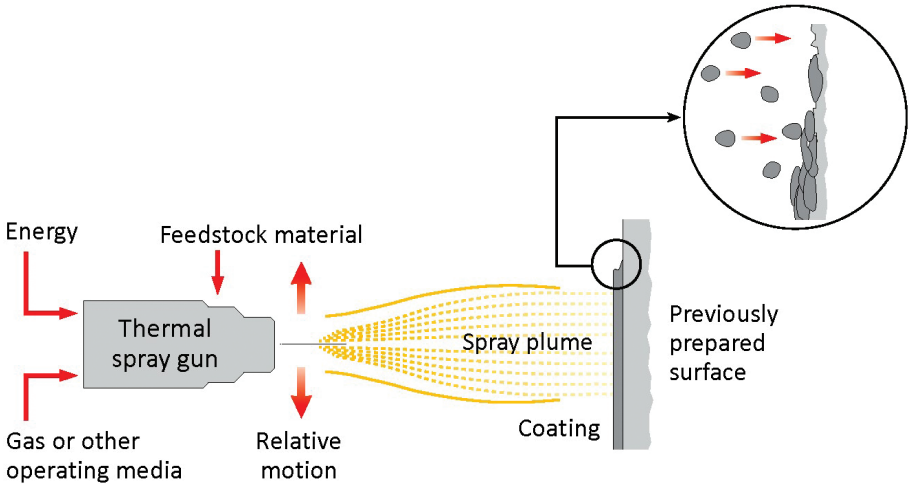

Fig. 1.6. Principle of thermal spraying [5] (Reproduced by permission of Oerlikon Metco)

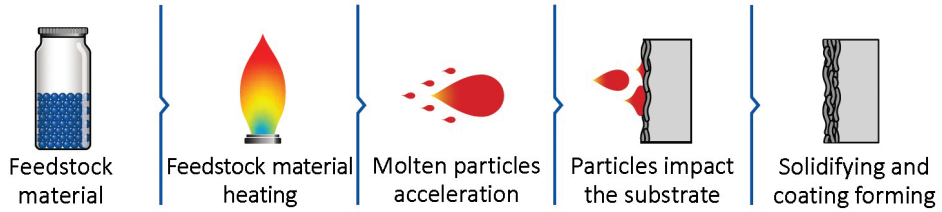

Fig. 1.7. Stages of the feedstock transformation and forming of the thermal spray coating

speed, flatten, and form thin platelets (splats) that conform and adhere to the substrate and to each other. By this way, splat by splat, a laminar structure coating is formed (**Fig. 1.7**). The feedstock material could be in the form of rods, wires or powder (which is most often case). When it is in the powder form, there should be a carrier gas which transports the feedstock material to the thermal spray gun.

The typically structure of the thermal spray coatings is lamellar [15, 16], with oxide particles and oxide layers and inclusions in between. The coating that is formed is not homogenous and typically contains a certain degree of porosity, and, in the case of sprayed metals in atmospheric conditions, the coating will contain oxides of the metal (**Fig. 1.8**). Upon impact, the deformed particles start to shrink and solidify, mechanically anchoring and hooking to the surface. Therefore, the main bonding mechanism between coating and substrate is physical interlocking and anchoring), i.e. mechanical bonding, although other bonding mechanisms exist like metallurgical bonding (diffu-

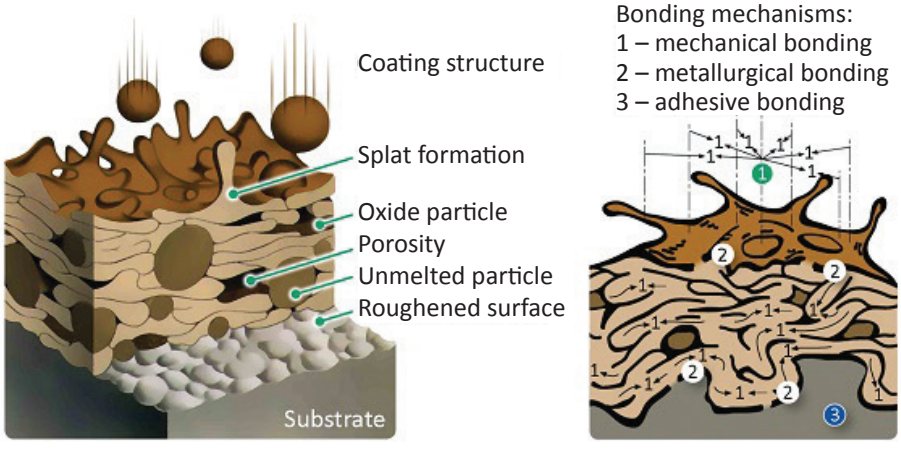

Fig. 1.8. Schematic structure of a thermal sprayed coating and bonding mechanisms [17]

sion) and adhesive bonding (chemisorption, adsorption, van der Waals forces, etc.), as shown in **Fig. 1.8**. Unlike hardfacing, the substrate material does not melt (it is not fused), so there are no problems connected with dilution.

Because the adhesion of the coating to the substrate predominantly consists of mechanical bonding, pretreatment of the surface is very important. The surface of the substrate is usually roughened and activated so the area for bonding is increased. The most frequently applied activation is by abrasive grit blasting. Before roughening, oxides, rust, grease and oils, paint and other contaminants should be removed from the substrate surface by the use of different solvents and chemicals or with ultra sound. Shaping of the substrate is sometimes necessary to eliminate potential localised stress concentration and places where it is difficult to deposit a coating or where its adherence to the substrate is poor (high concentration of thermal stresses).

Depending on the application of the thermal spray coating, different characteristics are important but there are some characteristics which are the same for all applications: coating thickness, porosity, structure, presence of unmelted particles and oxide inclusions, microhardness and bond strength [18]. These characteristics are mutually connected and are dependent on many parameters [19]. Generally, these parameters could be divided into two groups: substrate preparation parameters and spray deposition parameters. Detailed description of the influences these parameters have, can be found elsewhere [20, 21].

Thermal spraying is widely used coating deposition method because it presents process flexibility and coating quality in combination. It finds wide application in aerospace, petrochemical, automotive and other industries, where it is used to produce coatings with wear resistance, low coefficient of friction, high-temperature protection, corrosion resistance, electrical conductivity, electrical resistance, electromagnetic interference shielding, etc. There are several different processes for thermal spray coating deposition, and the main classification into two categories can be performed according to the thermal energy source used for melting of the feedstock material: flame (combustion) and electrical (electrical discharge) energy (**Fig. 1.9**). Cold gas spraying (CGS) process is something in between the mechanical (solid-state process) and thermo-mechanical process, since the kinetic energy, i.e. the particle velocity, is increased and the thermal energy is reduced comparing to the other processes. In this way the particles remain mainly in the solid state and are relatively cold. The most widely used processes for thermal spray coating deposition are: flame spraying (FS), electric arc wire spraying (AS), atmospheric plasma spraying (APS), plasma spray and high velocity oxygen fuel (HVOF) spraying [5, 22, 23].

Thermal spraying feedstock material may be any material that has a well defined melting point and which is not decomposed when heated. The choice is very wide and includes: pure metals and alloys (steels, Ni-, Cu-, Co- and Al-alloys, superalloys, M–Cr–Al–Y); ceramics (Al_2O_3, ZrO_2, Al_2O_3–TiO_2, Cr oxides, TiO_2, CaF_2, MgO–CaO); carbides (WC, Cr_3C_2, TiC) and cermets (WC–Co, WC–(Co–Cr), Cr_3C_2–(Ni–Cr)); polymers (polyethylene, polyamide, PEEK, PMMA, etc.); composites (Al-Si+graphite, Ni+graphite, Al-Si+polyester, CaF_2 with a metallic matrix, Al-Si+polyamide, Al-Si+polyethylene). The possible substrates are also various. Most metals, ceramics, glass and some plastics can be coated with thermal spraying [24, 25].

Compared to the other coating deposition processes, thermal spraying has many advantages, but also certain disadvantages. The advantages are: many possible combinations substrate-coating material; flexibility high-quality parts can be repaired, with low costs and relatively short downtimes in comparison to other repairing processes; substrates are only slightly heated up, in order to avoid microstructural changes; parts with complicated shape and variety of sizes could be coated. Disadvantages are: coating has different composition and behaviour than a feedstock material; microporosity of the coating is relatively high; limited bond strength of the sprayed layers; constrictions concerning the geometry (e.g. inner coating of bodies with a low inside diameter).

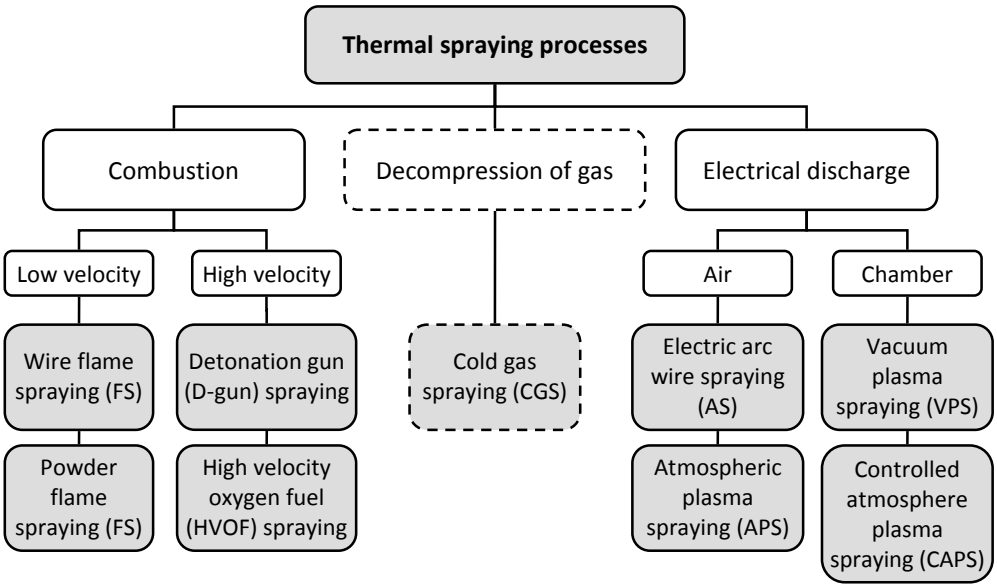

Fig. 1.9. Types of thermal spraying processes (names of the techniques are shown as shaded)

1.3. Principles of abrasive and erosive wear

Wear could be defined as a "process of progressive removal of material from the surface of solid body in contact and relative motion with a solid, liquid or gaseous counter-body". Therefore, wear is a result of surface loads and should be distinguished from fracture, i.e. from volume loads. Wear process leads to material and form changes at the material surfaces and to material losses. This can be seen by detached particles (wear products) from the tribologically stressed surface layer. Wear is usually undesired, as it diminishes the functional behaviour of a component and the value of the product. Wear of materials is the main reason for replacement of components, since in most cases it determines its useful lifetime. Indeed, wear is an important topic from an economical point of view because it represents one of a very limited number of ways in which material objects lose their usefulness. It is estimated that its economic importance is 50% [26]. It was also shown that over 30% of all failures in the main machine elements are direct consequence of wear [27]. Maintenance and other losses only increase this percentage.

Wear itself is a very complex process initiated by the action of different wear mechanisms, which in some cases act simultaneously or follow each other. The term of wear mechanism defines the physical/chemical elementary processes within the contact area of a tribosystem. A basic distinction is made between the four elementary wear mechanisms, as shown in **Fig. 1.10**, i.e. adhesion, abrasion, surface fatigue and tribochemical reactions (tribo-

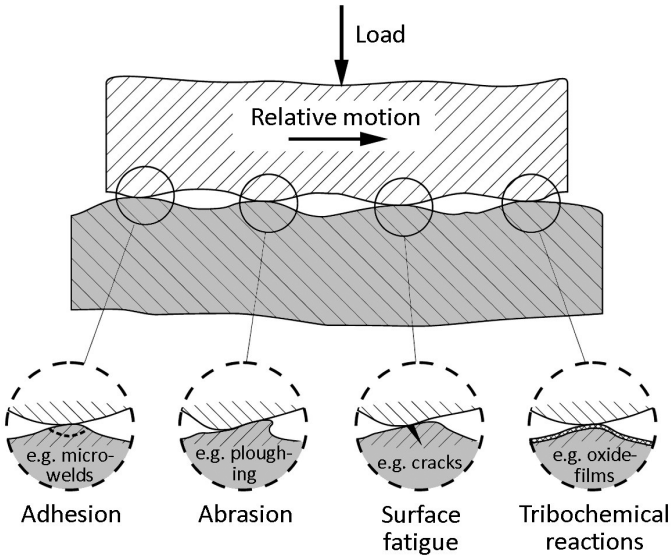

Fig. 1.10. Main wear mechanisms in tribosystems

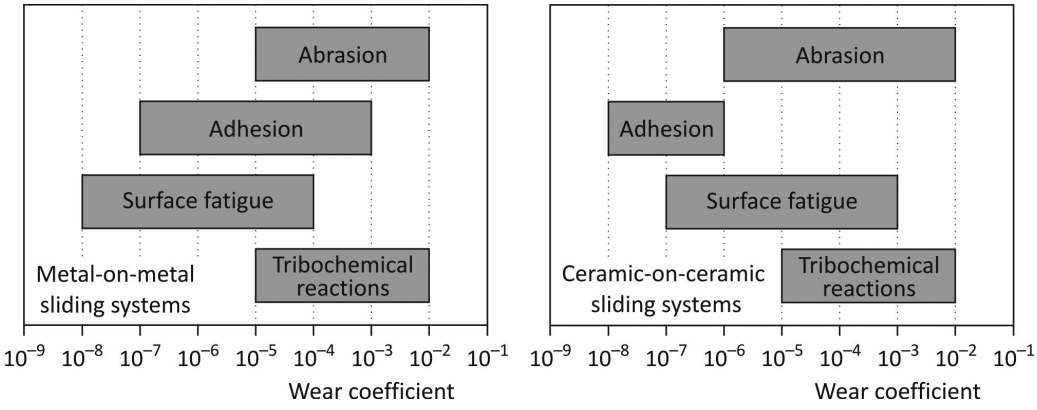

Fig. 1.11. Typical wear coefficient values for metal-on-metal and ceramic-on-ceramic sliding systems [28]

oxidation). In addition to these main mechanisms, and under special conditions, also diffusion and tribosublimation ought to be mentioned in the field of wear mechanisms. In these processes, the material changes have atomic dimensions at the mating bodies, when atoms and molecules from the tribologically stressed surface areas diffuse into the mating body, or sublimate into the surrounding medium.

Comparing by the severity through the dimensionless wear coefficient value, the abrasion wear mechanism is one of the most severe (**Fig. 1.11**). Wear mechanisms define most of the basic types of wear, and in most cases wear type is a result of the combined effects of different wear mechanisms. Nevertheless, wear types are investigated as isolated cases. Wear mechanism can be considered as a cause, and each wear type as a consequence (manifestation). According to the causes and manifestations eight different types of wear can be classified: adhesive wear, abrasive wear, surface fatigue wear (pitting), erosive wear, cavitation wear, fretting wear, oxidative wear and corrosive wear. First six are mechanical types of wear and the last two are chemical type of wear [29]. Beside these main wear types, there are some types of wear which have specific and isolated occurrence, such as diffusive wear, thermal wear, etc.

There are many parameters that affect wear process and influence its character, type, intensity, etc. These parameters can be divided into three categories: 1. Working parameters (type and character of movements, character and size of load, speed, operating temperature, time, etc.); 2. Characteristics of the system elements (real area of contact, chemical composition and structure, hardness, elastic modulus, density, thermal conductivity, surface roughness, thickness and structure of the surface layers, lubricant viscosity,

viscosity-temperature and viscosity-pressure dependence, relative humidity, etc.); 3. Types of interactions between the system elements (type of contact, type of friction, wear type and type of lubrication).

Analysis of the type of wear that can occur under certain operating conditions and for selected materials is very important in the construction and maintenance of machines, since it suggests what measures should be taken to reduce wear. Present dominant type of wear is determined by: experience; wear rate; working conditions (load, speed, temperature, etc.); environment (vacuum, air, lubricant, corrosive or reactive environment); chemical composition and appearance of the worn surface; chemical composition, quantity (concentration), size and morphology (form and structure) of the wear products; etc. Knowledge of expected wear values is necessary to allow equipment suppliers to design and provide guarantees of equipment lifetimes, and to allow operators to plan maintenance schedules. This is particularly important in the case of heavy-duty applications, where the costs of abrasive and erosive wear can be very significant.

1.3.1. Abrasive wear

Abrasive wear is one of the most common types of wear, which makes abrasive wear resistance very important in many industries. There are at least 17 active ASTM standards directly related to abrasive wear, and at least 4 directly related to erosive wear [30]. More than 50% of all wear-related failures of industrial equipment are caused by abrasive wear [27]. The estimated costs of abrasive wear are between 1 and 4% of the Gross national product of an industrialized nation [31]. For these reasons, the abrasive wear resistance is a subject of great importance in many industries, such as mining and minerals processing industry (bulldozer blades, excavator teeth, drills and chutes, etc.), automotive industry (cylinders, piston rings, clutches and brakes, etc.) as well as in other machines that work in contaminated environments (wind turbines, construction and agricultural machinery, etc.). The wear of machine parts, the cost of repair and replacement of these parts, and the associated downtime related to these activities result in significant costs for these industries.

Abrasive wear can be defined as “wear by displacement of material from surfaces in relative motion caused by the presence of hard particles either between the surfaces or embedded in one of them, or by the presence of hard protuberances on one or both of the surfaces” [32]. The second part of this definition corresponds to pure two-body abrasion, where tested material slides against harder and rougher counter-body material, while the first part corresponds to the three- and two-body abrasion, respectively. Another

interesting example of two-body abrasion is the abrasive erosion, which is the special case of erosive wear. Abrasive erosion has been defined as "erosive wear in which the loss of material from a solid surface is due to relative motion in contact with solid particles which are entrained in a fluid, moving nearly parallel to a solid surface" [32].

Abrasive wear processes are typically classified as two-body: abrasive particles or protuberances are fixed (**Fig. 1.12*a***) or abrasive particles freely slide and/or roll and act as a counter-body (**Fig. 1.12*b***) and three-body abrasion: abrasive particles are free to slide and/or to roll between mating bodies (**Fig. 1.12*c***). The origin of the abrasive particles (dust, dirt, sand, aerosol, debris, etc.) is either outside the tribological system (contaminants) or they are generated within the system itself (wear products). The rate of material removal in two-body abrasion can be one order of magnitude higher than that for three-body abrasion, because the loose abrasive particles abrade the solid surfaces between which they are situated only about 10% of the time, while they spend about 90% of the time rolling [33].

Another system of classification divides abrasion into gouging abrasion, high-stress (or grinding) abrasion and low-stress (or scratching) abrasion. In gouging abrasion, large particles are removed from the surface, leaving deep grooves and/or pits. The stresses in gouging abrasion are higher than those in high-stress abrasion and are often of a sufficient magnitude to cause generalised plastic deformation of materials. High-stress abrasion is accompanied by the fracture of the abrasive particles and the worn surface may exhibit varying degrees of scratching with plastic flow of sufficiently ductile phases or fracture of brittle phases. Debris may be formed after repeated plastic flow by a fatigue-like mechanism or by chipping. Low-stress abrasion occurs when the load is low enough that the abrasive particles are not fractured and a worn surface usually exhibits fine scratches [34].

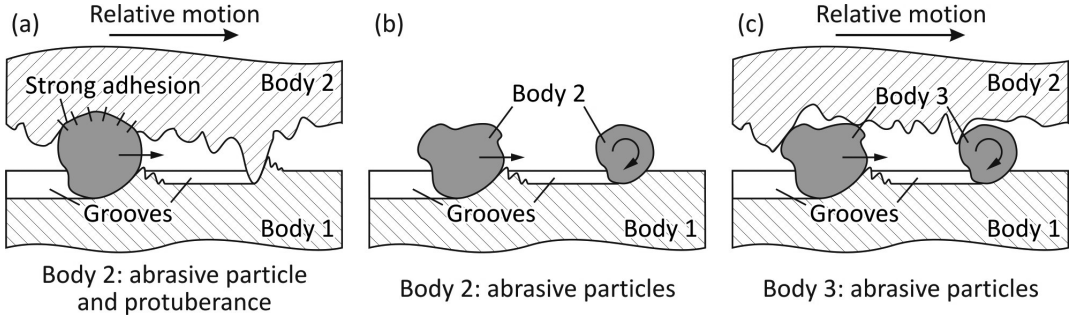

Fig. 1.12. Abrasive wear process: (a) and (b) two-body abrasion; and (c) three-body abrasion

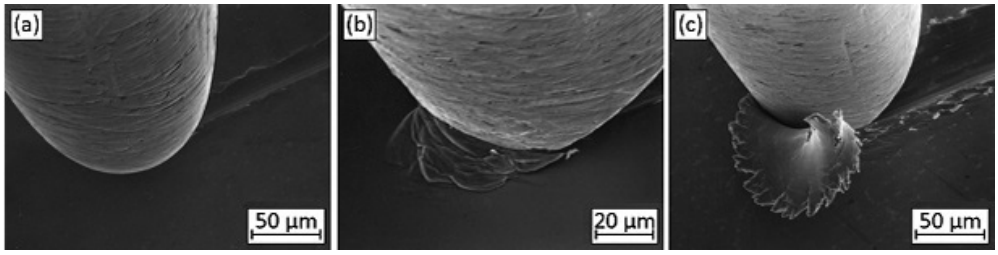

Fig. 1.13. Types of the abrasive mechanism: (a) ploughing and ridge formation; (b) wedge formation; and (c) cutting [35] (Reprinted with Authors' permission)

Regardless of the classification, abrasive wear mechanism could generally be divided into four types (modes): ploughing, fatigue, cutting and fracture (cracking), resulting with different surface appearance. Ploughing is characterised by a strong plastic deformation of the material caused by the effects of the abrasive particles in such a way, that its grooves bulge at their rims (**Fig. 1.13*a***). In the ideal case, ploughing due to a single pass of one abrasive particle does not result in any detachment of material from a wearing surface. During ploughing, material loss, however, can occur due to many abrasive particles which are acting simultaneously or successively. Material may be ploughed aside repeatedly by passing particles and may break off by low cycle fatigue. Pure cutting results in a material loss equal to the volume of the wear groove produced (**Fig. 1.13*c***). An intermediate case could also occur (**Fig. 1.13*b***), in which the wedge is formed in front of the abrasive particle. The wedge dimensions do not change too much during process and wear debris is generated by fragmentation of the formed wedge. Ploughing, fatigue and cutting types are more present in ductile materials. On the other hand, with brittle materials fracture (cracking) is more possible. It happens

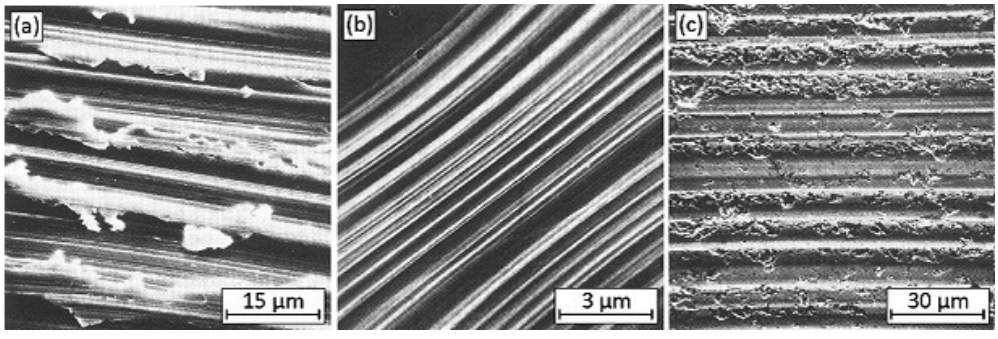

Fig. 1.14. Appearance of surfaces worn by different abrasive mechanism types: (a) ploughing and fatigue; (b) cutting; and (c) surface fracture (cracking)

when highly concentrated stresses are imposed by abrasive particles. In this case, large wear debris are detached from a surface due to crack formation and propagation [36].

Abrasive wear is the most obvious type of wear whose wear mechanism is prominently mechanical. It is manifested with grooves and chips, scratches, or pits and brittle surface cracks, depending on the present abrasive mechanism type (**Fig. 1.14**). Wear products formed by ploughing and fatigue are in the form of irregularly shaped fragments, while the wear products formed by cutting usually have spiral pattern.

Value of the abrasive wear depends on many parameters, such as normal load; sliding distance; hardness of the softer material in contact; hardness, amount and size of abrasive particles; etc. The increase of normal load induces a wear rate increase, and above some critical load the wear rate abruptly increases. This usually indicates the transition of the wear regime (**Fig. 1.15**). In the case presented in **Fig. 1.15** gray cast iron pins surface was not in full contact with the nodular cast iron counter-body at lower specific loads (1 and 2 MPa), and the basic lamellar structure of the material could be clearly noticed. At higher specific loads (3 and 4 MPa) more intensive,

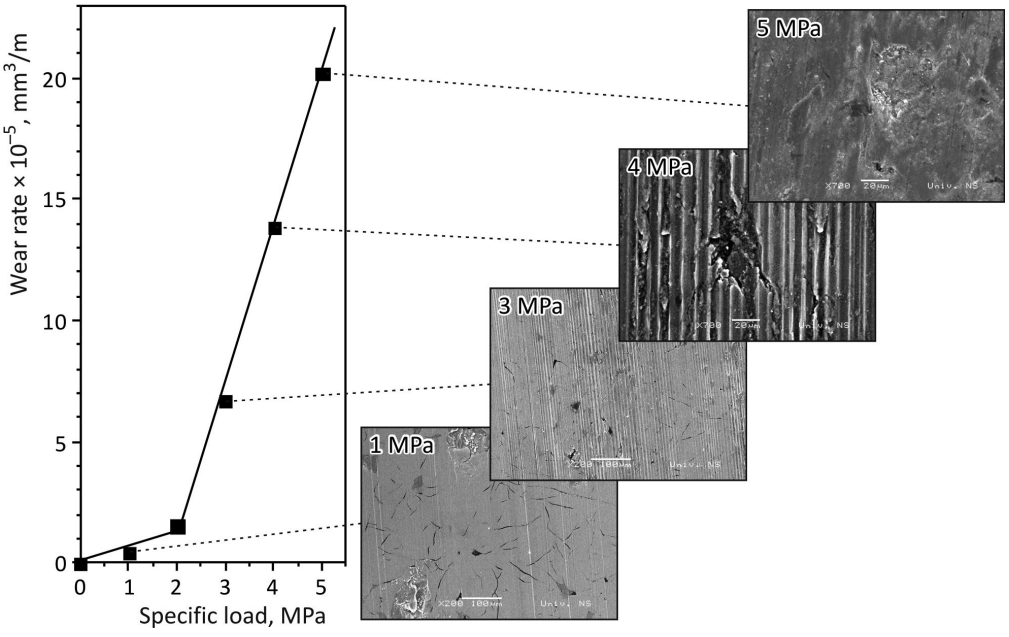

Fig. 1.15. Wear rate vs. specific load – change of the wear mechanism from light abrasion through normal and intensive abrasion to severe adhesive wear (gray cast iron pin in dry sliding contact with nodular cast iron disc) [37]

abrasive wear starts, and at highest specific load of 5 MPa intensive adhesive wear occurs, due to the presence of high pressure and contact temperature.

Higher hardness of the softer material in contact usually gives higher abrasive wear resistance, but this dependence is not proportional (except for pure metals). In some cases, as in composite materials, it is not even true [38]. It has been found that the abrasive wear depends on the correlation between the hardness of the abrasive particles (Ha) and the hardness of the softer material in contact (Hm), leading to three distinct wear regimes (**Fig. 1.16**). These three regimes are: I – light abrasion, II – transition zone, and III – severe abrasion [27]. In order to reduce abrasive wear of the softer material its hardness should be increased, and as the limits for metals should be Hm = 1.3 × Ha, because further increase of the hardness Hm beyond 1.3 times that of the Ha is unnecessary since no further significant improvement will be obtained [39].

The higher amount and higher size of abrasive particles generally increase the abrasive wear rate. Nevertheless, if the size of the abrasive particles do not exceeds a few tens of micrometer, it does not affect significantly the abrasive wear rate [22, 40]. **Fig. 1.17** illustrates the influence of the abrasive particles size of an abrasive paper on the wear coefficient, measured on carbon steel and copper. The value of wear coefficient increases up to a particle size of about 50 μm, and then stabilizes.

Basic ways to reduce the abrasive wear are: increasing of the material hardness (Hm); better machining (lower roughness); eliminating of the abrasive particles (filtering) and better sealing. Another way to reduce the abra-

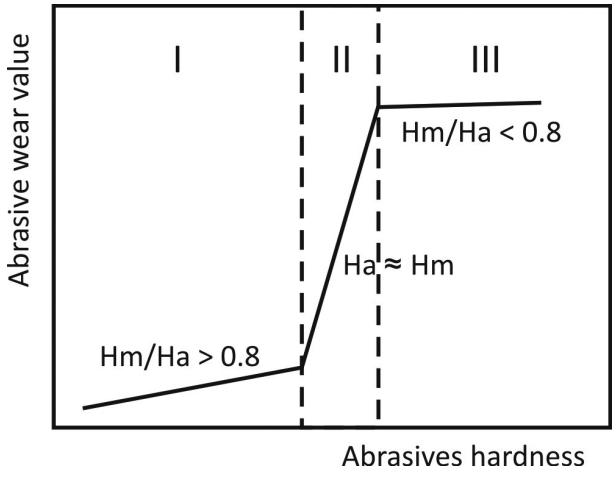

Fig. 1.16. Influence of the abrasive particles hardness on the abrasive wear of the softer material in contact [27]

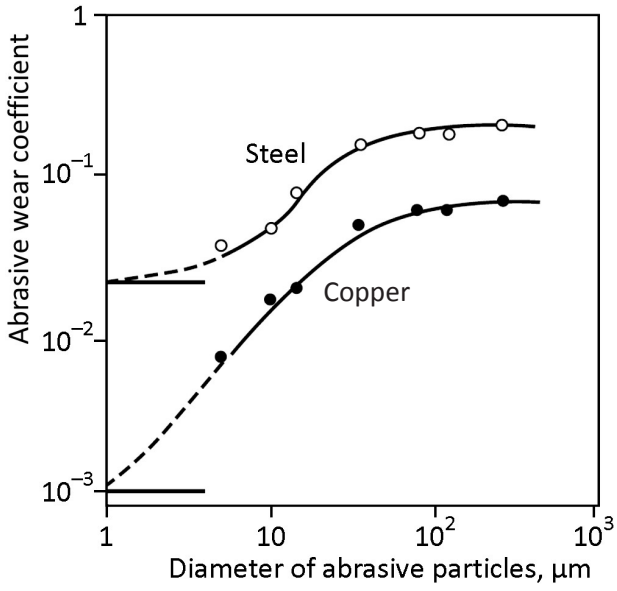

Fig. 1.17. Effect of diameter of abrasive particles on the wear coefficient [40] (Republished with permission of [Taylor and Francis Group LLC Books], from [Corrosion and Surface Chemistry of Metals, Dieter Landolt, 2006]; permission conveyed through Copyright Clearance Center, Inc.)

sive wear is using of the composite materials. Factors that affect the abrasive wear of these materials include the size, orientation, relative hardness, modulus of elasticity, and brittleness of the second phase (**Fig. 1.18**). When the size of the second phase is small relative to the abrasive groove depth, the second phase has little or no beneficial effect. Also, a reinforcing phase lying parallel to the surface is more easily removed than one that is anchored perpendicular to the surface. Reinforcing phases harder than the abrasive particles will protect the matrix, and reduce the abrasive wear. A low modulus of elasticity of the matrix and/or of the reinforcing phase favours debonding at the interfaces, and lead to pull-out and abrasive loss. Lastly, brittle materials (reinforcing phase and/or matrix) tend to crack to a larger area than the cross-section of the abrasive particle groove. This results in increasing abrasive wear [36].

1.3.2. Erosive wear

Erosive wear can be defined as “loss of material from a solid surface due to relative motion in contact with solid particles which are entrained in a fluid or due to the action of streaming liquid, gas or gas containing liquid droplets”

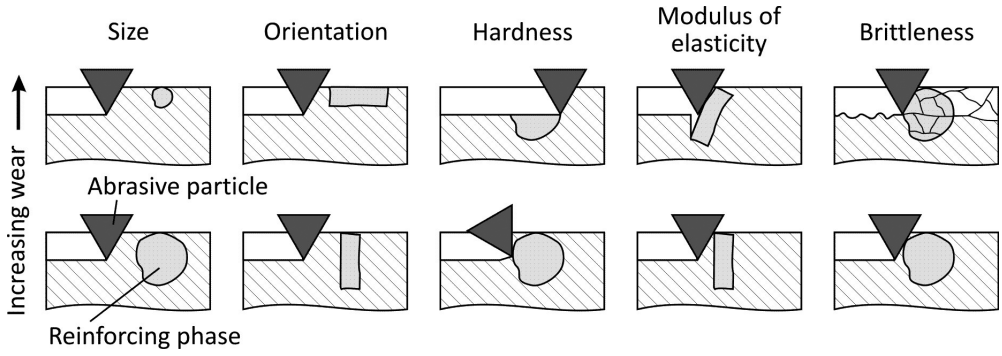

Fig. 1.18. Influence of various properties of reinforcing phase on abrasive wear of composite

[32]. The first part of this definition corresponds to solid particles erosion, and the second part to fluid erosion. Solid particles erosion has two special cases: abrasive erosion and impingement or impact erosion (erosion in which the relative motion of the solid particles is nearly normal to the solid surface). Fluid erosion does not normally include cavitation erosion (cavitation wear), nor electrical erosion (electrical pitting).

According to the aforementioned definition, two types of erosive wear could be distinguished: solid particles erosion and fluid erosion, i.e. erosion caused by the impact of fluid with or without solid particles. Solid particles erosion is more often in practice. In solid particles erosion wear is the result of abrasive action of solid particles carried by fluid in combination with surface fatigue, i.e. combination of abrasion and surface fatigue wear mechanism. Like in other wear types, mechanical strength does not guarantee erosive wear resistance.

In most cases failure damage caused by erosive wear is localized on specific areas. Damaged surface is characterised with smooth, broad grooves in direction of fluid flow or mate and clean texture (**Fig. 1.19**). In **Fig. 1.19*a***, erosive wear by fluid was noticed around oil holes of the journal bearing, and was manifested by removal of the material due to the fatigue mechanism. Most probably the inlet speed of lubricating oil was high, causing fluid erosion of the bearing. Erosive wear by solid particles is shown in **Fig. 1.19*b***. A piston pin retainer broke and the loose pieces severely eroded the piston pin bore. Erosion is worse at the top of the bore than it is at the bottom, due to the piston loading and movement against the broken retainer, i.e. downward piston movement is more sudden and violent than upward piston movement.

Erosive wear rate depends on many parameters, such as angle of particle/fluid impact; kinetic energy of the particle/fluid on impact; size, shape,

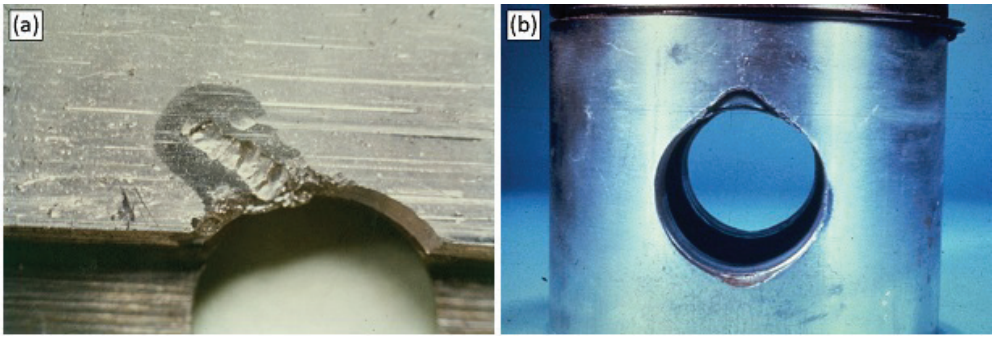

Fig. 1.19. Appearance of surfaces worn by different erosive wear types: (a) journal bearing surface damaged by erosive wear (fluid erosion) [Reprinted from Engineering Failure Analysis, 44, A. Vencl, A. Rac, Diesel engine crankshaft journal bearings failures: Case study, 217-228, Copyright (2014), with permission from Elsevier] and (b) piston pin bore damaged by erosive wear (solid particles erosion)

amount and type of particles carried by the fluid, and properties of the eroded material. The angle of impact (impingement) is the angle between the eroded surface and the trajectory of the particle/fluid immediately before impact. For ductile materials the highest erosive wear is when the impact angle is between 20 and 30°, while for brittle materials the highest erosive wear is when the impact angle is about 90° (**Fig. 1.20**).

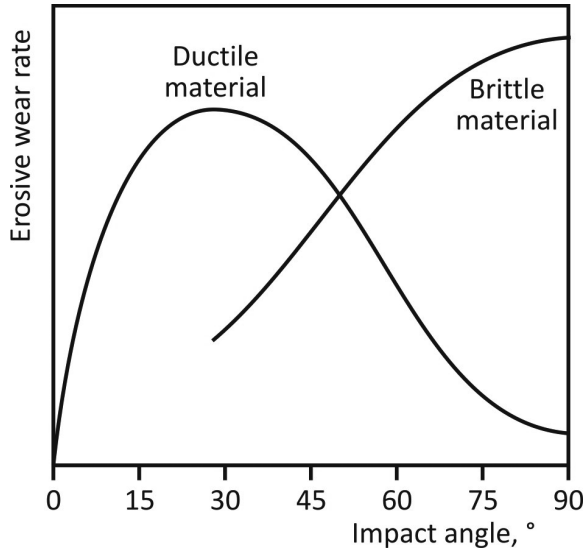

Fig. 1.20. Effect of impact angle on erosive wear rates of ductile and brittle materials [27]

The velocity of the erosive particle/fluid has a very strong effect on the wear process, since it influences the kinetic energy that will be transferred to the surface. If the velocity is very low then stresses at impact are insufficient for plastic deformation to occur and wear proceeds by surface fatigue. When the velocity is increased to, for example, 20 m/s it is possible for the eroded material to deform plastically on particle impact. In this regime, which is quite common for many engineering components, wear may occur by repetitive plastic deformation [22].

Effect of particle size is shown in **Fig. 1.21**, which reveals that as particle size was increased from 9 to 127 μm in diameter the mode of erosive wear changed from ductile to brittle. In both cases erosive agent was silicon carbide with velocity of 152.4 m/s. This change in wear mode is most probably a consequence of the average spacing of defects, e.g., holes or cracks in an eroded surface. With small particles only a minority of the impacted places will coincide with a defect. This will provide ductile erosive wear mode, with relatively slow wear increase. For larger particles, a defect is almost always present in the impacted place and material removal is by brittle processes. This will provide rapid formation of the cracks and fast increase of wear. The sharpness of the particle has also been recognized to increase erosive wear

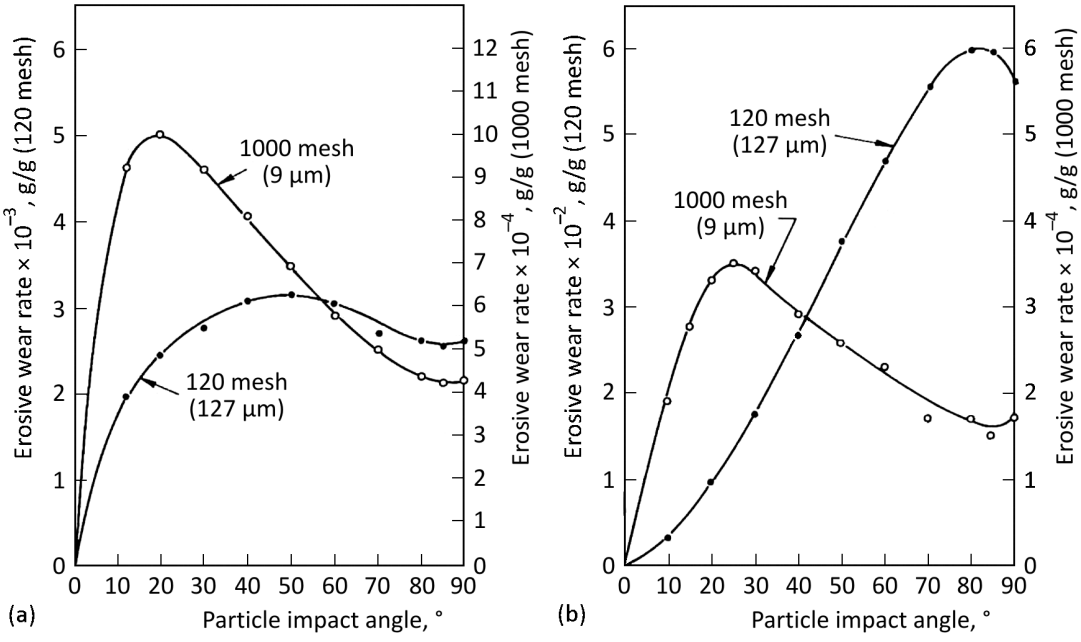

Fig. 1.21. Effect of particle size on mode and rates of erosive wear (grams removed/grams of abrasive): (a) hardened tool steel; and (b) plate glass; adapted from [41], with permission from ASME

[42], and it is known that hard particles cause higher wear rates than soft particles [43].

Basic ways to reduce the erosive wear are: decreasing of the fluid/particles velocity; eliminating of the solid particles; choosing the adequate material depending on the impact angle.

References to Chapter 1

[1] **Cotell, C. M., J. A. Sprague.** Preface. – In: *ASM Handbook, Vol. 5, Surface Engineering*, ASM International, Metals Park, 1994.

[2] **Martin, P. M.** *Introduction to Surface Engineering and Functionally Engineered Materials*. Hoboken: John Wiley & Sons, 2011.

[3] **Stupnišek, M., B. Matijević.** Pregled postupaka modificiranja i prevlačenja metala (Modification and coating of metal surface). – In: *Znanstveno stručni skup s međunarodnim učešćem "Toplinska obradba metala i inženjerstvo površina"*. Proceedings, Zagreb (Croatia), 08.06.2000, pp. 53-62.

[4] **Bhushan, B.** *Principles and Applications of Tribology*. New York: John Wiley & Sons, 2013.

[5] *An Introduction to Thermal Spray*. Brochure, Oerlikon Metco, Winterthur, 2015, (http://www.oerlikon.com/metco).

[6] **Holmberg, K., A. Matthews.** *Coatings Tribology: Properties, Mechanisms, Techniques and Applications in Surface Engineering*. Amsterdam: Elsevier, 2009.

[7] **Mellor, B. G.** Welding surface treatment methods for protection against wear. – In: Mellor, B. G. (Ed.), *Surface Coatings for Protection against Wear*. Cambridge: Woodhead Publishing, 2006, pp. 302-376.

[8] **Ponce de León, C., C. Kerr, F. C. Walsh.** Electroless plating for protection against wear. – In: Mellor, B. G. (Ed.), *Surface Coatings for Protection against Wear*. Cambridge: Woodhead Publishing, 2006, pp. 184-225.

[9] **Hajdu, J.** Surface preparation for electroless nickel plating. – In: Mallory, G. O., J. B. Hajdu (Eds.), *Electroless Plating: Fundamentals and Applications*. Norwich: Noyes Publications/William Andrew Publishing, 1990, pp. 193-206.

[10] **Schlesinger, M.** Electroless deposition of nickel. – In: Schlesinger, M., M. Paunovic (Eds.), *Modern Electroplating*. Hoboken: John Wiley & Sons, 2010, pp. 447-458.

[11] **Vencl, A., B. Gligorijević, B. Katavić, B. Nedić, D. Džunić.** Abrasive wear resistance of the iron- and WC-based hardfaced coatings evaluated with scratch test method. – *Tribology in Industry*, Vol. 35, 2013, No 2, pp. 123-127.

[12] **Davis, J. R. Hardfacing.** Weld cladding, and dissimilar metal joining. – In: *ASM Handbook Volume 6, Welding, Brazing, and Soldering*. ASM International, Metals Park, 1993, pp. 789-829.

[13] **Miller, B.** Frequently asked questions about hardfacing. – *Practical Welding Today*, Vol. 9, 2005, No 2.

[14] EN 14700:2005 *Welding consumables – Welding consumables for hard-facing*, European Committee for Standardization, Brussels, 2005.
[15] **Schorr, B. S., K. J. Stein, A. R. Marder.** Characterization of thermal spray coatings. – *Materials Characterization*, Vol. 42, 1999, No 2-3, pp. 93-100.
[16] **Vencl, A., M. Mrdak, M. Banjac.** Correlation of microstructures and tribological properties of ferrous coatings deposited by atmospheric plasma spraying on Al-Si cast alloy substrate. – Metallurgical and Materials Transactions A, Vol. 40, No 2, 2009, pp. 398-405.
[17]-- *About Thermal Spray*, Poster, Flame Spray Technologies, Duiven, (http://www.fst.nl).
[18] **Vencl, A., M. Mrdak, I. Cvijović.** Microstructures and tribological properties of ferrous coatings deposited by APS (atmospheric plasma spraying) on Al-alloy substrate. – *FME Transactions*, Vol. 34, 2006, No 3, pp. 151-157.
[19] **Vencl, A., S. Arostegui, G. Favaro, F. Zivic, M. Mrdak, S. Mitrović, V. Popovic.** Evaluation of adhesion/cohesion bond strength of the thick plasma spray coatings by scratch testing on coatings cross-sections. – *Tribology International*, Vol. 44, 2011, No 11, pp. 1281-1288.
[20] **Vencl, A., S. Avramović, A. Marinković.** Prevlaka na bazi gvožđa naneta na osnovu od Al legure plazma sprej postupkom u atmosferskim uslovima (Ferrous-based coating deposited on Al-alloy substrate by atmospheric plasma spraying (APS)). – In: *31. Savetovanje proizvodnog mašinstva Srbije i Crne Gore*, Kragujevac (Serbia), 19-21.09.2006, Proceedings, pp. 539-546.
[21] **Vencl, A.** Optimization of the deposition parameters of thick atmospheric plasma spray coatings. – *Journal of the Balkan Tribological Association*, Vol. 18, 2012, No 3, pp. 405-414.
[22] **Stachowiak, G. W., A. W. Batchelor.** – *Engineering Tribology*. Boston: Butterworth-Heinemann, 2000.
[23] **Stokes, J.** *Production of Coated and Free-Standing Engineering Components Using the HVOF (High Velocity Oxy-Fuel) Process*. PhD thesis. Dublin, School of Mechanical and Manufacturing Engineering, Dublin City University, 2003.
[24] **Guilemany, J. M., J. Nin.** Thermal spraying methods for protection against wear. – In: Mellor, B. G (Ed.), *Surface Coatings for Protection against Wear*, Cambridge, Woodhead Publishing, 2006, pp. 249-301.
[25] **Pawlowski, L.** *The Science and Engineering of Thermal Spray Coatings*. Chichester: John Wiley & Sons, 2008.
[26] **Rabinowicz , E.** *Friction and Wear of Materials*. New York: John Wiley & Sons, 1995, pp. 1-13.
[27] **Rac, A.** *Osnovi tribologije* (*Fundamentals of Tribology*). Belgrade: Mašinski fakultet Univerziteta u Beogradu, 1991.
[28] **Rabinowicz, E.** The least wear. – *Wear*, Vol. 100, 1984, No 1-3, pp. 533-541.
[29] **Vencl, A., A. Rac.** Diesel engine crankshaft journal bearings failures: Case study. – *Engineering Failure Analysis*, Vol. 44, 2014, pp. 217-228.

[30] *Annual Book of ASTM Standards*, ASTM International, West Conshohocken, 2016.
[31] **Bayer, R. G.** Fundamentals of wear failures. – In: *ASM Handbook*, *Volume 11, Failure Analysis and Prevention*, ASM International, Metals Park, 2002, pp. 901-905.
[32] OECD, Research Group on Wear of Engineering Materials, *Glossary of Terms and Definitions in the Field of Friction, Wear and Lubrication: Tribology*, Organisation for Economic Co-operation and Development, Paris, 1969.
[33] **Zum Gahr, K.-H.** Wear by hard particles. – *Tribology International*, Vol. 31, 1998, No 10, pp. 587-596.
[34] **Vencl, A., N. Manić, V. Popovic, M. Mrdak.** Possibility of the abrasive wear resistance determination with scratch tester. – *Tribology Letters*, Vol. 37, 2010, No. 3, pp. 591-604.
[35] **Kato, K., K. Hokkirigawa.** Abrasive wear diagram. – *Proceedings of 4th European Tribology Congress – Eurotrib 85, Vol. IV*, Ecully (France), 09-12.09.1985, Section 5.3, Paper 8.
[36] **Zum Gahr, K.-H.** *Microstructure and Wear of Materials*. Amsterdam: Elsevier, 1987.
[37] **Vencl, A.** A. *Istraživanje mogućnosti poboljšanja triboloških karakteristika Al-Si legura u uslovima klizanja* (*The Research of the Al-Si Alloys Tribological Properties Improvement Possibilities in Sliding Conditions*), PhD Thesis, Mašinski fakultet, Univerzitet u Beogradu, Belgrade, 2008.
[38] **Vencl, A., B. Katavić, D. Marković, M. Ristic, B. Gligorijević.** The tribological performance of hardfaced/thermal sprayed coatings for increasing the wear resistance of ventilation mill working parts. – *Tribology in Industry*, Vol. 37, 2015, No. 3, pp. 320-329.
[39] **Eyre, T. S.** Wear characteristics of metals. – *Tribology International*, Vol. 9, 1976, No 5, pp. 203-212.
[40] **Landolt, D.** *Corrosion and Surface Chemistry of Metals*. Lausanne: EPFL Press, 2007.
[41] **Sheldon, G. L., I. Finnie.** On the ductile behavior of nominally brittle materials during erosive cutting. – *Journal of Engineering for Industry*, Vol. 88, No 4, pp. 387-392.
[42] **Bahadur, S., R. Badruddin.** Erodent particle characterization and the effect of particle size and shape on erosion. – *Wear*, Vol. 138, 1990, No 1-2, pp. 189-208.
[42] **Goodwin, J. E., W. Sage, G. P. Tilly.** Study of erosion by solid particles. – *Proceedings of the Institution of Mechanical Engineers*, Vol. 184, 1969, No 1, pp. 279-292.

Chapter 2

ELECTROLESS NICKEL COMPOSITE COATINGS WITH NANOPARTICLES

2.1. Introduction

Electroless plating is a chemical deposition process, which can be defined as the deposition of a metal from an aqueous solution of its salt by a controlled chemical reduction that is catalyzed by the metal or alloy being deposited [1]. Nevertheless, the electroless plating process has an electrochemical mechanism, both oxidation and reduction, reactions involving the transfer of electrons between reacting chemical species. The oxidation of a substance is characterized by the *loss* of electrons (anodic process), while reduction is distinguished by a *gain* of electrons (cathodic action) [2]. The reduction reaction, which occurs between positively charged metal ions in solution M^+ and negative electrons e^-, can be represented as follows:

$$M^{n+} + ne^- \rightarrow M^0 . \tag{2.1}$$

The differences between the electroless plating (chemical deposition) and electroplating (electrochemical deposition) is in a way of providing electrons necessary for the reduction of metal ions in the solution. Electroplating is based on the reduction of metal ions at the cathode using electrons supplied by an external direct current source. The oxidation reaction occurs on anodes of the same nature as the metal being reduced at the cathode [3]. On the other hand, electroless plating uses only one electrode (cathode) without the use of external direct current source. Instead of an anode, the metal (coating) is supplied by the metal salt, and electrons are released from a suitable chemical reducing agent added to the solution. The reaction continues as long as the surface remains in contact with the electroless metal solution. Because the coating is deposited without an external electric current source, no lines of electric flux develop. As a consequence, the coating thickness is evenly distributed and uniform, without edge effects.

Since the electrons in electroless plating originate from within the system, the process is therefore also referred to as autocatalytic. The name electroless plating is somewhat misleading, however. There are no external electrodes present, but there is electric current (charge transfer) involved. More

descriptive term, which was used by the inventors, would be electrodeless plating. The name soon lost the *de*, and later the name autocatalytic was formally adopted, although electroless is still widely used [1].

Electroless plating has been used to obtain coatings of Ni, Co, Pd, Cu, Au, and Ag as well as some alloys containing these metals plus P or B. Electroless Cr deposition has also been claimed [1]. Among these, electroless nickel plating is the most widely used electroless plating process. The preferred source of nickel cations is nickel sulphate ($NiSO_4$). Other nickel salts, such as nickel chloride and nickel acetate, are used for very limited applications. The most common reducing agent used is sodium hypophosphite (NaH_2PO_2). Alternatives are sodium borohydride, dimethylamine borane and hydrazine but they are used much less frequently [2]. It is estimated that sodium hypophosphite is used in more than 99% of all electroless nickel plating [4].

The chemical deposition on nickel ions on catalytically active surface by hypophosphite in aqueous solution can be described by the following reaction [5]:

$$Ni^{2+}(SO)_4^- + 3Na^+(H_2PO_2)^- + 3H_2O \rightarrow Ni^0 + 3Na^+(H_2PO_3)^- + 2H_2\,. \quad (2.2)$$

The process is successful because it takes place only on catalytic surfaces, rather than throughout the solution. In other words, the electrons are not transferred to nickel directly but via the metal surface of the substrate (**Fig. 2.1**). If the process is not properly controlled, the reduction can take place throughout the solution, i.e., the two substances would react directly within the solution and produce a fine nickel powder.

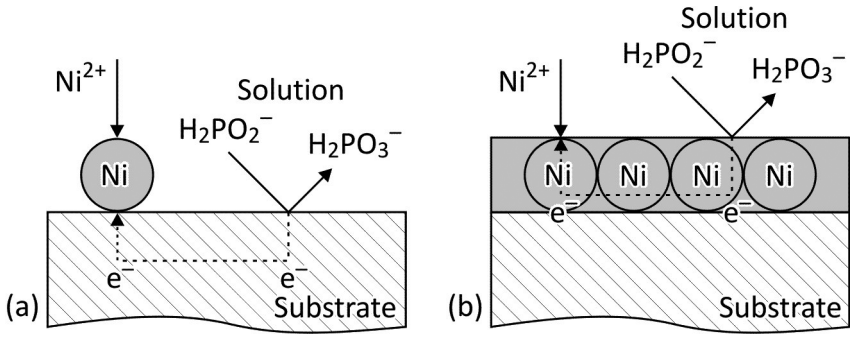

Fig. 2.1. Schematic diagram of the nickel plating from a hypophosphite bath: (a) initial layer on a ferrous substrate (electron transfer progresses from the hypophosphite layer to nickel via the substrate surface; thus, nickel is also deposited onto the substrate and does not precipitate in the solution); and (b) subsequent layer on a initial nickel layer

Part of the added hypophosphite decomposes to phosphorous acid and phosphorus in a side reaction [5]:

$$3Na^{+}(H_2PO_2)^{-} \rightarrow Na^{+}(H_2PO_3)^{-} + H_2O + 2Na^{+}(OH)^{-} + 2P^{0}. \quad (2.3)$$

The deposition rate of the electroless coatings varies between several micrometers per hour up to 25-30 μm/h. It depends on the quantity of energy added to the system in the form of heat [2], pH value of the solution [1], composition of the solution, and many other factors [3]. The thickness of the electroless nickel coating depends also on the composition of the solution, for instance. Typical coating thickness, depending on the industrial application, varies from 2 to 125 μm [3].

The Equation 2.3 reveals that also, in addition to elemental nickel, elemental phosphorus develops. The phosphorus is integrated into the coating, and its content has a great effect on coating properties. Phosphorus content can be varied over a wide range, typically 1 to 13 wt. %. According to their phosphorus content, electroless nickel coatings can be categorized into four principal groups: low phosphorus (1-3 wt. % P), low-medium phosphorus (3-6 wt. % P), medium phosphorus (6-9 wt. % P) and high phosphorus (9-13 wt. % P) alloys [6].

Chemical composition of the electroless nickel coatings affect its structure and produce often generally distinct physical, mechanical and tribolo-

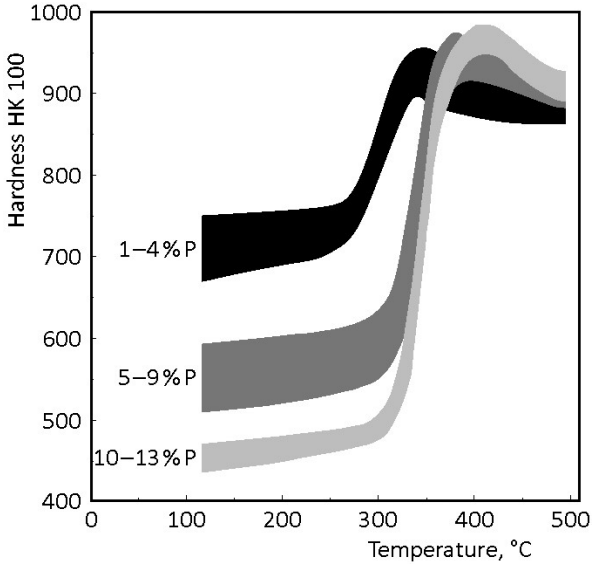

Fig. 2.2. Effect of one hour heat treatment and phosphorus content on electroless nickel coatings hardness [4] (Reproduced with permission from Nickel Institute)

gical properties of these coatings [1, 3, 4, 6, 7]. For instance, at high phosphorus contents coatings are no longer metallic but show partially ceramic properties, and the ferromagnetism of nickel thus disappears. Furthermore, electroless nickel coating can be heat treated, and the resulting coating will have much improved wear resistance, but diminished corrosion resistance [8]. Phosphorus and nickel form a solid solution, and 1 hour of heat treatment at 400 °C causes nickel phosphide precipitation [5]. Using this, hardness values of up to 1100 HV are obtainable that correspond to the hardness of the coatings known as hard chrome (**Fig. 2.2**).

For this reason, electroless nickel has been used to replace chrome coatings, which have negative environmental and health effects, in many decorative as well as functional applications. Although the environmental ramifications of nickel are still questionable, it is clearly less problematic than chrome. In applications requiring hardness and wear resistance, electroless nickel composite coatings have been even more successful in not only replacing chrome but actually surpassing the performance of hard chrome plating [9].

The deposition of nickel coating with electroless plating process is applied in industry mainly to improve the corrosion and wear resistance, to build up worn or undersized parts, to modify magnetic properties, etc. [10]. Estimation of the percentage uses of electroless nickel coatings for improving various characteristics is shown in **Fig. 2.3**.

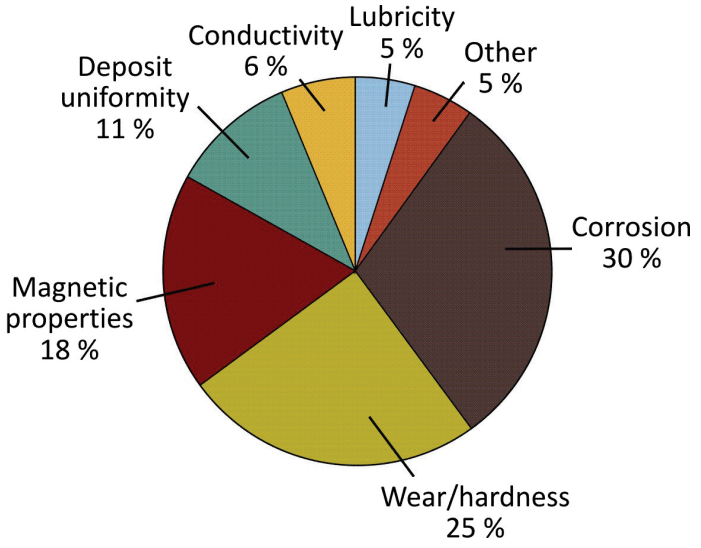

Fig. 2.3. Primary uses for electroless nickel coatings [11] (Reproduced with permission from Products Finishing)

Because of these properties, electroless nickel coatings are commonly used in engineering coating applications where wear resistance, hardness and corrosion protection are required. Applications include those in chemical process, food, oil and gas, automotive, aerospace, electronics, mining, printing, textile, paper and other industries [4, 6, 12].

The potential of the electroless nickel coatings increases due to the ability of easy production of functional composite coatings with incorporated various hard/soft particles. The application of electroless nickel composite coatings with particles of different materials, sizes and amounts is very interesting, since this generally leads to the improvement of mechanical and tribological characteristics. Generally, these particles are evenly and thoroughly distributed throughout the coating, which is firmly bonded to the substrate. These coatings, therefore, have all of the inherent features of electroless nickel as well as the properties of whatever particles are selected.

Theoretically, almost any type of particle could be incorporated, as long as it could withstand the conditions within an electroless nickel bath, and if it were of the appropriate size. Generally speaking, diamond and silicon carbide electroless nickel composite coatings are chosen for wear resistance, while boron nitride and PTFE composite coatings are selected for lubricity. However, depending on the application, any of these coatings might improve wear resistance or lubricity [13]. The method of formation, mechanism of particle incorporation, factors influencing particle incorporation, effect of particle incorporation on the coating structure, hardness, friction, wear and corrosion resistance, high temperature oxidation resistance and applications are discussed elsewhere [14, 15].

This chapter considers solutions for the improvement of the wear resistance and friction properties of working shafts (calenders) involved in the production of sheet-formed and foliate materials, such as paper, cardboard, leather, etc. Calender shafts work in dynamic conditions, i.e., in various temperature and contact interaction regimes, and are subjected to severe wear [16-19]. Usually, their resource is improved through wear resistant thin and hard Cr coatings. It was shown that enhanced tribological characteristics, especially abrasive and erosive wear and coefficient of friction, were obtained by using the electroless nickel composite coatings containing nano-sized particles of diamond [20, 21], silicon carbide [18, 19, 22-26] and boron nitride [27]. The idea of the researches was to investigate the influence of different nanoparticles addition, as well as heat treatment, on the coatings tribological properties.

2.2. Materials

The coatings were fabricated by electroless plating process EFTTOM-NICKEL, developed at Technical University of Sofia [28-31]. Three different types of nano-sized particles (5-7 vol. %) were incorporated in the nickel (Ni) coatings, i.e., particles of diamond (D), silicon carbide (SiC) and boron nitride (BN). Heat treatment was applied to some of the samples to improve its mechanical properties and adhesion in the substrate-coating interface. Applied heat treatment consists of heating at 300 °C during 6 hours. The substrate material for all coatings was a carbon steel Ст3кп (GOST 380-94), with chemical composition shown in **Table 2.1**. Hardness of the substrate was 135 HV 0.05. The roughness of the substrate was examined with mechanical profilometer. Measurement was performed in at least five points on the surface of coatings and the average roughness was *Ra* = 0.089 μm.

Table 2.1. Chemical composition (wt. %) of the coated material (substrate)

Element	C	Si	Mn	Ni	P	S	Cr	Fe
Percentage	0.4	0.20	0.55	0.30	0.45	0.045	0.30	Balance

2.2.1. Nickel coatings with diamond (D) nanoparticles

Ten different samples with electroless Ni coatings were investigated. They can be divided into two series, i.e., samples without and with heat treatment. In each series there are five samples: 1) coating without diamond nanoparticles; 2) coating with diamond nanoparticles of average size 4 nm; 3) coating with diamond nanoparticles of average size 100 nm; 4) coating with diamond nanoparticles of average size 200 nm; 5) coating with diamond nanoparticles of average size 250 nm. Volume concentration of diamond nanoparticles was the same in all coatings, i.e., from 5 to 7 vol. %. Designations of tested coatings are shown in **Table 2.2**. The ultradispersed diamond powder (diamond nanoparticles) was produced by the detonation synthesis method [20].

Coatings thickness was measured in 5 points on each coating surface, and the average values are shown in **Table 2.2**. Measurements of surface microhardness (HV 0.5) were carried out using Vickers microhardness tester under the load of 500 g. At least three measurements were made for each sample in order to eliminate possible segregation effects and to obtain a representative value of the material microhardness. Average values are presented in **Table 2.2**.

Table 2.2. Designation and thickness of tested coatings

Sample	Designation	Description	Thickness, µm	Microhardness HV 0.5
1	Ni	Electroless Ni coating without nanoparticles and heat treatment	25.6	543
2	Ni^{HT}	Electroless Ni coating without nanoparticles and with heat treatment	11.3	551
3	Ni-D4	Electroless Ni coating with D nanoparticles of 4 nm size and without heat treatment	23.2	289
4	$Ni\text{-}D4^{HT}$	Electroless Ni coating with D nanoparticles of 4 nm size and with heat treatment	8.0	543
5	Ni-D100	Electroless Ni coating with D nanoparticles of 100 nm size and without heat treatment	27.9	681
6	$Ni\text{-}D100^{HT}$	Electroless Ni coating with D nanoparticles of 100 nm size and with heat treatment	7.1	735
7	Ni-D200	Electroless Ni coating with D nanoparticles of 200 nm size and without heat treatment	26.2	531
8	$Ni\text{-}D200^{HT}$	Electroless Ni coating with D nanoparticles of 200 nm size and with heat treatment	9.1	787
9	Ni-D250	Electroless Ni coating with D nanoparticles of 250 nm size and without heat treatment	30.5	539
10	$Ni\text{-}D250^{HT}$	Electroless Ni coating with D nanoparticles of 250 nm size and with heat treatment	8.7	826

2.2.2. Nickel coatings with silicon carbide (SiC) nanoparticles

Six different samples with electroless Ni coatings were investigated. They can be divided into two series, i.e., samples without and with heat treatment. In each series there are three samples: 1) coating without silicon carbide nanoparticles; 2) coating with silicon carbide nanoparticles of average size 150 nm; 3) coating with silicon carbide nanoparticles of average size 700 nm. Volume concentration of silicon carbide nanoparticles was the same in all coatings, i.e., from 5 to 7 vol. %. Designations of tested coatings are shown in **Table 2.3**. Samples were tested only on abrasive wear resistance.

Coatings thickness was measured in 5 points on each coating surface, and the average values are shown in **Table 2.3**. Measurements of surface microhardness (HV 0.5) were carried out using Vickers microhardness tester

Table 2.3. Designation and thickness of tested coatings

Sample	Designation	Description	Thickness, µm	Microhardness HV 0.5
1	Ni	Electroless Ni coating without nanoparticles and heat treatment	25.6	543
2	Ni^{HT}	Electroless Ni coating without nanoparticles and with heat treatment	11.3	551
3	Ni-SiC150	Electroless Ni coating with SiC nanoparticles of 150 nm size and without heat treatment	25.1	499
4	$Ni\text{-}SiC150^{HT}$	Electroless Ni coating with SiC nanoparticles of 150 nm size and with heat treatment	11.1	959
5	Ni-SiC700	Electroless Ni coating with SiC nanoparticles of 700 nm size and without heat treatment	27.6	642
6	$Ni\text{-}SiC700^{HT}$	Electroless Ni coating with SiC nanoparticles of 700 nm size and with heat treatment	9.7	832

under the load of 500 g. At least three measurements were made for each sample in order to eliminate possible segregation effects and to obtain a representative value of the material microhardness. Average values are presented in **Table 2.3**.

2.2.3. Nickel coatings with boron nitride (BN) nanoparticles

Four different samples with electroless Ni coatings were investigated: 1) Ni coating without BN nanoparticles and without heat treatment (Ni); 2) Ni coating without BN nanoparticles and with heat treatment ($Ni\text{-}BN^{HT}$); 3) Ni coating with BN nanoparticles and without heat treatment (Ni-BN); 4) Ni coating with BN nanoparticles and with heat treatment ($Ni\text{-}BN^{HT}$). The average size of cubic boron nitride (c-BN) nanoparticles was 10 nm, and its volume concentration was from 5 to 7%. Designations of tested coatings are shown in **Table 2.4**.

Coatings thickness was measured in 5 points on each coating surface, and the average values are shown in **Table 2.4**. Measurements of surface microhardness (HV 0.5) were carried out using Vickers microhardness tester under the load of 500 g. At least three measurements were made for each sample in order to eliminate possible segregation effects and to obtain a representative value of the material microhardness. Average values are presented in **Table 2.4**.

Table 2.4. Designation and thickness of tested coatings

Sample	Designation	Description	Thickness, μm	Microhardness HV 0.5
1	Ni	Electroless Ni coating without nanoparticles and heat treatment	25.6	543
2	Ni^{HT}	Electroless Ni coating without nanoparticles and with heat treatment	11.3	551
3	Ni-BN10	Electroless Ni coating with BN nanoparticles and without heat treatment	23.2	520
4	$Ni\text{-}BN10^{HT}$	Electroless Ni coating with BN nanoparticles and with heat treatment	8.4	545

2.3. Experimental details

In order to investigate various influences on tribological properties (abrasive and erosive wear) of different electroless Ni coatings, two tribological experiments were done with different test equipments. The main goal was to determine the influence of different nanoparticles addition, as well as heat treatment.

In addition to the wear data, the hardness of each of tested materials was determined, as an ancillary mechanical property, to make appropriate correlations. It is well known that hardness of commercially pure metals influences its abrasive wear resistance and that higher hardness implies a higher wear resistance. Khruschov [32] finds out that increase of the wear resistance depends on the way in which the metal is being hardened (alloying, heat treatment or work-hardening) and that in some cases wear resistance decreases with increase of hardness. The results of other researchers also show that abrasive wear resistance of quenched and tempered steels has a much weaker dependency on bulk hardness [33]. The use of hardness as a parameter for predicting the wear behaviour of materials must be done with caution since these characteristics very often are not in correlation [34].

2.3.1. Abrasive wear testing

Abrasive wear tests were carried out on Taber Abraser (**Fig. 2.4**) with a modified standard test conditions (only one abrasive roller was used), in the ambient air at room temperature. The Taber Abraser generates a combination of

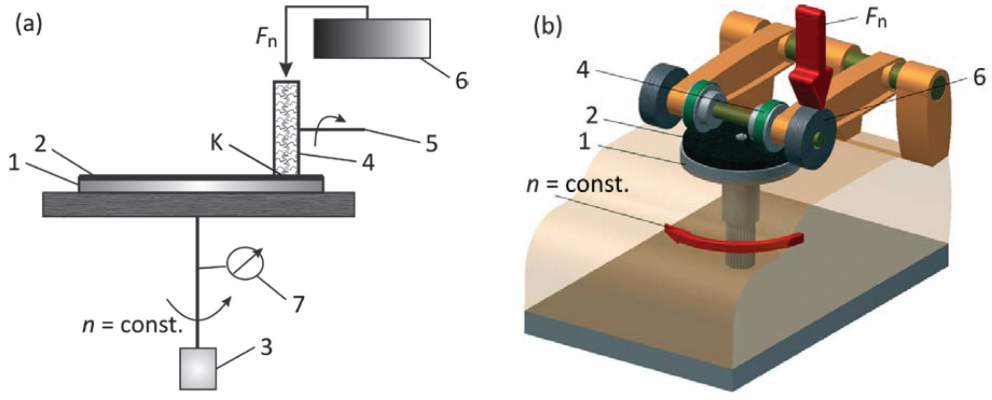

Fig. 2.4. Taber Abraser testing: (a) schematic diagram; and (b) 3D model

sliding and rolling motion and is primarily used for tests under mild abrasion condition [35].

A disc sample (1) of 100 mm diameter and 3 mm thickness with coating (2) is fixed on the horizontal turntable platform, driven with constant rotational speed (n) of 60 rpm by the electric motor (3). Abrasive roller (4), a Taber abrading wheel Calibrase® CS-10, is mounted on horizontal axis (5) and provides through weights (6) the necessary normal load (F_n). Abrasive roller (wheel) is driven by the rotating test sample. The wheels produce abrasion marks that form a pattern of crossed arcs over a circular ring. The width of the worn area (circular ring) is 12.7 mm, with the inner radius of 31.75 mm and outer radius of 44.45 mm. Therefore, the distance between the rotational axis of disc sample (1) and mass centre of the contact area (K) is 38.1 mm, and the worn area is approximately 30 cm^2 [36]. The sliding action between the coated disc sample and abrasive roller is due to the relative motion between them which is characterised by the roller slip. This occurs because the axe of the roller is shifted from the disc sample centre of rotation with the drifting angle of around 30° [37]. Thus, the average tangential (sliding) velocity of the coated disc sample is 0.239 m/s.

Abrasive wear is calculated as a mass loss, i.e. as a difference between the initial mass of the sample and its mass after given number of abrasion cycles (N), counted by the counter (pos. 7 in **Fig. 2.4**). Before and after testing, the coated disc was degreased and cleaned, and its mass is measured by the electronic balance with accuracy of 0.1 mg. Normal load of 250 g (2.45 N) was constant for all tests and coatings. The sliding distance (s) is calculated from the following equation:

$$s = 2r\pi \cdot N, \tag{2.4}$$

where r = 38.1 mm is the distance between the rotational axis of disc sample and mass centre of the contact area, and N is the number of abrasion cycles.

Obtained results of the mass loss are shown as a function of sliding distance, in the form of the comparative wear curves. Wear rate (W) in mg/m is calculated by fitting the wear curves (it is the slope of wear curve), assuming that the steady-state wear was from the beginning of the tests (which is common thing for the abrasive wear). In order of easier comparison of different coatings, a value of relative wear resistance (R) is also introduced (Eq. 2.5). The relative wear resistance (R) is calculated as a ratio of reference sample wear rate (W_y) and wear rate of the analysed sample (W_x), where **x** and **y** denote the designation number of the sample. Relative wear resistance of the reference sample is always R = 1.

$$R_{x,y} = \frac{W_y}{W_x}. \tag{2.5}$$

2.3.2. Erosive wear testing

Erosive wear tests were carried out on jet nozzle type erosion equipment (**Fig. 2.5**) in the ambient air, at room temperature. This testing utilizes repeated gas-entrained solid particle impingement erosion, and involves a small

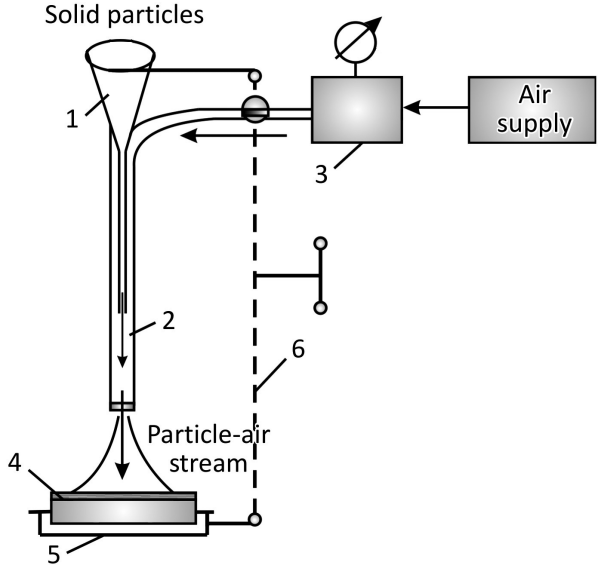

Fig. 2.5. Schematic diagram of erosive wear testing

nozzle delivering a stream of gas containing solid particles which impacts the surface of a test specimen.

Solid particles are poured from the reservoir (1) by freefalling to the nozzle tube (2). Length of the nozzle is 200 mm, diameter is 8 mm, and exit diameter is 6 mm. Before the tests, solid particles material was sieved through a set of sieves and dried in an oven for removal of moisture from the particles. The air stream is provided by the compressed air at controlled pressure, purified from particles and moisture (3). Air stream also enters the nozzle tube (2), where the formation of two-phase (particle-air) working stream takes place. The test sample (4), in the rectangular shape (20 × 25 mm) and 3 mm thickness, is fixed in a holder (5) attached to the reversing mechanism (6). With reversing mechanism (6), two working parameters are controlled: (a) distance of the sample from the nozzle, and (b) impact angle of the particles. Parameters used in the erosive wear testing (solid particles material, maximum size of the particles, air stream pressure, particles flow, particles impact angle, distance between the sample and the nozzle and duration of the test) were the same for all tested coatings (**Table 2.5**).

Erosive wear is calculated as a mass loss, i.e., as a difference between the initial mass of the sample and its mass after the end of test. Before and after testing, the coated sample was degreased and cleaned, and its mass is measured by the electronic balance with accuracy of 0.1 mg. Wear rate (W) is given in mg/min as the mass loss of the sample material divided by the duration of the test. In order of easier comparison of different coatings, a value of relative wear resistance (R) is also introduced (Eq. 2.5). The relative wear resistance (R) is calculated as a ratio of reference sample wear rate (W_y) and wear rate of the analysed sample (W_x), where **x** and **y** denote the designation number of the sample. Relative wear resistance of the reference sample is always R = 1.

Table 2.5. Parameters used in the erosive wear testing

Test parameter	Value
Solid particles material	Black corundum (Al_2O_3)
Maximum size of the particles	600 μm
Air stream pressure	0.1 MPa
Particles flow	166.67 g/min
Particles impact angle	90°
Distance between the sample and the nozzle	10 mm
Duration of the test	3 minutes

2.4. Results and discussion

2.4.1. Nickel coatings with diamond (D) nanoparticles

Abrasive wear: Abrasive wear of the coatings was determined at various number of cycles, i.e., at N = 300, 600, 800 and 1000, and corresponding mass losses are presented in **Table 2.6**. By calculating the linear wear of the coatings (which is not presented), it was confirmed that it was lower than the thickness of all tested coatings.

Using the results from **Table 2.6**, wear curves are constructed and wear rates (*W*) in mg/m are calculated by fitting the wear curves for all tested coatings. The wear curves for coatings without nanoparticles (Ni and Ni^{HT}) are shown in **Fig. 2.6** and for coatings with D nanoparticles (Ni-D4, Ni-$D4^{HT}$, Ni-D100, Ni-$D100^{HT}$, Ni-D200, Ni-$D200^{HT}$, Ni-D250 and Ni-$D250^{HT}$) in **Figs. 2.7** to **2.10**.

The obtained experimental result for coating without heat treatment and nanoparticles correspond to the result obtained by Krishnamoorthy et al. [38]. They used four times higher load and the abrasive wear value after 1000 cycles was also approximately four times higher, i.e., 36.7 mg. These au-

Table 2.6. Abrasive wear of tested coatings

Sample	Coating designation	Number of cycles (N)			
		300	600	800	1000
		Sliding distance, m			
		71.8	143.6	191.5	239.4
		Mass loss, mg			
1	Ni	3.3	5.7	6.6	8.7
2	Ni^{HT}	1.5	2.5	3.3	3.8
3	Ni-D4	3.2	4.7	5.8	7.3
4	Ni-$D4^{HT}$	1.8	3.1	3.6	4.3
5	Ni-D100	0.2	0.9	1.4	1.7
6	Ni-$D100^{HT}$	0.8	1.3	1.6	1.9
7	Ni-D200	2.7	4.7	5.2	5.9
8	Ni-$D200^{HT}$	1.0	2.4	2.6	2.8
9	Ni-D250	0.9	2.4	2.7	3.2
10	Ni-$D250^{HT}$	1.1	1.6	1.9	2.3

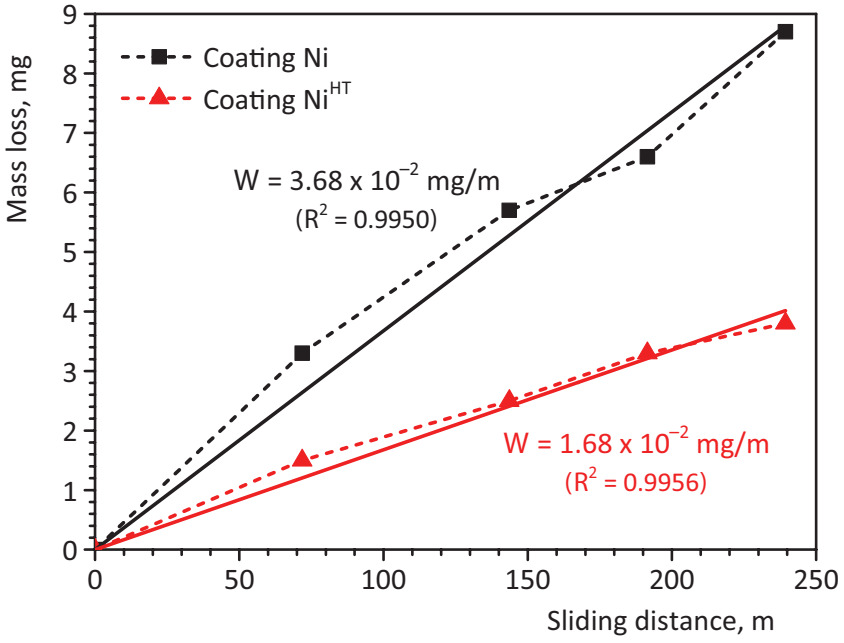

Fig. 2.6. Mass loss vs. sliding distance for coatings without nanoparticles (without and with heat treatment)

thors found that structural changes occurring in the coatings at various heat treatment temperatures, during crystallization process, are very important for the properties of these coatings. They also found that there is optimal heat treatment temperature, below and above which the properties deteriorate. Finding optimal heat treatment temperature is even more difficult for the electroless nickel composite coatings.

Presence of diamond nanoparticles decreases the abrasive wear. The heat treatment also leads to reduction of wear for both version of Ni coating (with and without D nanoparticles). The lowest wear rate of 0.68×10^{-2} mg/m is observed for coating Ni-SiC100, i.e. coating with D nanoparticles of 100 nm size, and without heat treatment. The increase of wear resistance for this coating was approximately 5.37 times in comparison to coating Ni (coating without nanoparticles and heat treatment) which shows the highest wear rate of 3.68×10^{-2} mg/m. The wear process is more stable for coatings without D nanoparticles, which can be seen from the R^2 (R-squared) value. Nevertheless, the influence of imbedded D nanoparticles on wear process stability can be neglected, since generally all R-squared shows acceptable goodness of fit ($R^2 = 1$ is a perfect fit). Presence of short running-in process was noticed for all coatings.

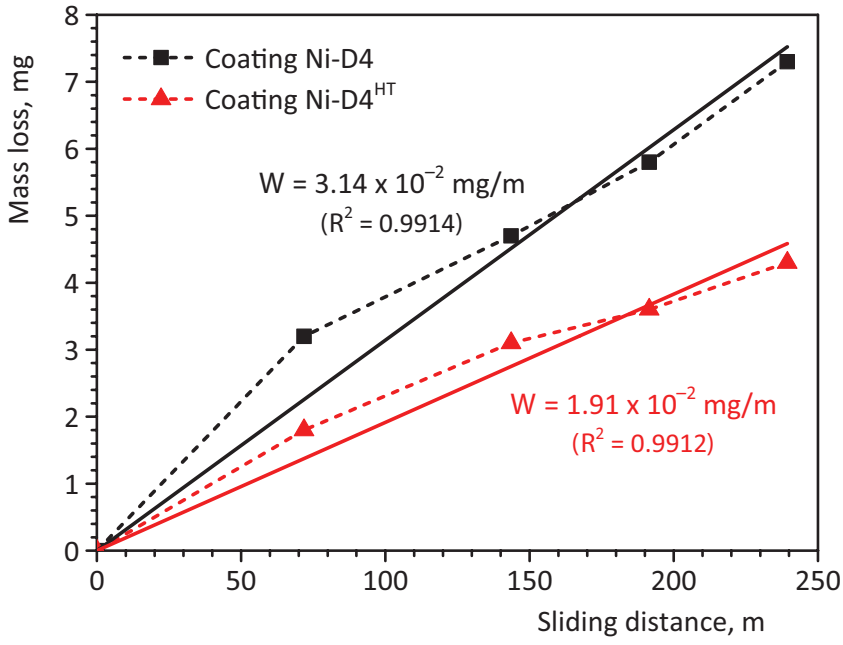

Fig. 2.7. Mass loss vs. sliding distance for coatings with diamond nanoparticles of 4 nm size (without and with heat treatment)

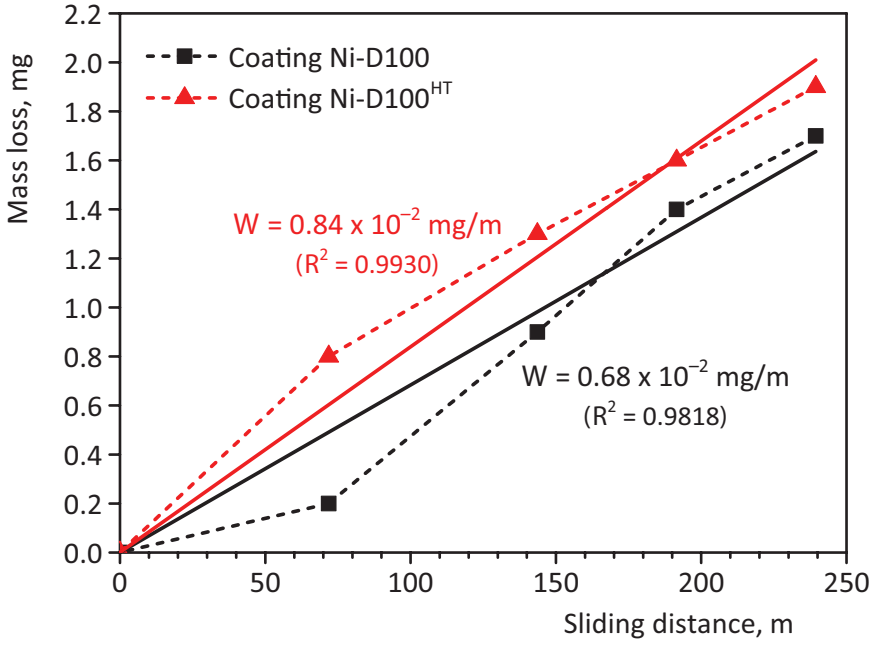

Fig. 2.8. Mass loss vs. sliding distance for coatings with diamond nanoparticles of 100 nm size (without and with heat treatment)

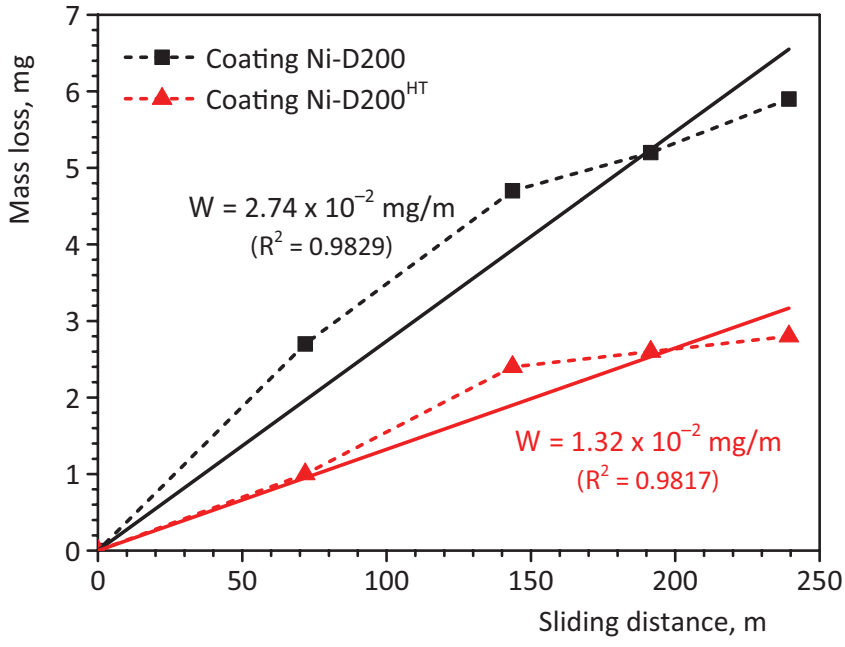

Fig. 2.9. Mass loss vs. sliding distance for coatings with diamond nanoparticles of 200 nm size (without and with heat treatment)

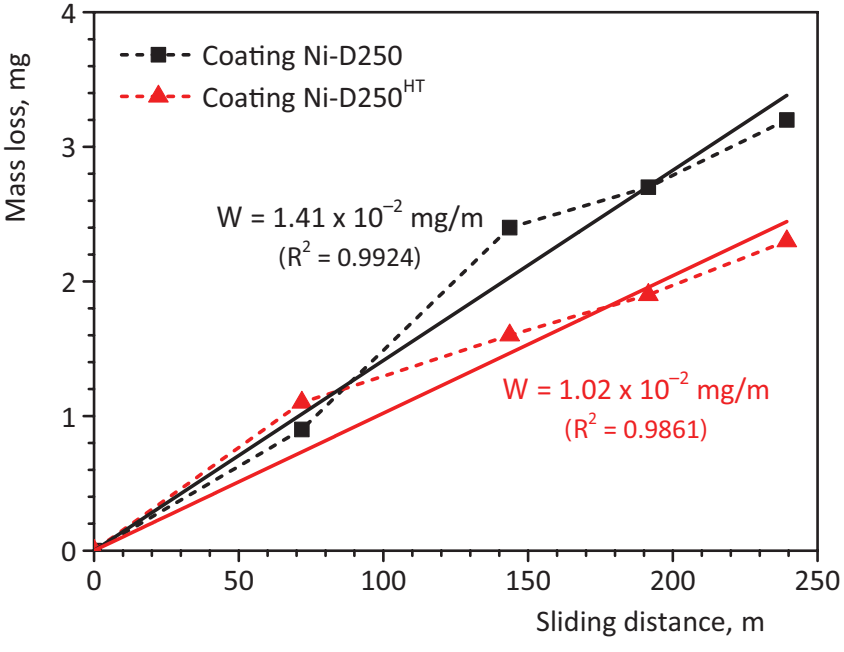

Fig. 2.10. Mass loss vs. sliding distance for coatings with diamond nanoparticles of 250 nm size (without and with heat treatment)

Influences of heat treatment and addition of nanoparticles on the increase of the abrasive wear resistance are analysed separately and together. It was done by comparing the wear rates of tested coatings, and it was expressed by using the relative wear resistance (R). Relative wear resistance (R) was calculated according to the Equation 2.5. In analysing the influence of heat treatment, five coatings without heat treatment (samples 1, 3, 5, 7 and 9) were the reference coatings, with the relative wear resistance R = 1, for the same coatings with heat treatment (samples 2, 4, 6, 8 and 10). In analysing the influence of nanoparticles addition two coatings without nanoparticles (samples 1 and 2) were the reference coatings, with the relative wear resistance R = 1, for the corresponding (with or without heat treatment) coatings with nanoparticles. In analysis of both influences one coating without heat treatment and nanoparticles (sample 1) was the reference coating, with the relative wear resistance R = 1, for all other coatings. Calculated relative wear resistances were presented in **Table 2.7**.

In order to visually perceive the results shown in **Table 2.7**, three diagrams are presented, showing the influence of heat treatment (**Fig. 2.11**),

Table 2.7. Relative wear resistance and the influences of heat treatment and addition of diamond nanoparticles on the increase of abrasive wear resistance of tested coatings

Sample	Coating designation	Wear rate, mg/m	Relative wear resistance (R)		
			Influence of heat treatment	Influence of particles addition	Both influences
1	Ni	3.68×10^{-2}	$R_{1,1} = 1$	$R_{1,1} = 1$	$R_{1,1} = 1$
2	Ni^{HT}	1.68×10^{-2}	$R_{2,1} = 2.19$	$R_{2,2} = 1$	$R_{2,1} = 2.19$
3	Ni-D4	3.14×10^{-2}	$R_{3,3} = 1$	$R_{3,1} = 1.17$	$R_{3,1} = 1.17$
4	$Ni\text{-}D4^{HT}$	1.91×10^{-2}	$R_{4,3} = 1.64$	$R_{4,2} = 0.88$	$R_{4,1} = 1.92$
5	Ni-D100	0.68×10^{-2}	$R_{5,5} = 1$	$R_{5,1} = 5.37$	$R_{5,1} = 5.37$
6	$Ni\text{-}D100^{HT}$	0.84×10^{-2}	$R_{6,5} = 0.82$	$R_{6,2} = 2.00$	$R_{6,1} = 4.38$
7	Ni-D200	2.74×10^{-2}	$R_{7,7} = 1$	$R_{7,1} = 1.34$	$R_{7,1} = 1.34$
8	$Ni\text{-}D200^{HT}$	1.32×10^{-2}	$R_{8,7} = 2.07$	$R_{8,2} = 1.27$	$R_{8,1} = 2.78$
9	Ni-D250	1.41×10^{-2}	$R_{9,9} = 1$	$R_{9,1} = 2.60$	$R_{9,1} = 2.60$
10	$Ni\text{-}D250^{HT}$	1.02×10^{-2}	$R_{10,9} = 1.38$	$R_{10,2} = 1.64$	$R_{10,1} = 3.60$

influence of nanoparticles addition (**Fig. 2.12**), and both influences (**Fig. 2.13**) on the increase of abrasive wear resistance of tested coatings. The analysis of the results shows that the heat treatment principally increases abrasive wear resistance (**Fig. 2.11**). Coatings with heat treatment show average wear resistance increase of 1.62 times, comparing to the same coatings without heat treatment. An exception is coating Ni-D100, which shows lower wear resistance when it is heat treated. This is possibly related to increment of the brittleness of this coating with heat treatment, since fracture processes play an important role in material removal during abrasion of brittle solids [39].

From **Fig. 2.12**, it can be noticed that the influence of nanoparticle addition on abrasive wear resistance was higher than the heat treatment influence. It can also be noticed that the increase of wear resistance becomes bigger as the size of nanoparticles increase. An exception is again coating Ni-D100, regardless the initial treatment condition of the coating (with or without heat treatment). The average wear resistance increase for coatings containing nanoparticles was 2.03 times, comparing to the same coatings without nanoparticles. Combined influences of diamond nanoparticles addition and heat treatment (**Fig. 2.13**) produce the best effect on the abrasive wear resistance increase. Nevertheless, both influences (heat treatment and diamond nanoparticles addition) on abrasive wear resistance increase are significant.

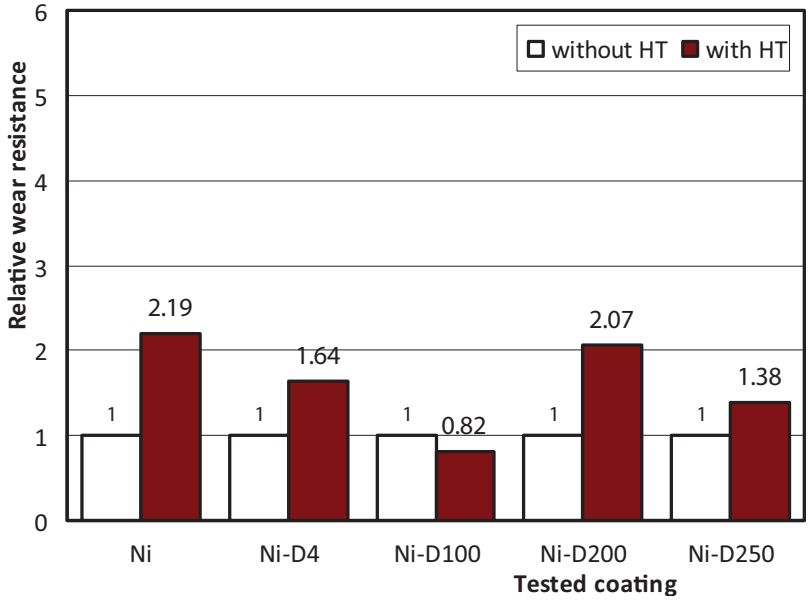

Fig. 2.11. Influence of heat treatment (HT) on the abrasive wear resistance of tested coatings

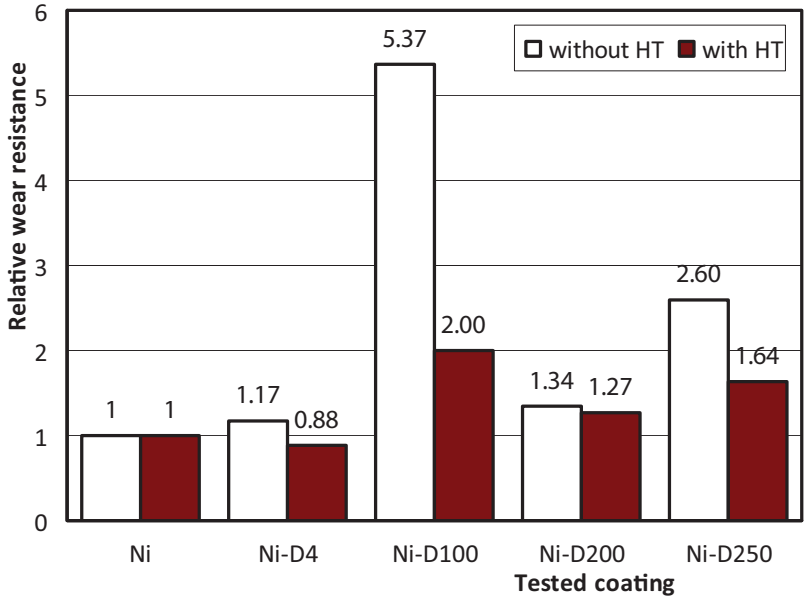

Fig. 2.12. Influence of nanoparticles addition on the abrasive wear resistance of tested coatings

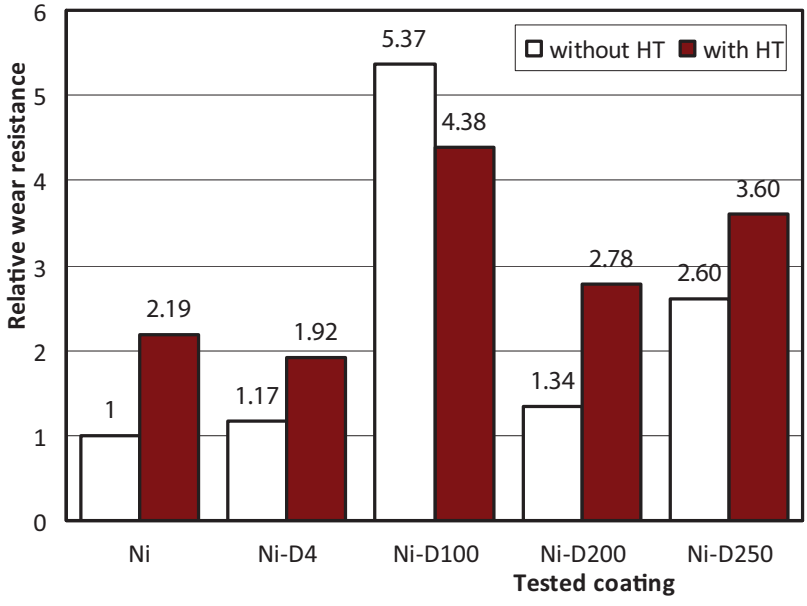

Fig. 2.13. Influence of heat treatment (HT) and nanoparticles addition on the abrasive wear resistance of tested coatings

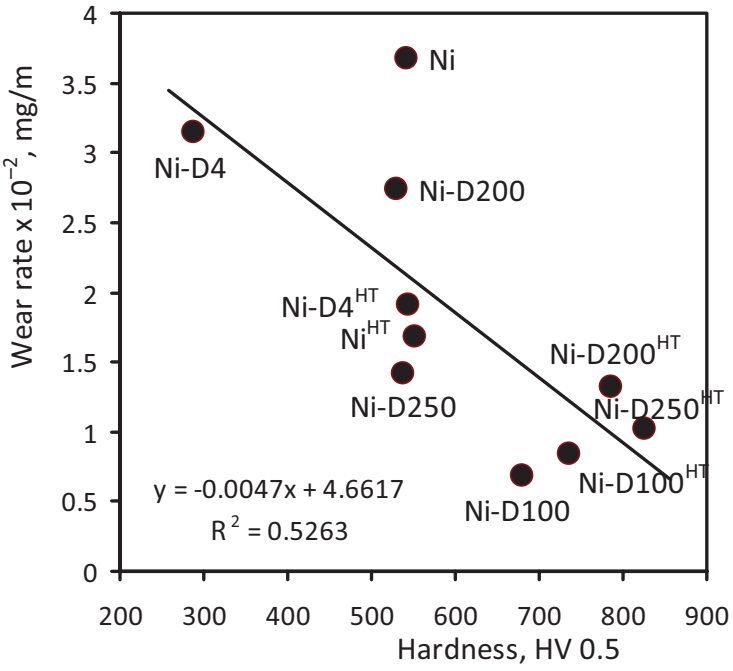

Fig. 2.14. Abrasive wear rate vs. hardness of tested coatings

The relationship between obtained abrasive wear values and hardness (**Table 2.2**) of tested coatings is shown in **Fig. 2.14**. The wear rate generally decreases as hardness increase, as it could be expected, but it is obvious that relationship between the abrasive wear and hardness values is questionable (R^2 value is very low).

Erosive wear: Experimental results for mass loss and calculated wear rate for all tested materials are given in **Table 2.8**. Based on the results given in **Table 2.8**, appropriate diagram is drawn for the dependences of wear rate on diamond nanopatricles size, for coatings without and with heat treatment (**Fig. 2.15**).

The obtained experimental results show that the presence of diamond nanoparticles decreases the erosive wear. Size of the nanoparticles does not show some significant influence, regardless the initial treatment condition of the coating (with or without heat treatment). On the other hand, heat treatment seems to improve wear resistance, since heat treated coating in all cases show lower wear rate than the same coating without heat treatment. The lowest wear rate of 4.17 mg/min shows coating Ni-D200^{HT}, i.e., heat treated coating with nanoparticles of 200 nm size. The increase of wear resistance for this coating was approximately 3.37 times in comparison to coating Ni

Table 2.8. Erosive wear of tested coatings

Sample	Coating designation	Mass before erosion test, g	Mass after erosion test, g	Mass loss, mg	Wear rate, mg/min
1	Ni	6.3321	6.2900	42.1	14.03
2	Ni^{HT}	6.3804	6.3559	24.5	8.17
3	Ni-D4	6.2894	6.2638	25.6	8.53
4	$Ni\text{-}D4^{HT}$	6.2172	6.2036	13.6	4.53
5	Ni-D100	6.2278	6.2073	20.5	6.83
6	$Ni\text{-}D100^{HT}$	6.3535	6.3399	13.6	4.53
7	Ni-D200	6.3000	6.2755	24.5	8.17
8	$Ni\text{-}D200^{HT}$	6.2361	6.2236	12.5	4.17
9	Ni-D250	6.2088	6.1840	24.8	8.27
10	$Ni\text{-}D250^{HT}$	6.2465	6.2325	14.0	4.67

(coating without nanoparticles and heat treatment) which shows the highest wear rate of 14.03 mg/min.

Influences of heat treatment and addition of nanoparticles on the increase of the erosive wear resistance are analysed separately and together. It was done by comparing the wear rates of tested coatings, and it was expressed by using the relative wear resistance (R). Relative wear resistance (R) was calculated according to the Equation 2.5. In analysing the influence

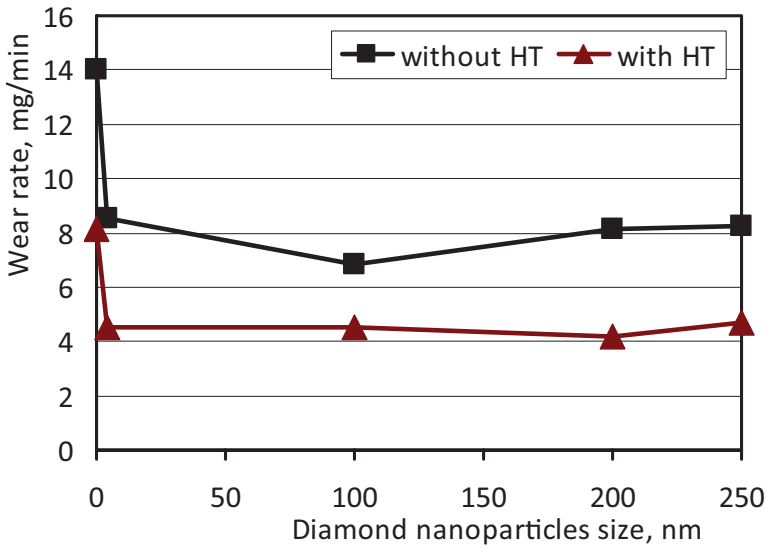

Fig. 2.15. Dependence of erosive wear rate on diamond nanoparticles size

of heat treatment five coatings without heat treatment (samples 1, 3, 5, 7 and 9) were the reference coatings, with the relative wear resistance R = 1, for the same coatings with heat treatment (samples 2, 4, 6, 8 and 10). In analysing the influence of nanoparticles addition two coatings without nanoparticles (samples 1 and 2) were the reference coatings, with the relative wear resistance R = 1, for the corresponding (with or without heat treatment) coatings with nanoparticles. In analysing of both influences one coating without heat treatment and nanoparticles (sample 1) was the reference coating, with the relative wear resistance R = 1, for all other coatings. Calculated relative wear resistances were presented in **Table 2.9**.

In order to visually perceive the results shown in **Table 2.9**, three diagrams are presented, showing the influence of heat treatment (**Fig. 2.16**), influence of nanoparticles addition (**Fig. 2.17**), and both influences (**Fig. 2.18**) on the increase of erosive wear resistance of tested coatings.

The analysis of the results shows that the heat treatment increases erosive wear resistance (**Fig. 2.16**), and that its influence was higher than the nanoparticle addition influence. Coatings with heat treatment show average wear resistance increase of 1.77 times, comparing to the same coatings without heat treatment.

Table 2.9. Relative wear resistance and the influences of heat treatment and addition of diamond nanoparticles on the increase of erosive wear resistance of tested coatings

Sample	Coating designation	Wear rate, mg/min	Relative wear resistance (R)		
			Influence of heat treatment	Influence of particles addition	Both influences
1	Ni	14.03	$R_{1,1} = 1$	$R_{1,1} = 1$	$R_{1,1} = 1$
2	Ni^{HT}	8.17	$R_{2,1} = 1.72$	$R_{2,2} = 1$	$R_{2,1} = 1.72$
3	Ni-D4	8.53	$R_{3,3} = 1$	$R_{3,1} = 1.64$	$R_{3,1} = 1.64$
4	$Ni\text{-}D4^{HT}$	4.53	$R_{4,3} = 1.88$	$R_{4,2} = 1.80$	$R_{4,1} = 3.10$
5	Ni-D100	6.83	$R_{5,5} = 1$	$R_{5,1} = 2.05$	$R_{5,1} = 2.05$
6	$Ni\text{-}D100^{HT}$	4.53	$R_{6,5} = 1.51$	$R_{6,2} = 1.80$	$R_{6,1} = 3.10$
7	Ni-D200	8.17	$R_{7,7} = 1$	$R_{7,1} = 1.72$	$R_{7,1} = 1.72$
8	$Ni\text{-}D200^{HT}$	4.17	$R_{8,7} = 1.96$	$R_{8,2} = 1.96$	$R_{8,1} = 3.37$
9	Ni-D250	8.27	$R_{9,9} = 1$	$R_{9,1} = 1.70$	$R_{9,1} = 1.70$
10	$Ni\text{-}D250^{HT}$	4.67	$R_{10,9} = 1.77$	$R_{10,2} = 1.75$	$R_{10,1} = 3.01$

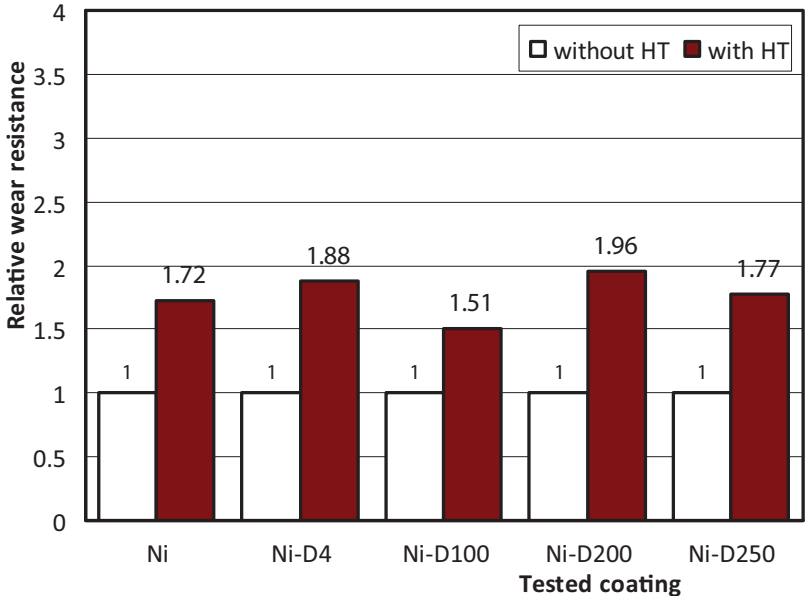

Fig. 2.16. Influence of heat treatment (HT) on the erosive wear resistance of tested coatings

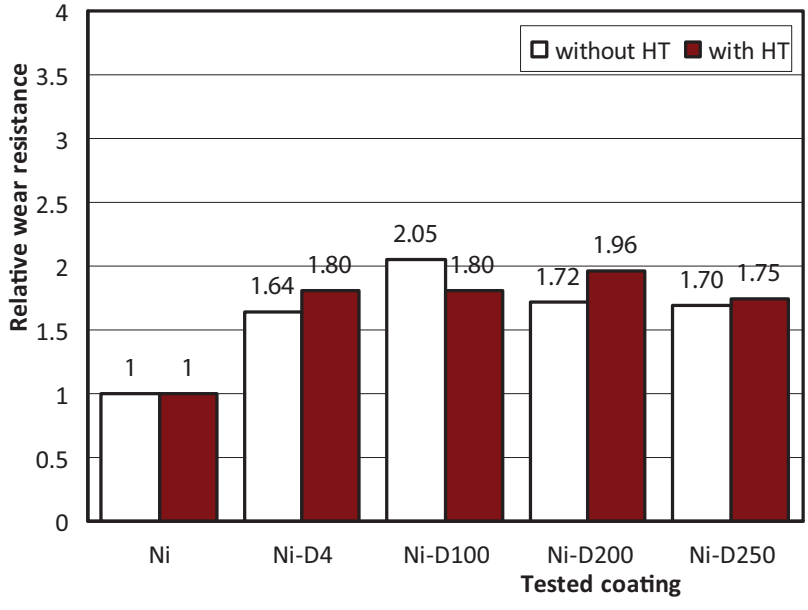

Fig. 2.17. Influence of nanoparticles addition on the erosive wear resistance of tested coatings

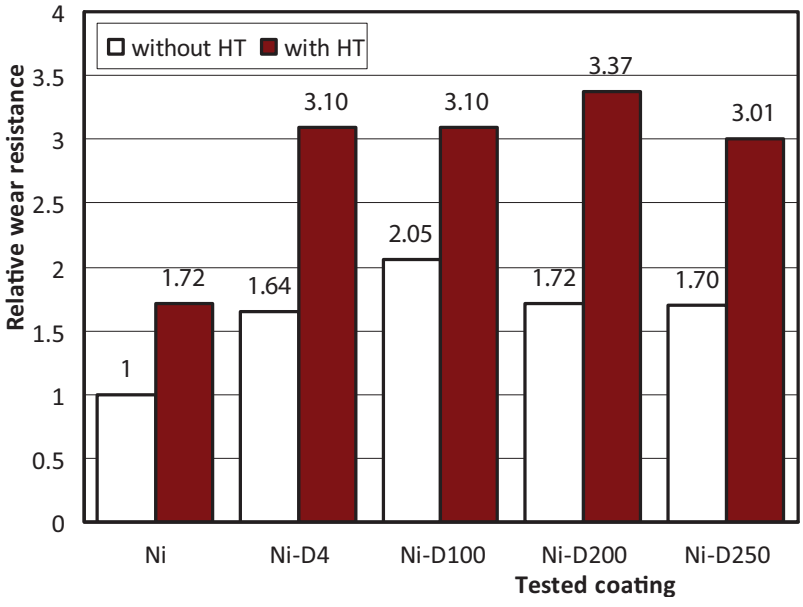

Fig. 2.18. Influence of heat treatment (HT) and nanoparticles addition on the erosive wear resistance of tested coatings

Presence of diamond nanoparticles also increased erosive wear resistance but this increase was less pronounced for all coatings except for coating Ni-D100 (**Fig. 2.17**). This coating also showed lower abrasive wear resistance in heat treated condition (**Fig. 2.12**), which was related to increment of the brittleness. The erosive wear results of this coating could be explained with the nature of coating and testing conditions, since it is well known that brittle materials show the highest erosive wear at particles impact angle close to 90° [40]. The average wear resistance increase for coatings containing nanoparticles was 1.80 times, comparing to the same coatings without nanoparticles. The increase of wear resistance becomes bigger as the size of nanoparticles increase, and after some nanoparticle size (100 nm for coatings without heat treatment, and 200 nm for heat treated coatings) starts to become smaller. This indicates that there is an optimum nanoparticle size for the best erosive wear resistance. Nevertheless, both influences (heat treatment and diamond nanoparticles addition) on erosive wear resistance increase are significant, and their combined influence (**Fig. 2.18**) produce the best effect on the erosive wear resistance increase.

The relationship between obtained erosive wear and abrasive wear values of tested coatings is shown in **Fig. 2.19**. The first feature from **Fig. 2.19**

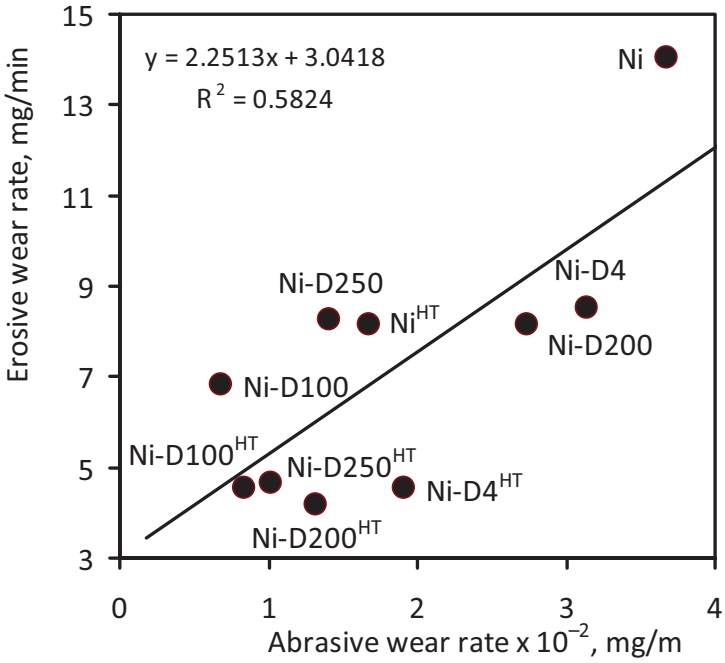

Fig. 2.19. Erosive wear rate vs. abrasive wear rate of tested coatings

is that the erosive and abrasive wear are not in good correlation, since the R-squared (R^2) value is relatively low (R^2 = 0.58).

Both, abrasive and erosive wear resistance depend on many characteristics and cannot be connected only with hardness, especially for composite materials. Further discussion of the obtained results requires additional experimental work and analysis of the microstructure and other mechanical characteristics. In addition, repeatability of the obtained results should be evaluated, i.e., more replicate tests should be run (especially for the erosive wear testing) for all materials in order to achieve a higher confidence level in evaluating test results.

2.4.2. Nickel coatings with silicon carbide (SiC) nanoparticles

Abrasive wear: Abrasive wear of the coatings was determined at various number of cycles, i.e., at N = 300, 600, 800 and 1000, and corresponding mass losses are presented in **Table 2.10**. By calculating the linear wear of the coatings (which is not presented), it was confirmed that it was lower than the thickness of all tested coatings.

Using the results from **Table 2.10**, wear curves are constructed and wear rates (W) in mg/m are calculated by fitting the wear curves for all tested

Table 2.10. Abrasive wear of tested coatings

Sample	Coating designation	Number of cycles (N)			
		300	600	800	1000
		Sliding distance, m			
		71.8	143.6	191.5	239.4
		Mass loss, mg			
1	Ni	3.3	5.7	6.6	8.7
2	Ni^{HT}	1.5	2.5	3.3	3.8
3	Ni-SiC150	2.2	4.5	5.3	6.0
4	Ni-$SiC150^{HT}$	1.4	2.6	3.5	4.2
5	Ni-SiC700	2.0	3.3	4.6	5.1
6	Ni-$SiC700^{HT}$	2.3	3.3	4.1	4.8

coatings. The wear curves for coatings without nanoparticles (Ni and Ni^{HT}) are previously shown in **Fig. 2.6** and for coatings with SiC nanoparticles (Ni-SiC150, Ni-$SiC150^{HT}$, Ni-SiC700 and Ni-$SiC700^{HT}$) in **Figs. 2.20** and **2.21**.

The obtained experimental results show that the heat treatment decreases the abrasive wear, and the decrease was the biggest for the coating

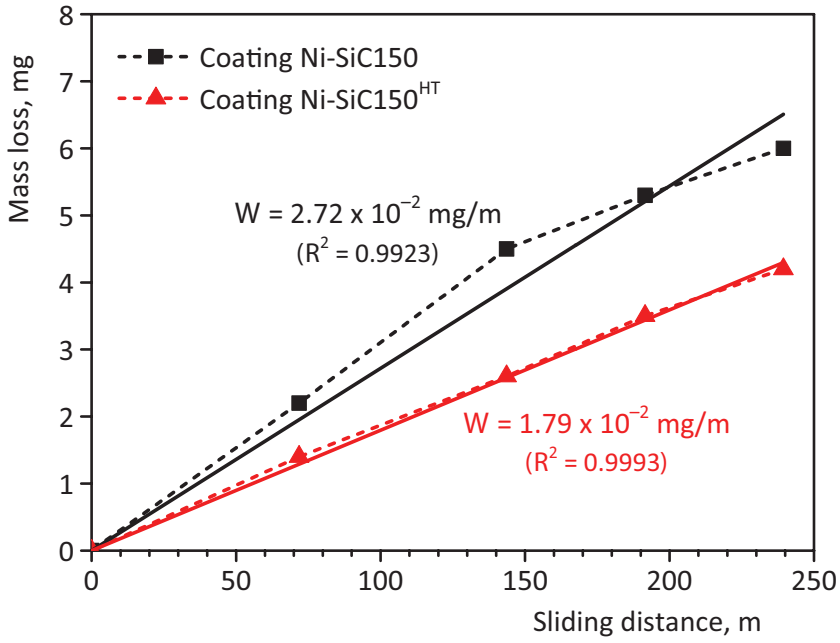

Fig. 2.20. Mass loss vs. sliding distance for coatings with silicon carbide nanoparticles of 150 nm size (without and with heat treatment)

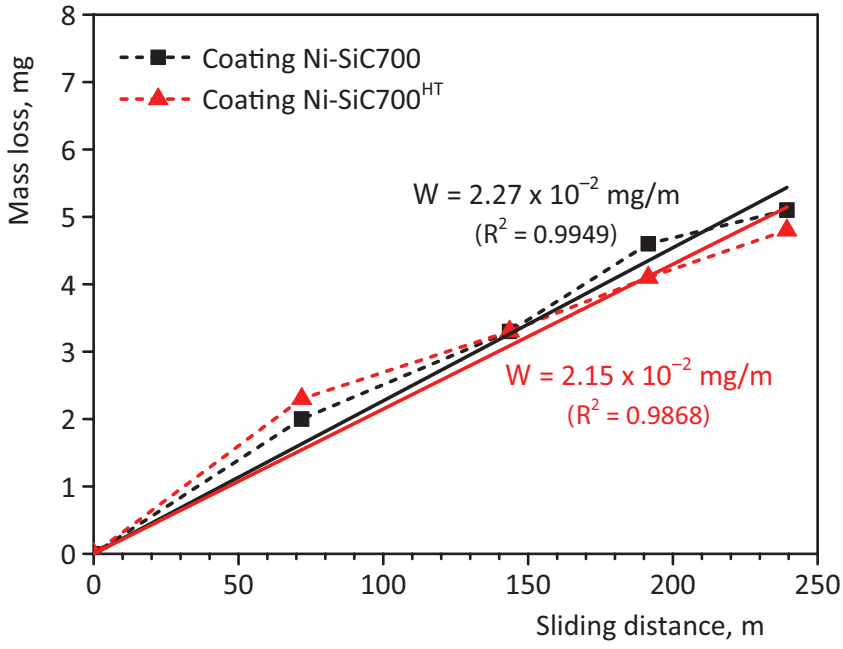

Fig. 2.21. Mass loss vs. sliding distance for coatings with silicon carbide nanoparticles of 700 nm size (without and with heat treatment)

without silicon carbide nanoparticles (coating Ni^{HT}). The influence of heat treatment was lower for coating Ni-$SiC150^{HT}$, and even lower for coating Ni-$SiC700^{HT}$.

Influences of heat treatment and addition of nanoparticles on the increase of the abrasive wear resistance are analysed separately and together. It was done by comparing the wear rates of tested coatings, and it was expressed by using the relative wear resistance (R). Relative wear resistance (R) was calculated according to the Equation 2.5. In analysing the influence of heat treatment three coatings without heat treatment (samples 1, 3 and 5) were the reference coatings, with the relative wear resistance R = 1, for the same coatings with heat treatment (samples 2, 4 and 6). In analysing the influence of nanoparticles addition two coatings without nanoparticles (samples 1 and 2) were the reference coatings, with the relative wear resistance R = 1, for the corresponding (with or without heat treatment) coatings with nanoparticles. In analysing of both influences one coating without heat treatment and nanoparticles (sample 1) was the reference coating, with the relative wear resistance R = 1, for all other coatings. Calculated relative wear resistances were presented in **Table 2.11**.

Table 2.11. Relative wear resistance and the influences of heat treatment and addition of silicon carbide nanoparticles on the increase of abrasive wear resistance of tested coatings

Sample	Coating designation	Wear rate, mg/m	Relative wear resistance (R)		
			Influence of heat treatment	Influence of particles addition	Both influences
1	Ni	3.68×10^{-2}	$R_{1,1} = 1$	$R_{1,1} = 1$	$R_{1,1} = 1$
2	Ni^{HT}	1.68×10^{-2}	$R_{2,1} = 2.19$	$R_{2,2} = 1$	$R_{2,1} = 2.19$
3	Ni-SiC150	2.79×10^{-2}	$R_{3,3} = 1$	$R_{3,1} = 1.35$	$R_{3,1} = 1.35$
4	$Ni\text{-}SiC150^{HT}$	1.79×10^{-2}	$R_{4,3} = 1.51$	$R_{4,2} = 0.93$	$R_{4,1} = 2.05$
5	Ni-SiC700	2.27×10^{-2}	$R_{5,5} = 1$	$R_{5,1} = 1.62$	$R_{5,1} = 1.62$
6	$Ni\text{-}SiC700^{HT}$	2.15×10^{-2}	$R_{6,5} = 1.06$	$R_{6,2} = 0.78$	$R_{6,1} = 1.71$

In order to visually perceive the results shown in **Table 2.11**, three diagrams are presented, showing the influence of heat treatment (**Fig. 2.22**), influence of nanoparticles addition (**Fig. 2.23**), and both influences (**Fig. 2.24**) on the increase of abrasive wear resistance of tested coatings.

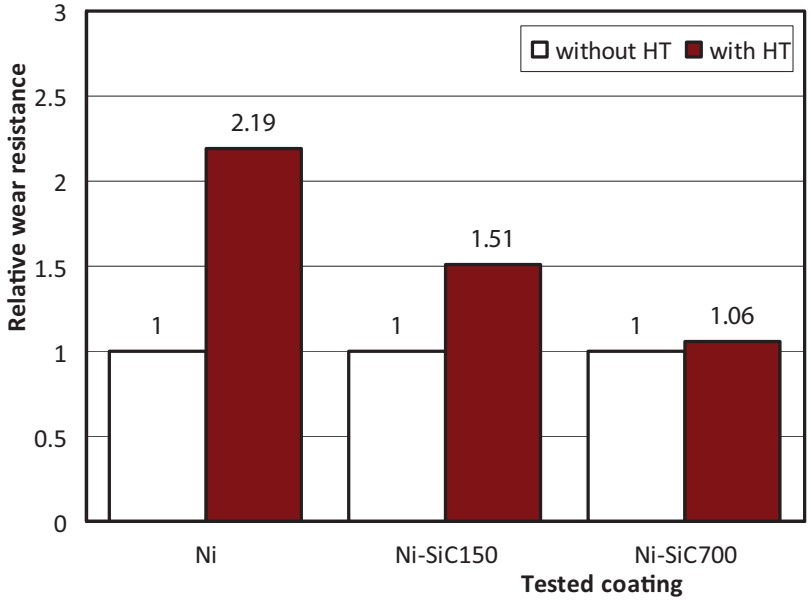

Fig. 2.22. Influence of heat treatment (HT) on the abrasive wear resistance of tested coatings

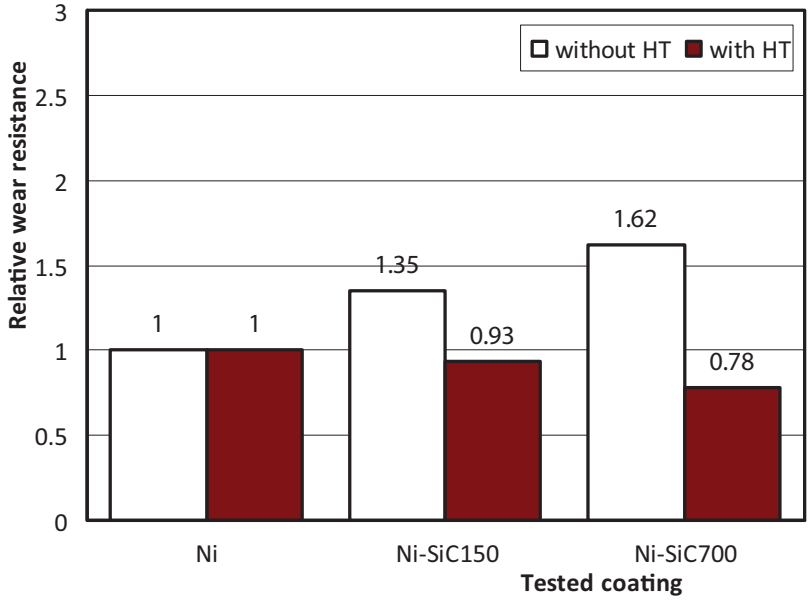

Fig. 2.23. Influence of nanoparticles addition on the abrasive wear resistance of tested coatings

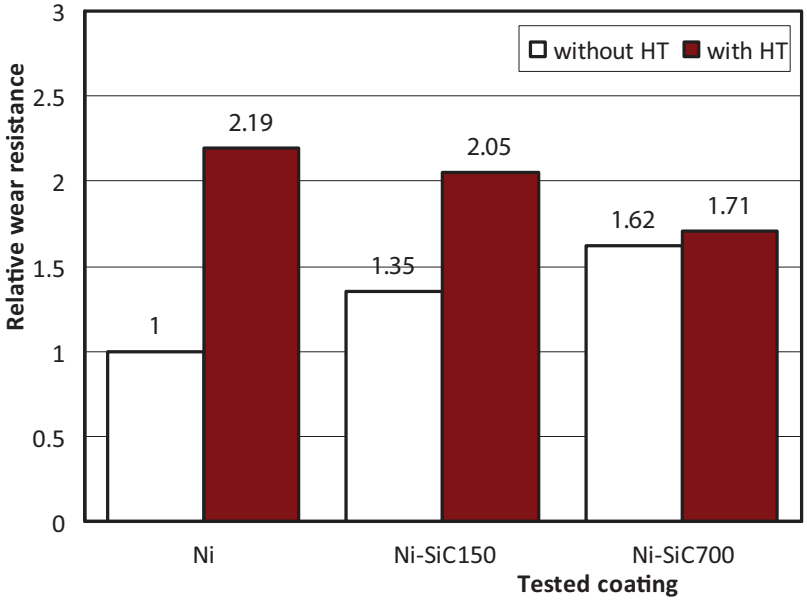

Fig. 2.24. Influence of heat treatment (HT) and nanoparticles addition on the abrasive wear resistance of tested coatings

The analysis of the results shows that the heat treatment principally increases abrasive wear resistance (**Fig. 2.22**), but these increases become lower as silicon carbide nanoparticles are added, and even lower as the size of these nanoparticles become bigger. Coatings with heat treatment show average wear resistance increase of 1.59 times, comparing to the same coatings without heat treatment.

Presence of silicon carbide nanoparticles also leads to increase of abrasive wear resistance, but only for coatings without heat treatment (**Fig. 2.23**). This increase was bigger as the size of these nanoparticles become bigger. The average wear resistance increase for these coatings was 1.49 times, comparing to the same coatings without nanoparticles. As opposed to that, presence of silicon carbide nanoparticles in heat treated coatings leads to decrease of abrasive wear resistance (**Fig. 2.23**). This decrease was bigger as the size of these nanoparticles become bigger. The average wear resistance decrease for these coatings was 0.86 times, comparing to the same coatings without nanoparticles. Combined influence of silicon carbide nanoparticles addition and heat treatment (**Fig. 2.24**) is not favourable, since it leads to the decrease of abrasive wear resistance.

The relationship between obtained abrasive wear values and hardness (**Table 2.3**) of tested coatings is shown in **Fig. 2.25*a***. The wear rate generally decreases as hardness increase, as it could be expected. Exceptions are coatings Ni and Ni^{HT}, i.e. coatings without silicon carbide nanoparticles. Indeed, coatings with SiC nanoparticles (**Fig. 25*b***) showed good correlation, since the R-squared (R^2) value in this case is relatively high (R^2 = 0.93).

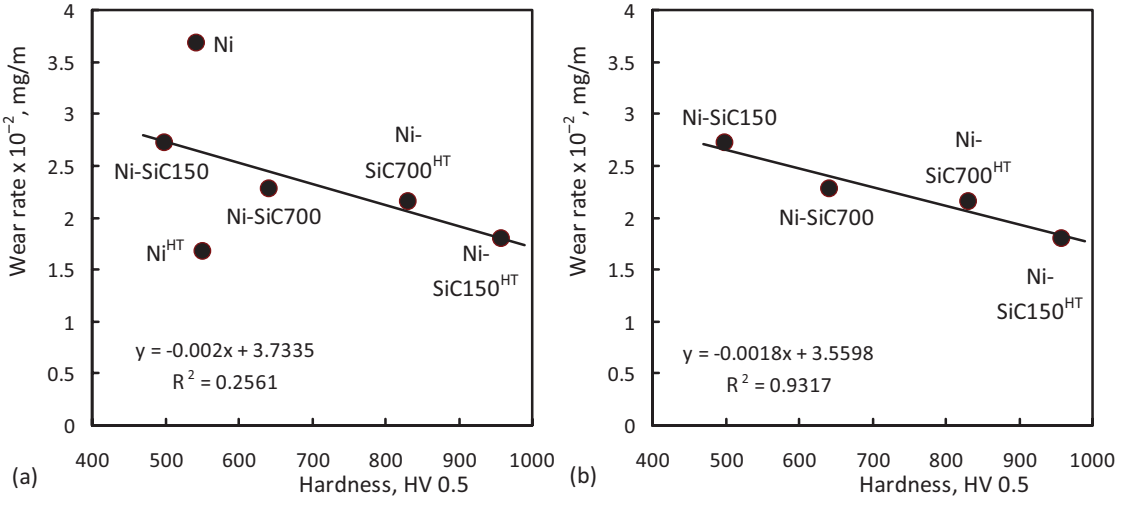

Fig. 2.25. Abrasive wear rate vs. hardness of tested coatings: (a) all catings; and (b) only coatings with SiC nanoparticles

2.4.3. Nickel coatings with boron nitride (BN) nanoparticles

Abrasive wear: Abrasive wear of the coatings was determined at various number of cycles, i.e., at N = 300, 600, 800 and 1000, and corresponding mass losses are presented in **Table 2.12**. By calculating the linear wear of the coatings (which is not presented), it was confirmed that it was lower than the thickness of all tested coatings.

Using the results from **Table 2.12**, wear curves are constructed and wear rates (*W*) in mg/m are calculated by fitting the wear curves for all tested coatings. The wear curves for coatings without nanoparticles (Ni and Ni^{HT}) are previously shown in **Fig. 2.6** and for coatings with BN nanoparticles (Ni-BN10 and Ni-$BN10^{HT}$) in **Fig. 2.26**.

The obtained experimental results show that the presence of boron nitride nanoparticles decreases the abrasive wear. The heat treatment also leads to reduction of wear for both version of Ni coating (with and without BN nanoparticles). The lowest wear rate of 0.83×10^{-2} mg/m is observed for coating Ni-$BN10^{HT}$, i.e., heat treated coating with BN nanoparticles. The increase of wear resistance for this coating was approximately 4.42 times in comparison to coating Ni (coating without nanoparticles and heat treatment) which shows the highest wear rate of 3.68×10^{-2} mg/m. The wear process is stable, since generally all R^2 (R-squared) value shows acceptable goodness of fit ($R^2 = 1$ is a perfect fit).

Influences of heat treatment and addition of nanoparticles on the increase of the abrasive wear resistance are analysed separately and together. It was done by comparing the wear rates of tested coatings, and it was expressed by using the relative wear resistance (R). Relative wear resistance (R) was calculated according to the Equation 2.5. In analysing the influence of

Table 2.12. Abrasive wear of tested coatings

Sample	Coating designation	Number of cycles (N)			
		300	600	800	1000
		Sliding distance, m			
		71.8	143.6	191.5	239.4
		Mass loss, mg			
1	Ni	3.3	5.7	6.6	8.7
2	Ni^{HT}	1.5	2.5	3.3	3.8
3	Ni-BN10	2.0	3.8	4.4	5.5
4	Ni-$BN10^{HT}$	0.2	1.0	1.5	2.3

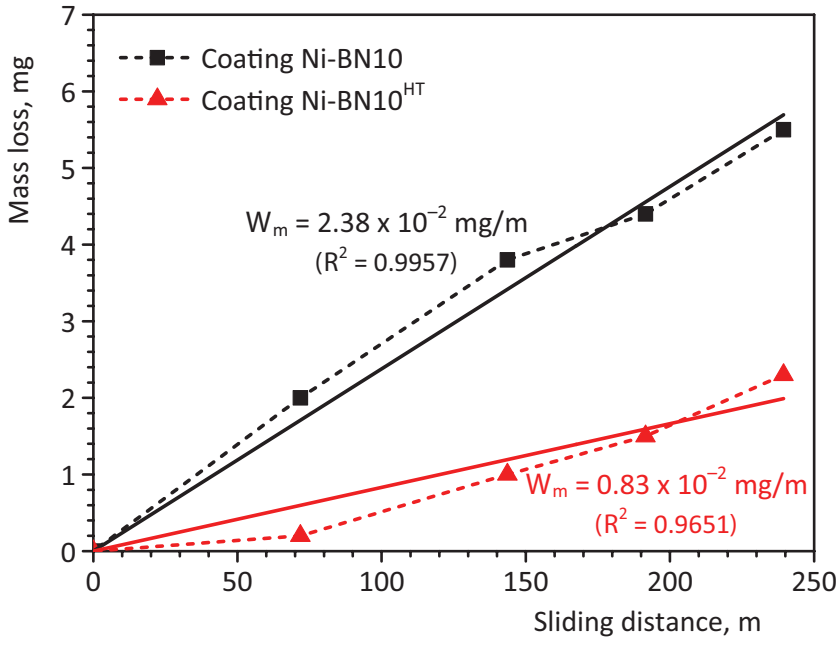

Fig. 2.26. Mass loss vs. sliding distance for coatings with boron nitride nanoparticles of 10 nm size (without and with heat treatment)

heat treatment two coatings without heat treatment (samples 1 and 3) were the reference coatings, with the relative wear resistance R = 1, for the same coatings with heat treatment (samples 2 and 4). In analysing the influence of nanoparticles addition two coatings without nanoparticles (samples 1 and 2) were the reference coatings, with the relative wear resistance R = 1, for the corresponding (with or without heat treatment) coatings with nanoparticles. In analysing of both influences one coating without heat treatment and nanoparticles (sample 1) was the reference coating, with the relative wear resistance R = 1, for all other coatings. Calculated relative wear resistances were presented in **Table 2.13**.

In order to visually perceive the results shown in **Table 2.13**, three diagrams are presented, showing the influence of heat treatment (**Fig. 2.27**), influence of nanoparticles addition (**Fig. 2.28**), and both influences (**Fig. 2.29**) on the increase of abrasive wear resistance of tested coatings.

The analysis of the results shows that the heat treatment increases abrasive wear resistance (**Fig. 2.27**), and that this influence was much higher than the nanoparticle addition influence. Coatings with heat treatment show average wear resistance increase of 2.53 times, comparing to the same coatings without heat treatment.

Table 2.13. Relative wear resistance and the influences of heat treatment and addition of boron nitride nanoparticles on the increase of abrasive wear resistance of tested coatings

Sample	Coating designation	Wear rate, mg/m	Relative wear resistance (R)		
			Influence of heat treatment	Influence of particles addition	Both influences
1	Ni	3.68×10^{-2}	$R_{1,1} = 1$	$R_{1,1} = 1$	$R_{1,1} = 1$
2	Ni^{HT}	1.68×10^{-2}	$R_{2,1} = 2.19$	$R_{2,2} = 1$	$R_{2,1} = 2.19$
3	Ni-BN10	2.38×10^{-2}	$R_{3,3} = 1$	$R_{3,1} = 1.54$	$R_{3,1} = 1.54$
4	$Ni\text{-}BN10^{HT}$	0.83×10^{-2}	$R_{4,3} = 2.86$	$R_{4,2} = 2.02$	$R_{4,1} = 4.42$

Presence of boron nitride nanoparticles also increased wear resistance (**Fig. 2.28**), but this increase was less pronounced than heat treatment influence. The average wear resistance increase for coatings containing nanoparticles was 1.78 times, comparing to the same coatings without nanoparticles. Combined influences of boron nitride nanoparticles addition and heat treatment (**Fig. 2.29**) produce the best effect on the abrasive wear resistance increase. Nevertheless, both influences (heat treatment and boron nitride nanoparticles addition) on abrasive wear resistance increase are significant.

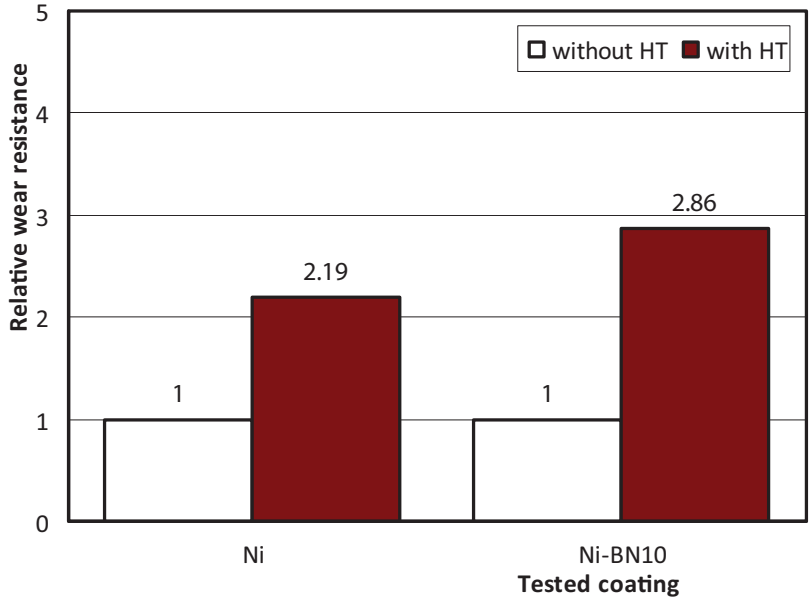

Fig. 2.27. Influence of heat treatment (HT) on the abrasive wear resistance of tested coatings

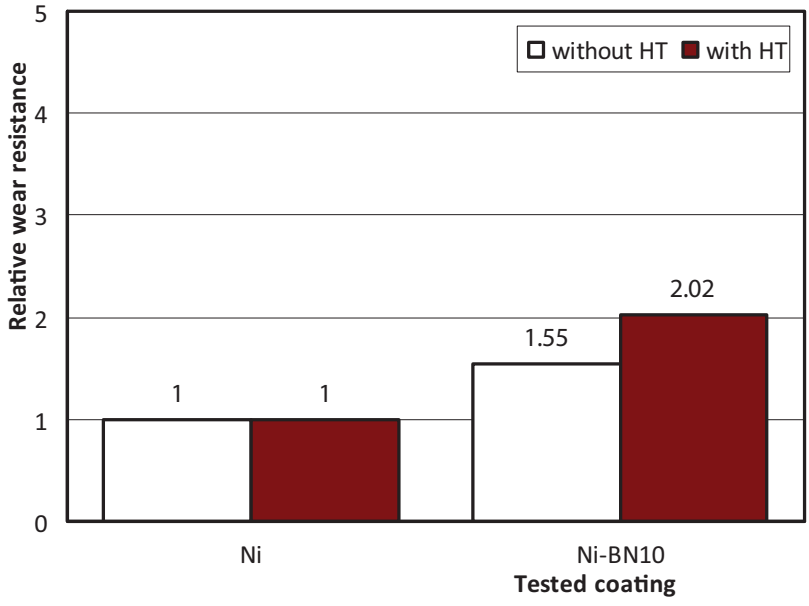

Fig. 2.28. Influence of nanoparticles addition on the abrasive wear resistance of tested coatings

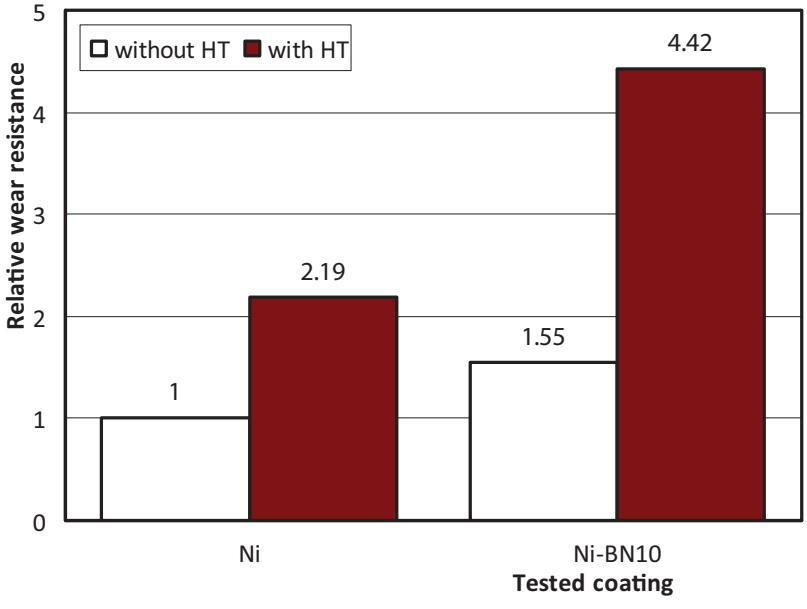

Fig. 2.29. Influence of heat treatment (HT) and nanoparticles addition on the abrasive wear resistance of tested coatings

The relationship between obtained abrasive wear values and hardness (**Table 2.4**) of tested coatings is shown in **Fig. 2.30**. There are no correlation between the wear rate and hardness of coatings (R^2 = 0.06), since coatings had similar values of hardness while its wear rate differ significantly. In addition number of values for the statistical analysis could not be statistically significant.

Erosive wear: Experimental results for mass loss and calculated wear rate for all tested materials are given in **Table 2.14**. The obtained experimental results show that the presence of boron nitride nanoparticles, as well as heat treatment, decreases the erosive wear. As a consequence, the lowest wear rate of 5.40 mg/min shows coating Ni-BN^{HT}, i.e., heat treated coating with boron nitride nanoparticles. The increase of wear resistance for this coating was approximately 2.60 times in comparison to coating Ni (coating without nanoparticles and heat treatment) which shows the highest wear rate of 14.03 mg/min.

Influences of heat treatment and addition of nanoparticles on the increase of the erosive wear resistance are analysed separately and together. It was done by comparing the wear rates of tested coatings, and it was expressed by using the relative wear resistance (R). Relative wear resistance (R)

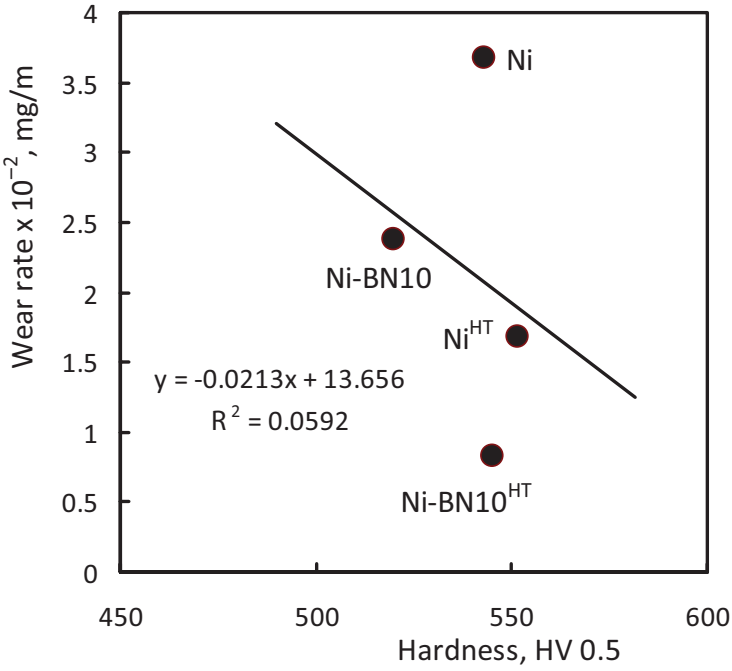

Fig. 2.30. Abrasive wear rate vs. hardness of tested coatings

Table 2.14. Erosive wear of tested coatings

Sample	Coating designation	Mass before erosion test, g	Mass after erosion test, g	Mass loss, mg	Wear rate, mg/min
1	Ni	6.3321	6.2900	42.1	14.03
2	Ni^{HT}	6.3804	6.3559	24.5	8.17
3	Ni-BN	6.2203	6.1819	38.4	12.80
4	$Ni\text{-}BN^{HT}$	6.2263	6.2101	16.2	5.40

was calculated according to the Equation 2.5. In analysing the influence of heat treatment two coatings without heat treatment (samples 1 and 3) were the reference coatings, with the relative wear resistance R = 1, for the same coatings with heat treatment (samples 2 and 4). In analysing the influence of nanoparticles addition two coatings without nanoparticles (samples 1 and 2) were the reference coatings, with the relative wear resistance R = 1, for the corresponding (with or without heat treatment) coatings with nanoparticles. In analysing of both influences one coating without heat treatment and nanoparticles (sample 1) was the reference coating, with the relative wear resistance R = 1, for all other coatings. Calculated relative wear resistances were presented in **Table 2.15**.

In order to visually perceive the results shown in **Table 2.15**, three diagrams are presented, showing the influence of heat treatment (**Fig. 2.31**),

Table 2.15. Relative wear resistance and the influences of heat treatment and addition of boron nitride nanoparticles on the increase of erosive wear resistance of tested coatings

Sample	Coating designation	Wear rate, mg/min	Relative wear resistance (R)		
			Influence of heat treatment	Influence of particles addition	Both influences
1	Ni	14.03	$R_{1,1} = 1$	$R_{1,1} = 1$	$R_{1,1} = 1$
2	Ni^{HT}	8.17	$R_{2,1} = 1.72$	$R_{2,2} = 1$	$R_{2,1} = 1.72$
3	Ni-BN	12.80	$R_{3,3} = 1$	$R_{3,1} = 1.10$	$R_{3,1} = 1.10$
4	$Ni\text{-}BN^{HT}$	5.40	$R_{4,3} = 2.37$	$R_{4,2} = 1.51$	$R_{4,1} = 2.60$

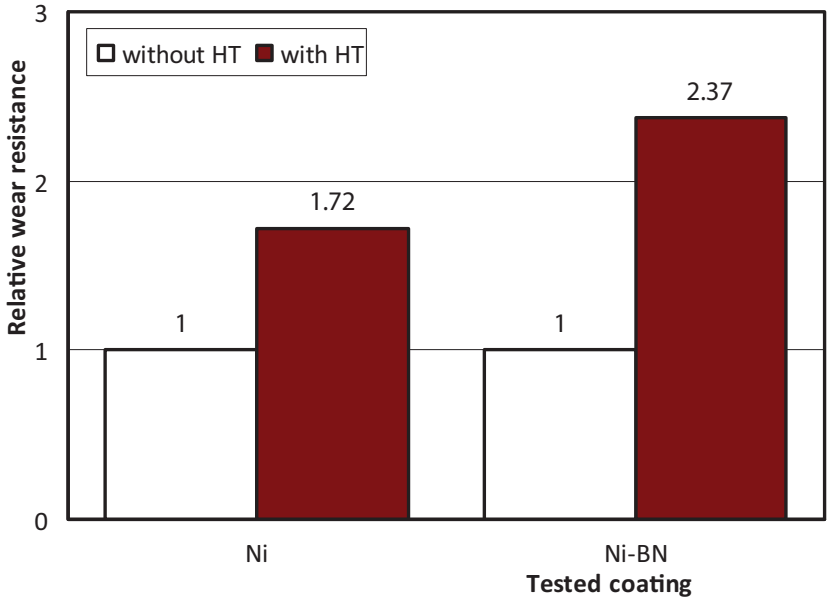

Fig. 2.31. Influence of heat treatment (HT) on the erosive wear resistance of tested coatings

influence of nanoparticles addition (**Fig. 2.32**), and both influences (**Fig. 2.33**) on the increase of erosive wear resistance of tested coatings.

The analysis of the results shows that the heat treatment increases erosive wear resistance (**Fig. 2.31**), and that its influence was higher than the nanoparticle addition influence. Coatings with heat treatment show average wear resistance increase of 2.04 times, comparing to the same coatings without heat treatment.

On the other hand, presence of boron nitride nanoparticles also increased wear resistance but this increase was less pronounced (**Fig. 2.32**). The average wear resistance increase for coatings containing nanoparticles was 1.30 times, comparing to the same coatings without nanoparticles. Combined influences of boron nitride nanoparticles addition and heat treatment (**Fig. 2.33**) produce the best effect on the erosive wear resistance increase.

The relationship between obtained erosive wear and abrasive wear values of tested coatings is shown in **Fig. 2.34**. The first feature from Figure 2.34 is that the erosive and abrasive wear are in good correlation, since the R-squared (R^2) value is relatively high (R^2 = 0.89). This proofs that hardness was not the best parameter for predicting the tribological parameters of these coatings, even for the materials intend to be used in hard conditions

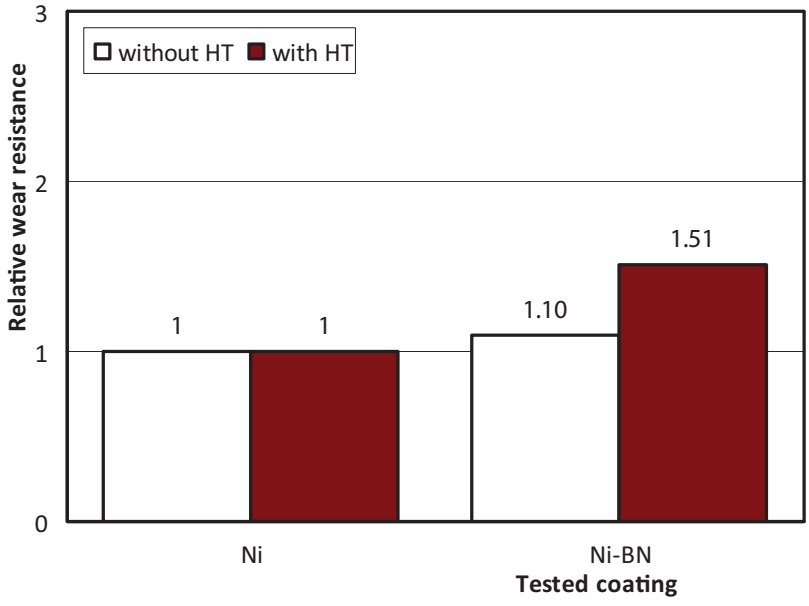

Fig. 2.32. Influence of nanoparticles addition on the erosive wear resistance of tested coatings

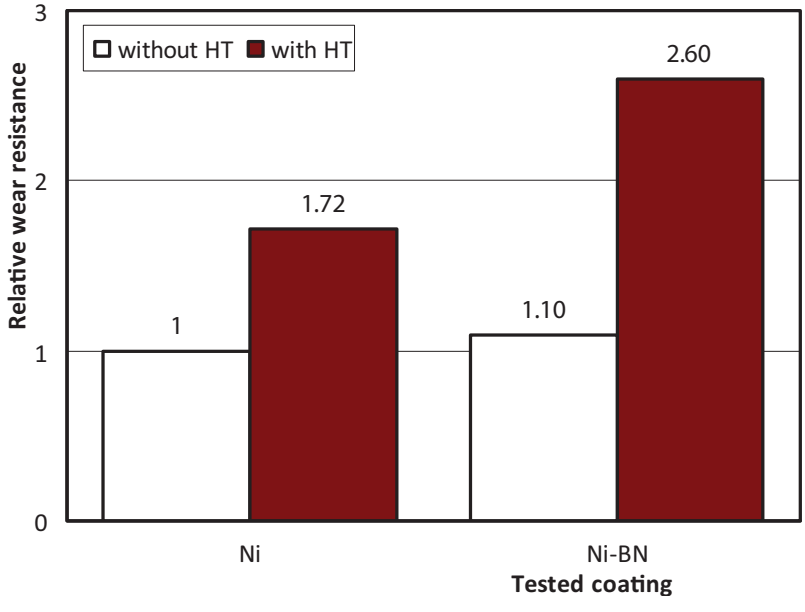

Fig. 2.33. Influence of heat treatment (HT) and nanoparticles addition on the erosive wear resistance of tested coatings

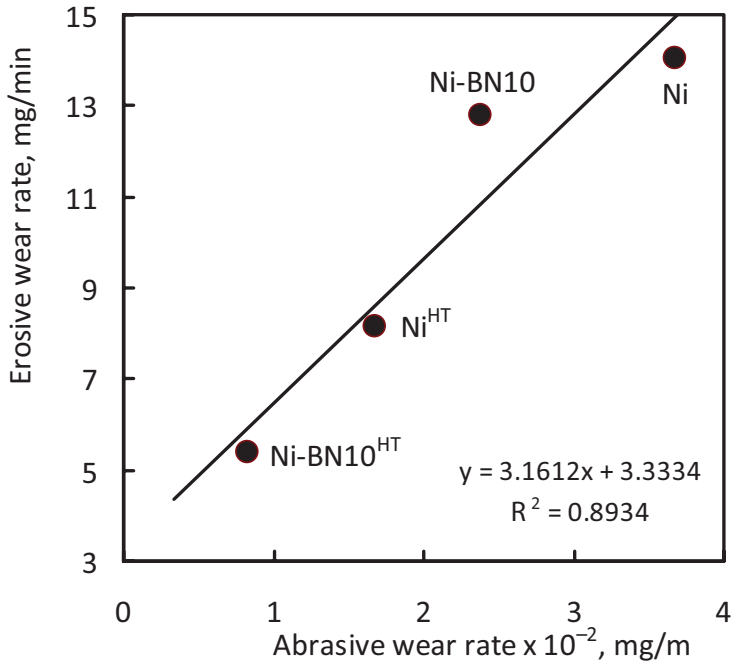

Fig. 2.34. Erosive wear rate vs. abrasive wear rate of tested coatings

with dominant abrasive and erosive wear mechanism. **Fig. 2.34** is a good representation of the influence of heat treatment and/or nanoparticles addition on the resistance to wear in hard conditions of tested coatings. Addition of boron nitride nanoparticles improve wear resistance; wear resistance is even more improved with the heat treatment, and the best wear resistance is obtained when these two influences are combined, i.e., when the coating have imbedded nanoparticles and it is heat treated.

2.5. Conclusions

Many influences should be concerned in projecting the tribological properties of the composite coatings. Some of the important are the reinforcements (its type, shape, dimension, distribution and amount) and applied heat treatment. For every specific application and working conditions, there is an optimal value. Tribological properties (abrasive and erosive wear) of various electroless nickel composite coatings with nanoparticles were investigated. Three different types of nanoparticles (diamond, silicon carbide and boron nitride), in the same volume concentration and different sizes, were incorporated in the

nickel coatings. The same heat treatment was applied to all samples in order to investigate its influence on abrasive and erosive wear resistance. All composite coatings were compared with nickel coating without nanoparticles.

Heat treatment principally increased abrasive and erosive wear resistance of nickel coatings with diamond (D) nanoparticles. The abrasive wear resistance increase was approximately 1.62 times, and erosive wear resistance approximately 1.77 times, comparing to the same coatings without heat treatment. Presence of diamond nanoparticles also increased abrasive and erosive wear resistance of nickel coatings. The average abrasive wear resistance increase was 2.03 times, and average erosive wear resistance increase was 1.80 times, comparing to the same coatings without nanoparticles. Combined influences of diamond nanoparticles addition and heat treatment produce the best effect on the abrasive and erosive wear resistance increase. Generally, but with some exceptions, the increase of abrasive and erosive wear resistance becomes bigger as the size of diamond nanoparticles increase. General rule that harder coating have higher abrasive and erosive wear resistance is valid, but the relationship between abrasive and erosive wear values and hardness of tested coatings is not linear. Therefore, hardness could not be the appropriate parameter for abrasive or erosive wear resistance of these coatings.

Nickel coatings with silicon carbide (SiC) nanoparticles showed the lowest abrasive wear resistance increase comparing with coatings reinforced with diamond (D) and boron nitride (BN) nanoparticles. Heat treatment increased abrasive wear resistance by approximately 1.59 times, but this increase becomes lower as the size of silicon carbide nanoparticles increase. Presence of silicon carbide nanoparticles also increased abrasive wear resistance, by approximately 1.49 times, but only for coatings without heat treatment. This increase was bigger as the size of these nanoparticles become bigger. As a consequence, combined influence of silicon carbide nanoparticles addition and heat treatment for these coatings is not favourable, since it generally decreases abrasive and erosive wear resistance. The relationship between obtained abrasive wear values and hardness is more or less linear and, as it could be expected, the abrasive wear rate generally decreases as hardness increase.

Heat treatment increased abrasive and erosive wear resistance of nickel coatings with boron nitride (BN) nanoparticles. The abrasive wear resistance increase was approximately 2.53 times, and erosive wear resistance approximately 2.04 times, comparing to the same coatings without heat treatment. Presence of boron nitride nanoparticles also increased abrasive and erosive wear resistance of nickel coatings, but this increase was less pronounced than

heat treatment influence. The average abrasive wear resistance increase was 1.78 times, and average erosive wear resistance increase was 1.30 times, comparing to the same coatings without nanoparticles. Combined influences of boron nitride nanoparticles addition and heat treatment produce the best effect on the abrasive and erosive wear resistance increase. Correlation of any kind between obtained abrasive wear values and hardness of tested coatings could not be established, since coatings had similar values of hardness while their wear rates differ significantly. On the other hand, relationship between obtained erosive wear and abrasive wear values of tested coatings is almost linear, i.e. they are in good correlation. This proofs that hardness was not the best parameter for predicting the tribological parameters of these coatings.

References to Chapter 2

[1] **Schlesinger, M.** Electroless deposition of nickel. – In: M. Schlesinger, M. Paunovic (Eds.), *Modern Electroplating.* Hoboken: John Wiley & Sons, 2010, pp. 447-458.

[2] **Mallory, G. O.** The fundamental aspects of electroless nickel plating. – In: G. O. Mallory, J. B. Hajdu (Eds.), *Electroless Plating: Fundamentals and Applications.* Norwich, Noyes Publications/William Andrew Publishing, 1990, pp. 1-56.

[3] **Ponce de León, C., C. Kerr, F. C. Walsh.** Electroless plating for protection against wear. – In: B.G. Mellor (Ed.), *Surface Coatings for Protection against Wear*. Cambridge, Woodhead Publishing, 2006, pp. 184-225.

[4] **Parkinson, R.** Properties and applications of electroless nickel. *Nickel Development Institute Technical Series, 1997, Paper 10081*.

[5] **Olberding, W.** An introduction to electrodeposition and electroless plating processes. – In: F.-W. Bach, A. Laarmann, T. Wenz (Eds.), *Modern Surface Technology*. Weinheim, WILEY-VCH Verlag, 2006, pp. 101-118.

[6] **Gillespie, P.** Electroless nickel coatings: Case study. – In: J. S. Burnell-Gray, P. K. Datta (Eds.), *Surface Engineering Casebook: Solutions to Corrosion and Wear-Related Failures.* Cambridge, Woodhead Publishing, 1996, pp. 49-72.

[7] **Weil, R., K. Parker.** The properties of electroless nickel. – In: G.O. Mallory, J.B. Hajdu (Eds.), *Electroless Plating: Fundamentals and Applications*, Noyes Publications/William Andrew Publishing, Norwich, 1990, pp. 111-137.

[8] **Kennedy, F. E., U. J. Gibson**. Tribological surface treatments and coatings. – In: E. Richard Booser (Ed.), *Tribology Data Handbook: An Excellent Friction, Lubrication, and Wear Resource*, CRC Press, Boca Raton, 1997, pp. 581-593.

[9] **Feldstein, M. D.** The environmental benefits of composite electroless nickel coatings. – *Products Finishing*, Vol. 66, 2002, No 11, pp. 52-56.

[10] **Baudrand, D. W.** (Rev.). Electroless nickel plating. – In: *ASM Handbook, Vol. 5, Surface Engineering*, ASM International, Metals Park, 1994, pp. 290-310.

[11] **Morcos, B., M. Barnstead.** Electroless nickel plating. – *Products Finishing*, Vol. 75, 2011, No 5, pp. 44-48.

[12] **Colaruotolo, J., D. Tramontana.** Engineering applications of electroless nickel. – In: G. O. Mallory, J. B. Hajdu (Eds.), *Electroless Plating: Fundamentals and Applications*. Norwich: Noyes Publications/William Andrew Publishing, 1990, pp. 207-227.
[13] **Ploof, L.** Electroless nickel composite coatings. – *Advanced Materials & Processes*, Vol. 166, 2008, No 5, pp. 36-38.
[14] **Feldstein, N.** Composite electroless plating. – In: G. O. Mallory, J. B. Hajdu (Eds.), *Electroless Plating: Fundamentals and Applications*. Norwich: Noyes Publications/William Andrew Publishing, 1990, pp. 269-287.
[15] **Balaraju, J. N. T. S. N. Sankara Narayanan, S. K. Seshadri.** Electroless Ni-P composite coatings. – *Journal of Applied Electrochemistry*, Vol. 33, 2003, No 9, pp. 807-816.
[16] **Oswald, T. A., J. P. Hernández-Ortiz.** *Polymer Processing: Modelling and Simulation*. Munich: Carl Hanser Verlag, 2006.
[17] **Frydel, J., D. Mewes, S. Luther, R.H. Schuster.** Rubber sheets calendering: Contribution to preventing the occurrence of gas entrapments. – *Kautschuk, Gummi, Kunststoffe*, Vol. 61, 2008, No 6, pp. 286-293.
[18] **Karastoyanov, D., T. Penchev, G. Gavrilov.** Coating with nano components for renovating of extrusing shafts. – *Problems of Engineering Cybernetics and Robotics*, Vol. 63, 2011, pp. 49-57.
[19] **Karastoyanov, D., V. Monov.** An advanced technology for renovation of extruding shafts. – *International Journal of Mechanical, Aerospace, Industrial, Mechatronic and Manufacturing Engineering*, Vol. 7, 2013, No 8, pp. 1679-1682.
[20] **Kaleicheva, J., Z. K. Karaguiozova, E. Lyubchenko, M. Kandeva, V. Mishev, S. Stavrev.** Composite Ni-nanodiamond coating deposited by electroless method. – *Journal of Chemistry and Chemical Engineering*, Vol. 6, 2012, No 7, pp. 599-603.
[21] **Kandeva, M., D. Karastoianov, B. Ivanova, V. Pojidaeva.** Influence of nano-diamond particles on the tribological characteristics of nickel chemical coatings. – *Tribology in Industry*, Vol. 36, 2014, No 2, pp. 181-187.
[22] **Kandeva, M., D. Karastoyanov, A. Andonova.** Tribology of nanostructured nickel chemical coatings. – *Problems of Engineering Cybernetics and Robotics*, Vol. 64, 2011, pp. 52-59.
[23] **Kandeva, M., D. Karastoyanov, A. Andonova.** Wear and tribotermal effects of nanostructured nickel chemical coatings. – *Applied Mechanics and Materials*, Vol. 157-158, 2012, pp. 960-963.
[24] **Kandeva, M., D. Karastoyanov, B. Ivanova, A. Dimitrova, Y. Sofronov, N. Nikolov.** Friction and wear of Ni coatings with nanosize particles of SiC. – *Proceedings of 5th World Tribology Congress (WTC 2013)*, Turin (Italy), 08-13.09.2013, Paper 1241.
[25] **Кандева, М., Д. Карастоянов, А. Венцл.** Ерозийно износване на никелови покрития с наноразмерни частици от силициев карбид (Erosion wear of nickel coatings with nano-size particles of silicon carbide). – *Tribological Journal BULTRIB*, Vol. 3, 2013, pp. 264-271.

[26] **Vencl, A., K. Jakimovska, B. Ivanova, J. Ruzic, S. Simeonov, M. Kandeva.** Static and kinetic friction of electroless Ni composite coatings. – *Journal of Achievements in Materials and Manufacturing Engineering*, Vol. 70, No 1, 2015, pp. 13-21.

[27] **Kandeva, M., A. Vencl, E. Assenova, D. Karastoyanov, T. Grozdanova.** Abrasive wear of chemical nickel coatings with boron nitride nano-particles. – *Proceedings of 11th International Conference in Manufacturing Engineering THE "A" Coatings*, Thessaloniki (Greece), 01-03.10.2014, pp. 319-325.

[28] **Гаврилов, Г., Ц. Николов.** *Химическо никелиране и дисперсни покрития* (*Chemical Nickel Deposition and Disperse Coatings*). София: Техника, 1985.

[29] **Бучков, Д.** *Научни изследвания, технологии, съоръжения, производство, промишлени услуги* (*Scientific Research, Technology, Equipment, Manufacturing, Industrial Service*). София: Технически университет – София, 2011.

[30] **Karaguiozova, Z., S. Stavrev, T. Babul, A. Ciski.** Influence of cubic nanostructured additions on the properties of electroless coatings. – *International Journal of Nanomanufacturing*, Vol. 5, 2010, No 1-2, pp. 129-138.

[31] **Карагьозова, З. К.** *Микро- и наноструктурни композитни никелови покрития, отложени по безтоков метод* (*Micro- and Nanostructured Composite Nickel Coatings Deposited by Electroless Method*). PhD Thesis, Faculty of Industrial Technology. Sofia: Technical University of Sofia, 2014.

[32] **Khruschov, M. M.** Resistance of metals to wear by abrasion, as related to hardness. – In: *Proceedings of International Conference on Lubrication and Wear*, London (UK), 01-03.10.1957, pp. 654-658.

[33] **Sundararajan, G.** The differential effect of the hardness of metallic materials on their erosion and abrasion resistance. – *Wear*, Vol. 162-164, 1993, No B, pp. 773-781.

[34] **Vencl, A., N. Manić, V. Popovic, M. Mrdak.** Possibility of the abrasive wear resistance determination with scratch tester. – *Tribology Letters*, Vol. 37, 2010, No 3, pp. 591-604.

[35] **Franek, F., E. Badisch, M. Kirchgaßner.** Advanced methods for characterisation of abrasion/erosion resistance of wear protection materials. – *FME Transactions*, Vol. 37, 2009, No 2, pp. 61-70.

[36] http://www.taberindustries.com/taber-rotary-abraser (Accessed: 28.12.2015).

[37] **Csanády, E., E. Magoss, L. Tolvaj.** *Quality of Machined Wood Surfaces. – Springer International*. Cham, Switzerland, 2015.

[38] **Krishnamoorthy, P. R. B. H. Narayana, T. V. Ramakrishna, M. Shekhar Kumar.** Properties of electroless nickel-phosphorus deposits after crystallization. – *Metal Finishing*, Vol. 90, 1992, No 11, pp. 13-17.

[39] **Moore, M. A., F. S. King.** Abrasive wear of brittle solids. – *Wear*, Vol. 60, 1980, No 1, pp. 123-140.

[40] **Stachowiak, G.W., A.W. Batchelor.** – *Engineering Tribology*. Amsterdam: Elsevier, 2014, pp. 525-576.

Chapter 3

FERROUS-BASED COATINGS HARDFACED BY GAS METAL ARC WELDING (GMAW)

3.1. Introduction

Hardfacing by gas metal arc welding (**GMAW**) technique belongs to the arc welding group, and externally provided shielding gas subgroup. In hardfacing by arc welding, the heat from an electric arc is used to melt the coating material onto the substrate surface. The electric arc is developed by impressing a voltage between an electrode and the substrate. The voltage required to sustain the arc varies with the distance between the electrode and substrate and with the arc welding technique. The coating (filler) material is provided by the electrode used to form the arc or can be externally introduced into the arc. Arc welding processes in which the filler derives directly from the electrode are sometimes referred to as consumable electrode processes. Arc welding processes in which the filler is externally introduced into the arc are sometimes referred to as nonconsumable electrode processes. As a rule, nonconsumable electrode processes are accomplished at lower power requirements than are consumable electrode processes, resulting in less dilution and lower deposition rates [1]. Consumable and nonconsumable electrode hardfacing processes both require that the filler materials be protected from oxidation as they are melted and joined to the substrate surface.

GMAW sometimes referred to by its subtypes metal inert gas (**MIG**) welding or metal active gas (**MAG**) welding is a consumable electrode hard-

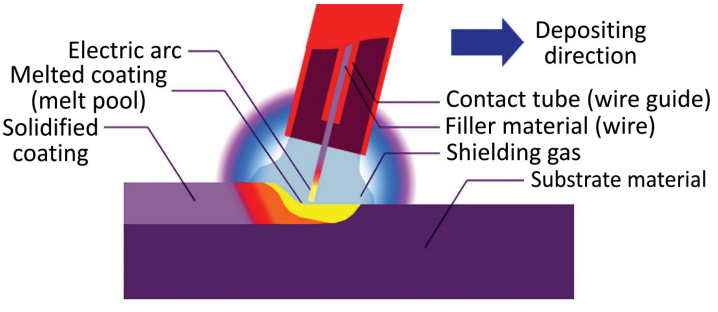

Fig. 3.1. Schematic drawing of the hardfacing by gas metal arc welding (GMAW) technique

facing process in which the filler material and substrate surface are protected by a flowing shielding gas (carbon dioxide, argon, or helium), either singly or in combination with a small amount of oxygen (**Fig. 3.1**). Shielding is provided by an externally supplied shielding gas. MIG welding means the use of an inert (i.e. non active) gas, and MAG welding requires the use of an active gas (i.e. carbon dioxide and oxygen).

The deposition rates are generally high (0.9-5 kg/h). Minimum coating thickness is 1.6 mm, and deposit efficiency is 90-95%. The dilution range is wide (10-40%) and depends on the applied technique and used gas for shielding, so the obtained hardness of the coatings are also in wide range [1]. Required hardness can be obtained in the first layer already (**Fig. 3.2**).

Gas-metal arc hardfacing wires can be deposited in either spray-arc or short-arc modes. The spray-arc mode produces a continuous stream of droplets about the same diameter as the hardfacing wire. Deposition rates are high, as is dilution. To avoid deformation of the part, cracking, warping, or other heat damage, a GMAW deposition is typically applied with a short-arc mode (sometimes called "skip" hardfacing). In this process, material is applied in short intervals along the surface to be coated, leaving equal spaces of uncoated substrate. These uncoated areas are then coated during a second

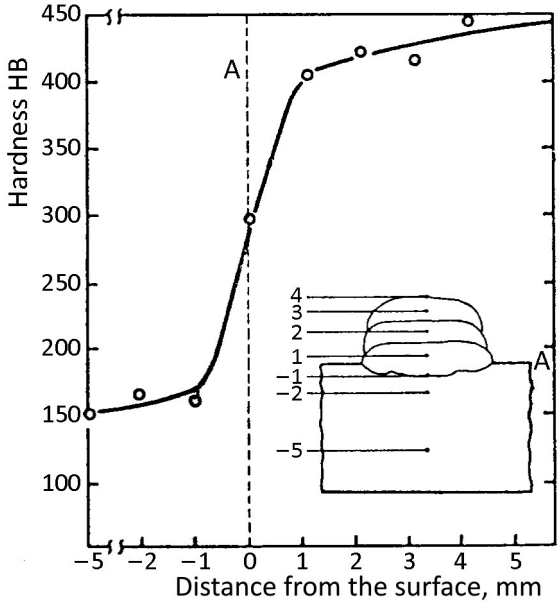

Fig. 3.2. Hardness variation as a function of distance from the hardfaced surface (MIG; hardfacing; shielding gas: Ar + O_2; substrate: steel X6 CrNiTi 18-10; filler material: Co-Cr-W)

pass across the substrate. In the short-arc mode, lower voltages are used, and there are less dilution compared with spray-arc mode.

Hardfacing by GMAW technique is one of the most widely used. The advantage of hardfacing by GMAW is that it is suitable for semiautomatic hardfacing, and the versatility of the process lends itself to the hardfacing of complex shapes. In addition, coating is visible at all times, thereby enabling high-quality deposits. Another advantage is that since it uses shielding gas, there is no slag and no slag removal is required (faster cleanup). On the other hand, disadvantages of GMAW are: relatively high dilution in spray-arc mode, the equipment is expensive and non-portable, and the use of auxiliary shielding gases adds to the cost of hardfacing by GMAW. However, the higher cost is generally offset by the higher coating quality associated with GMAW.

This chapter considers solutions for the regeneration (repair or build-up coatings) of equipment used in road construction, agricultural and mining industry, which are exposed to heavy-duty operating conditions, under the impact loads in abrasive and corrosive environment. The presented results consider optimisation of the deposition parameters for various ferrous-based coatings, based on the minimization of the mechanical treatment (machining) of the obtained coatings through the selected geometrical parameters. After the optimisation, wear resistance of the obtained coatings were investigated and analysed. The idea of the researches was to compare different coatings according to their wear resistance under conditions of abrasive wear, and under conditions of abrasive wear induced vibrations (vibro-abrasive wear). In addition, influences of normal load and vibration velocity were also investigated.

3.2. Materials

3.2.1. Chemical compositions

The substrate material for all coatings was a low-carbon steel, with chemical composition shown in **Table 3.1**. Hardness of the substrate was between 193.6 and 219.5 HV.

Five different commercial coating (filler) materials from different manufacturers have been used in experiments, and their chemical compositions are shown in **Table 3.2**.

Table 3.1. Chemical composition (wt. %) of the coated material (substrate)

Element	C	Si	Mn	Ni	P	S	Cr	Fe
Percentage	0.15	0.21	0.8	0.30	0.011	0.025	0.30	Balance

Table 3.2. Designation, form and chemical composition (wt. %) of the coating (filler) materials

Coating (filler) material		Element, wt. %							
Designation	Product form	C	Cr	Mn	Mo	W	Si	Nb	Fe
UTP DUR 350	Covered electrode	0.2	1.8	1.4	–	–	1.2	–	Balance
EH 550	Covered electrode	0.50	9.00	0.40	–	–	2.40	–	Balance
LNM 420FM	Solid wire	0.5	9.0	0.4	–	–	3.0	–	Balance
Fluxofil 58	Cored wire	0.45	5.50	1.60	0.60	–	0.60	–	Balance
Wearshield 70	Covered electrode	4.2	18	–	8.5	7.0	2.7	9.0	Balance

UTP DUR 350 is the commercial brand names of *Böhler Welding* (covered electrode EN 14700 E Fe1). It is particularly suited for wear resistant hardfacing on Mn-Cr-V alloyed parts, such as frogs, track rollers, chain support rolls, sprocket wheels, guide rolls, etc. This coating has a very good resistance against compression and rolling strain in combination with slight abrasion [2].

EEH 550 is covered electrode of the unknown manufacturer, which is very similar to UTP DUR 600, a commercial brand names of Böhler Welding (covered electrode EN 14700 E Fe8). UTP DUR 600 is universally applicable for cladding on parts of steel, cast steel and high Mn steel, subject simultaneously to abrasion, impact and compression. Typical application fields are the earth moving and stone treatment industry, e.g. excavator teeth, bucket knives, crusher jaws and cones, and mill hammers, but also for cutting edges on cold cutting tools [2].

LNM 420FM is the commercial brand name of *Lincoln Electric* (solid wire EN 14700 S Fe8). Typical applications are for wear resistant hardfacing of dies, parts for agricultural machinery, transport rolls and sand pumps. This coating has a high resistance against corrosion, abrasion and impact deformation [3].

Fluxofil 58 is the commercial brand name of *Oerlikon* (cored wire EN 14700 T Fe8). This Cr-Mo alloyed wire has high abrasion resistance and is suitable for hardfacing of wear parts, such as excavator parts, scraper blades, dipper teeth, worm conveyors, beaters, crusher jaws, crusher cones, screw conveyors, mixer blades, and plough tips, subjected to heavy wear. The weld metal is tough, free of cracks and therefore resistant to shock and impact [4].

Wearshield 70 is the commercial brand name of *Lincoln Electric* (covered electrode EN 14700 E Fe16). It is a highly alloyed electrode that produces carbide coatings. Typical microstructure of these coatings consists mainly of chromium carbides with other carbides of molybdenum, niobium, tungsten and vanadium in an austenite-carbide eutectic matrix. It is designed for ap-

plications of high stress abrasion (crushing of abrasive particles), severe abrasion and abrasion at elevated temperatures (> 760 °C). Typical applications include: augers, cement crushers, furnace chains, screw conveyors, etc. [3].

3.2.2. Optimisation of the deposition parameters and deposition conditions

Dilution of the coating (filler) material in hardfacing, among others, depends on the chosen hardfacing parameters, which are numerous. **Table 3.3** details the effect of some of the hardfacing parameters on dilution.

Four different parameters were varied in the optimisation of the deposition parameters, i.e., current intensity (amperage), electric power (voltage), deposition speed, and electrode extension. These parameters also in-

Table 3.3. The effect of hardfacing parameters on dilution [5, 6]

Parameter	Change in variable	Influence of change on dilution
Amperage and/or current density	Lower	Decreases
Electrode polarity	Direct current electrode negative	Decreases
	Direct current electrode positive	Increases
	Alternating current	Intermediate
Arc length	Greater	Decreases
Electrode diameter	Smaller	Decreases
Electrode extension (for consumable electrode processes)	Higher (longer)	Decreases
Filler metal feed rate	Higher	Decreases
Bead spacing or pitch (overlapping)	More overlap	Decreases
Electrode oscillation	Greater width and/or frequency of electrode oscillation	Decreases
Travel speed (deposition speed)	Lower	Decreases
Hardfacing position	Vertical up (forehand welding)	Highest
	Downhill	Higher
	Uphill	Lower
	Vertical up (backhand welding)	Lowest
Shielding medium	More	Decreases

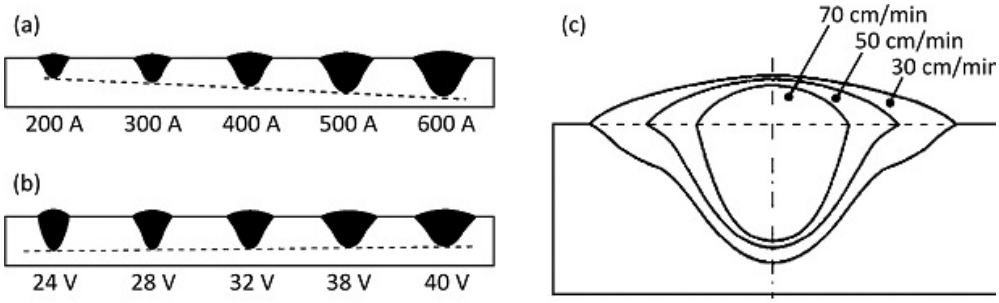

Fig. 3.3. Influence of different deposition parameters on shape and geometry of the hardfaced coating: (a) influence of amperage, (b) influence of voltage, and (c) influence of deposition speed

fluence the shape and geometry of the hardfaced coating, and characterize the efficiency and quality of the hardfacing repair process. With increased amperage the arc becomes hotter, it penetrates more deeply, and more base metal melting occurs, so the dilution is increased (**Fig. 3.3a**). Electric power (voltage) has low influence on penetration depth and dilution, but affects significantly the geometry, i.e., weld bead width (**Fig. 3.3b**). Higher power values are more suitable for hardfacing. A decrease in travel (deposition) speed decreases the amount of base material melted and increases the amount of filler material added per unit time or distance (feed rate), thus decreasing dilution. This reduction in dilution is brought about by the change in bead shape and thickness (**Fig. 3.3c**) and by the fact that the arc force is expended on the weld pool rather than the base metal. A longer electrode extension decreases dilution by increasing the melting rate of the electrode (Joule heating, $P = I^2R$) and diffusing the energy of the arc that impinges base material.

Optimisation of the deposition parameters was directed toward minimization of the mechanical treatment (machining) of the obtained coatings. For that purpose three geometrical parameters were analysed, i.e., hardfacing cap height (H) and width (B) and limit tolerance for mechanical treatment ($H - h$), as shown in **Fig. 3.4**. Optimal deposition parameters were obtained after a full factorial experiment which is described elsewhere [7-9].

Equipment used for coatings deposition is presented in **Fig. 3.5**. All coatings were deposited by hardfacing in a multiple pass (three layers). The deposition of the filler materials, to produce the corresponding coatings, is done with the deposition speed of 0.6 m/min (5 rpm) and electric current of 210 A and 21.5 V. Electrode extension was 16 mm. Shielding (protecting) gas was a two-component mixture comprising 83% argon and 17% carbon dioxide.

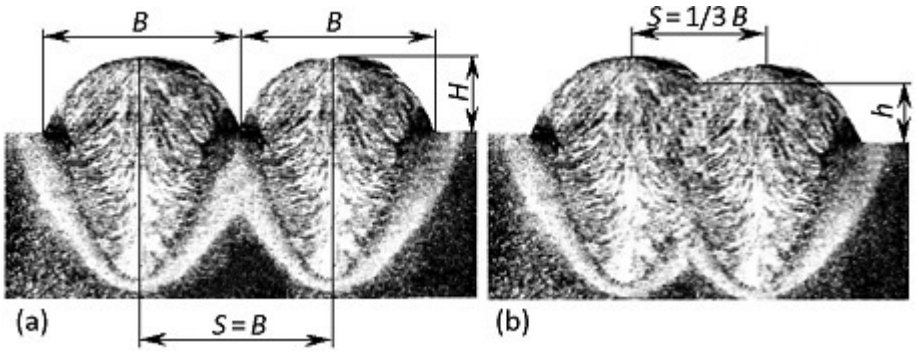

Fig. 3.4. Geometrical parameters of the GMAW coatings: (a) without overlapping, and (b) with overlapping [7]

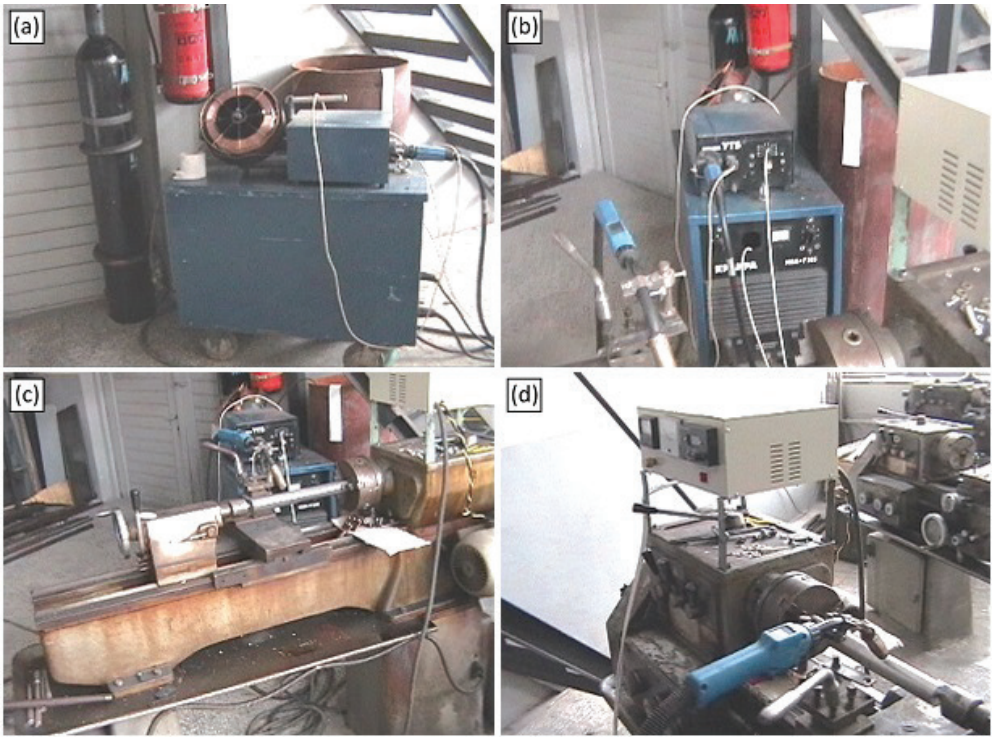

Fig. 3.5. Equipment utilized in the coatings deposition: (a) power supply, (b) wire feeder (УТ5), (c) substrate holder (lathe), and (d) device for electronic control of lathe speed and gas torch [9]

3.2.3. Microstructures and hardness

Microstructural characterizations of coatings were performed on the cross-section of the samples, by means of optical microscopy. Samples hard-faced with UTP DUR 350 and Wearshield 70 coatings were etched in a 4% of nitric acid solution in ethanol, and other samples were etched by Vilella's reagent (1 g of picric acid, 5 ml of hydrochloric acid and 100 ml of ethanol) [10]. The microstructures of the obtained coatings are shown in **Fig. 3.6**, and the description of the microstructures in **Table 3.4**.

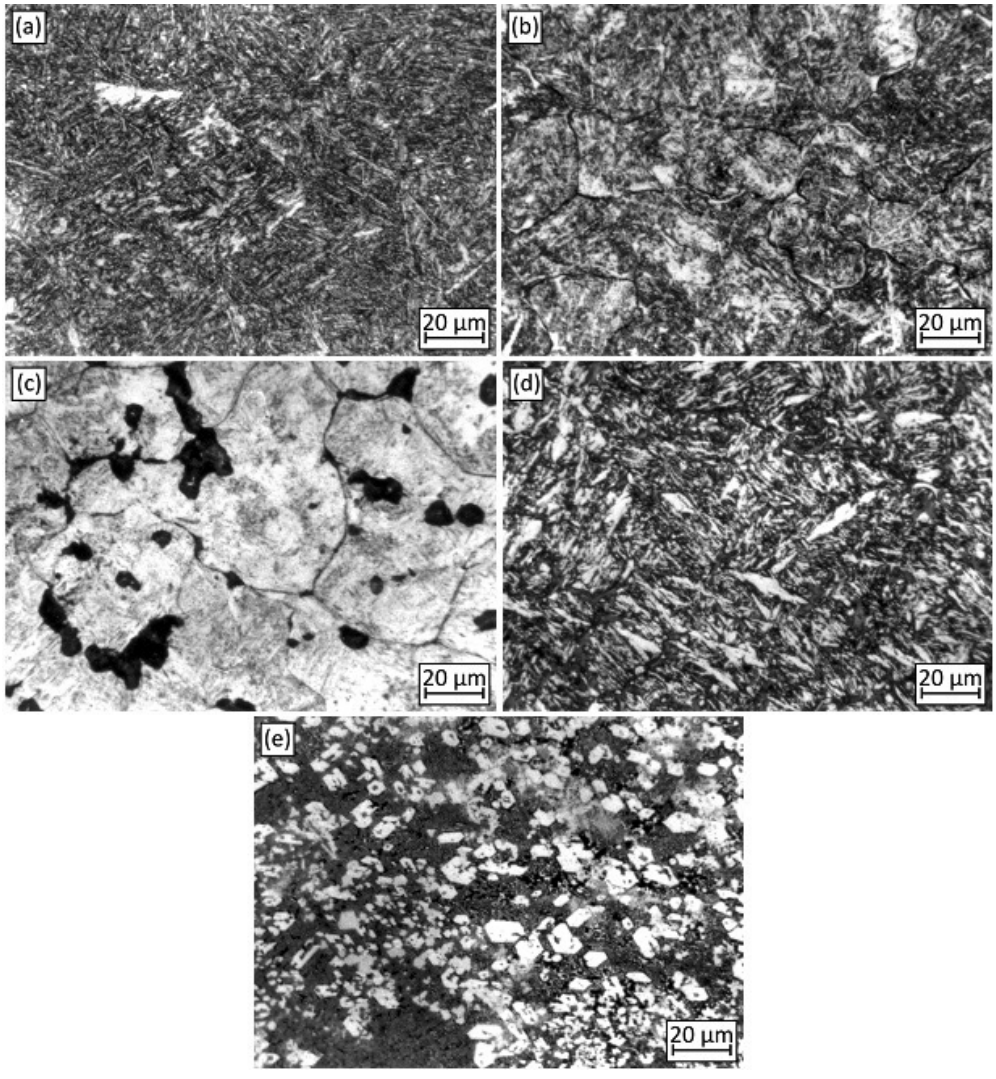

Fig. 3.6. Microstructure properties of tested coatings: (a) UTP DUR 350, (b) EH 550, (c) LNM 420FM, (d) Fluxofil 58, and (e) Wearshield 70 [9]

Table 3.4. Description of the microstructures and measured hardness [9]

Coating designation	Microsctructure	Hardness HRC
UTP DUR 350	Bainite	40
EH 550	Martensite and Cr carbides	60
LNM 420FM	Martensite and Cr carbides in the compound of pearlite structure	58
Fluxofil 58	Martensite and Cr carbides	60
Wearshield 70	Complex W-Mo and Nb carbides and eutecticum	63

Measurements of surface hardness (HRC) were carried out using Rockwell hardness tester. At least three measurements were made for each sample in order to eliminate possible segregation effects and to obtain a representative value of the material hardness. The results are shown in **Table 3.4**.

3.3. Experimental details

In order to compare different hardfaced coatings and to investigate various influences on their tribological properties (abrasive and vibro-abrasive wear), two tribological experiments were done with similar test equipments. The main goal was to compare different coatings, as well as, to investigate and analyse influences of normal load and vibration velocity on wear resistance of these coatings.

Abrasive wear is one of the most common types of wear, since more than 50% of all wear-related failures of industrial equipment are caused by abrasive wear [11]. The equipment used in road construction, agricultural and mining industry is exposed to heavy-duty operating conditions, under the impact loads in abrasive and corrosive environment. This means that this equipment always operate under lower of higher amount of vibration load caused by various reasons. Vibrations in most cases intensify the wear processes, which affects in turn the vibration parameters [12, 13]. High changes in the operation regime can cause resonance effects, which result in speed up of fatigue and wear mechanisms [14]. One of the basic ways to diminish the vibration affect on wear, and wear itself is wear resistance improvement of contact surfaces through coatings [15]. Regeneration (repair) of the equipment used in road construction, agricultural and mining industry, which is exposed to heavy-duty operating conditions, is mainly by hardfacing coating [16].

3.3.1. Abrasive wear testing

Abrasive wear tests were carried out on pin-on-drum tribometer according to the standard test method for pin abrasion testing (ASTM G 132), in the ambient air at room temperature. A schematic diagram of pin-on-drum tribometer is presented in **Fig. 3.7**.

Vertical cylindrical specimen (3) with deposited coating (4) is positioned perpendicularly to the impregnated corundum abrasive paper (5) with grain size of 125 μm (P120 grit). The abrasive paper is fastened to, and supported by a horizontal cylinder (2). The cylinder, driven by AC motor (1), rotates with given constant rotational speed about its horizontal axis. Specimen (3) is fixed in the loading head (6) though elastic connection, which allow self-adjustment of the specimen to the abrasive paper (5) and provide possibility for rotation of the specimen around its vertical axis. The loading head (6) engages the static rack bar (7) through the horizontal gear ring, providing worm drive and rotation of the specimen around its vertical axis. Static rack bar also provides horizontal movement (L) of the loading head and test specimen (3). In this way a helical wear track is formed. Rotation of the specimen around its vertical axis provides the homogeneous wear in all points of the contact area. Cleaning of the abrasive paper (5) from wear debris is done by an appropriate brush fixed to the loading head (6), together with a vacuum pump. The normal load (F_n) is given by means of dead weights (8).

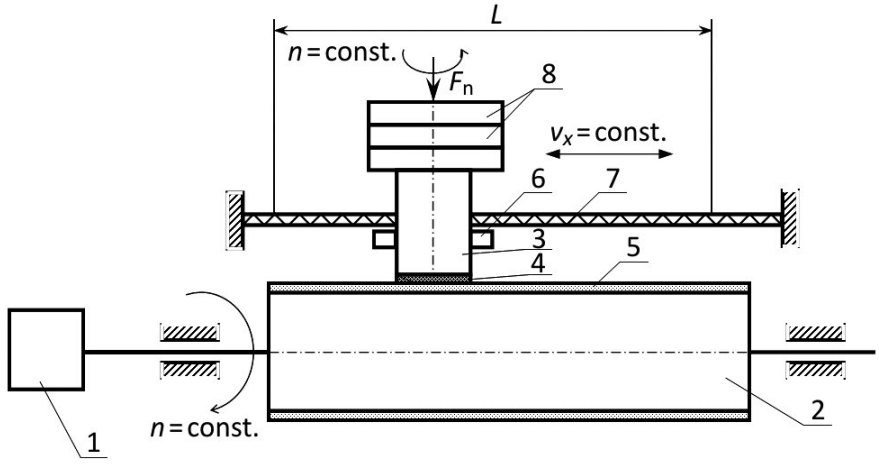

Fig. 3.7. Schematic diagram of abrasive wear testing on pin-on-drum tribometer (1 – AC motor; 2 – drum (horizontal cylinder); 3 – pin (specimen); 4 – coating; 5 – abrasive surface (abrasive paper); 6 – loading head; 7 – static rack bar; 8 – loading weights)

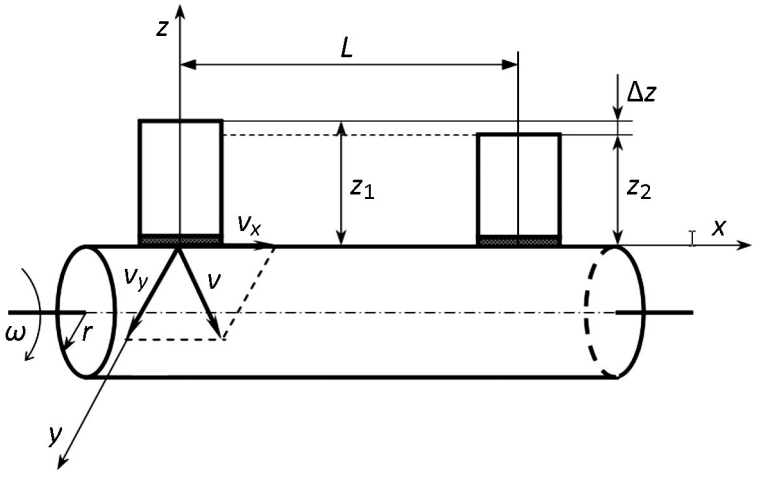

Fig. 3.8. Schematic diagram of the specimen sliding velocities

Due to the horizontal movement of the specimen and rotation of the cylinder (helical wear track), sliding velocity (v) of the specimen has two components (v_x and v_y) which, in accordance with **Fig. 3.8**, are defined as follows:

$$v_x = \frac{L}{t};\ v_y = r \cdot \omega = r\frac{n\pi}{30};\ v = \sqrt{v_x^2 + v_y^2}\ , \tag{3.1}$$

where L = 0.6 m is the horizontal length of the specimen path in one cycle, t is the duration of one cycle (time in which the specimen travels the length L), r = 0.075 m is the cylinder radius, and n = 40 rpm is the rotational speed of the cylinder.

The sliding distance (s) is calculated from the following equation:

$$s = v \cdot t \cdot \mathrm{N}\,, \tag{3.2}$$

where N is the number of cycles.

Two experiments were conducted in the abrasive wear test. In the first experiment the normal load of 0.40 kg (3.92 N) was constant. Taking into account the assumed contact area (specimen cross-section area) of approximately 1.77 cm^2 (diameter of the cylindrical test specimens was 15 mm), the specific load was 2.22 N/cm^2. Duration of one cycle (t) was 137 s, and there were five cycles as in total (N = 5). The sliding velocity and sliding distance, calculated according to the Equations 3.1 and 3.2, were: v = 0.31 m/s and s = 215.22 m.

In the second experiment four different normal loads were applied: 0.82 kg (8.04 N), 1.46 kg (14.32 N), 2.26 kg (22.16 N), and 3.14 kg (30.79 N). Taking into account the assumed contact area of approximately 1.77 cm^2 (diameter of the cylindrical test specimens was the same), the specific load were: 4.55, 8.10, 12.54, and 17.43 N/cm^2, respectively. Duration of cycle (t) was 78 s, and there was only one cycle (N = 1). The sliding velocity and sliding distance, calculated according to the Equations 3.1 and 3.2, were: v = 0.31 m/s and s = 24.51 m.

Abrasive wear is calculated as a mass loss, i.e., as a difference between the initial mass of the specimen and its mass after appropriate sliding time (t). Before and after testing, the specimen was degreased and cleaned, and its mass is measured by the electronic balance with accuracy of 0.1 mg. The abrasive wear is presented and analysed through the mass wear rates and relative wear resistances (experiment I) and through the mass wear rates and specific wear rates (wear factors) of the coatings (experiment II).

3.3.2. Vibro-abrasive wear testing

Vibro-abrasive wear tests were carried out on the modified pin-on-drum tribometer which is used for abrasive wear tests without vibrations. The tests were performed in the ambient air at room temperature. A schematic diagram of modified pin-on-drum tribometer is presented in **Fig. 3.9**.

Vertical cylindrical specimen (3) with deposited coating is positioned perpendicular to the impregnated corundum abrasive paper (5) with grain size of 125 μm (P120 grit). The abrasive paper is fastened to, and supported by a horizontal cylinder (2). The cylinder, driven by AC motor (1), rotates with given constant rotational speed about its horizontal axis. Specimen (3) is fixed in the loading head (4) though elastic connection, which allow self-adjustment of the specimen to the abrasive paper (5) and provide possibility for rotation of the specimen around its vertical axis. The loading head (4) engages the static rack bar (7) through the horizontal gear ring (6), providing worm drive and rotation of the specimen around its vertical axis. Static rack bar also provides horizontal movement (L) of the loading head and test specimen (3). In this way a helical wear track is formed. Rotation of the specimen around its vertical axis provides the homogeneous wear in all points of the contact area. Cleaning of the abrasive paper (5) from wear debris is done by an appropriate brush fixed to the loading head (4), together with a vacuum pump.

Due to the horizontal movement of the specimen and rotation of the cylinder (helical wear track), sliding velocity (v) of the specimen has two components (v_x and v_y) which, in accordance with **Fig. 3.8**, are defined in Equation 3.1. The sliding distance (s) is calculated from the Equation 3.2.

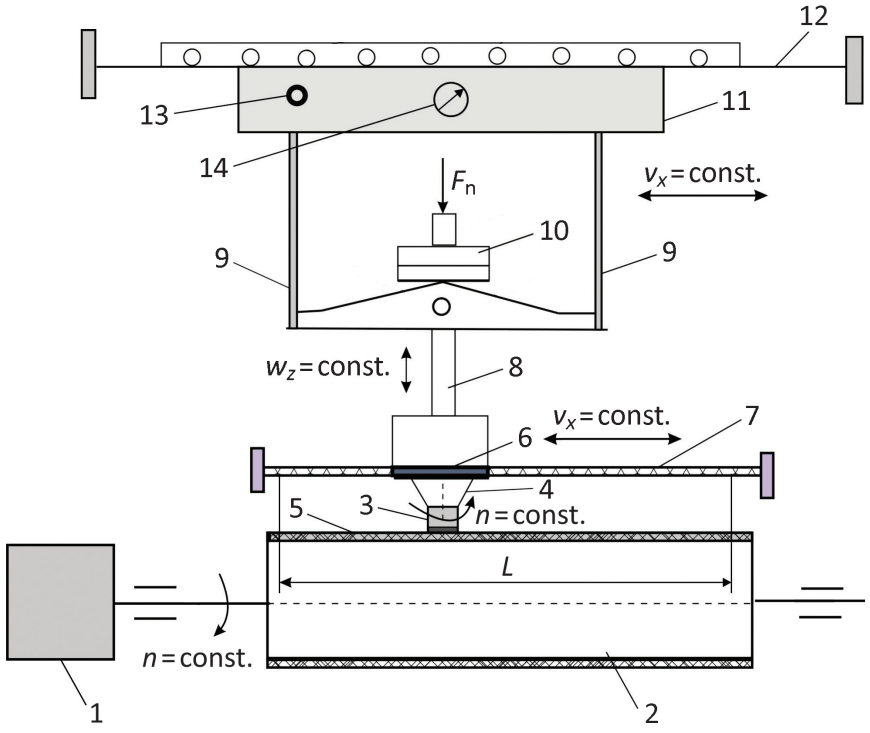

Fig. 3.9. Schematic diagram of vibro-abrasive wear testing on modified pin-on-drum tribometer: 1 – AC motor; 2 – drum (horizontal cylinder); 3 – pin (specimen) with coating; 4 – loading head; 5 – abrasive surface (abrasive paper); 6 – gear ring; 7 – static rack bar; 8 – specimen fastening mechanism; 9 – vibrating frame; 10 – loading weights; 11 – vibrator; 12 – vibrator supporting structure with driving mechanism; 13 – on/off button of the vibrator; 14 – regulator of vibrations parameters

Modification of the standard pin-on-drum tribometer is done by adding of the vibration frame (9), which is fastened through the appliance (8) to the loading head (4) and test specimen (3). The normal load (F_n) is given by means of dead weights (10). Vertical vibrations, along the axis of the specimen, are provided by the vibrator (11). The vibrator is mounted on the supporting structure (12), which provides translational movement of the vibration frame (9), simultaneously with the loading head (4) and the specimen (3), parallel to the cylinder (2). Switch-on of the vibrator is given by the button (13), and the vertical vibration velocity by the regulator (14). The vibration regulator (14) allows setting of various values of vertical vibration velocity (w_z) in the interval $3 < w_z < 20$ mm/s. This interval is selected in ac-

cordance with the ISO standard for evaluation of vibration severity in machines and equipment [17].

Vibration parameters: vibration displacement in mm; vibration velocity in mm/s; and vibration acceleration in mm/s^2 are measured by the vibration meter PCE-VT 204. Only the vibration velocity parameter is used and presented in this study. The Table 3.5 shows the measured values of the vibration velocity in three directions (**Fig. 3.10a**): vertical (*z* axis), i.e., vertical vibration velocity (w_z), axial (*x* axis), i.e., axial vibration velocity (w_x) and horizontal (*y* axis), i.e., horizontal vibration velocity (w_y). Relationship between measured velocity components is shown in **Fig. 3.10b**. Total vibration velocity (w), in accordance with **Fig. 3.10a**, is calculated as follows:

$$w = \sqrt{w_x^2 + w_y^2 + w_z^2} \ . \tag{3.3}$$

As it can be seen from **Table 3.5**, testing was performed with five different vibration velocities, as well as tests without vibration, for all coatings. Other parameters were also the same for all coatings. The normal load of 0.40 kg (3.92 N) was constant. Taking into account the assumed contact area (specimen cross-section area) of approximately 2.27 cm^2 (diameter of the cylindrical test specimens was 17 mm), the specific load was 1.73 N/cm^2. Duration of one cycle (t) was 156 s, and there was only one cycle (N = 1). The sliding velocity and sliding distance, calculated according to the Equations 3.1 and 3.2, were: v = 0.31 m/s and s = 49.01 m.

Vibro-abrasive wear is calculated as a mass loss, i.e., as a difference between the initial mass of the specimen and its mass after appropriate sliding time (t). Before and after testing, the specimen was degreased and cleaned, and its mass is measured by the electronic balance with accuracy of 0.1 mg. The vibro-abrasive wear is presented and analysed through the mass wear rates and relative wear resistances of the coatings.

Table 3.5. Values of the vibration velocity components and total vibration velocity

Vibration velocity	Reference position on the vibration regulator				
	1	5	7	9	10
w_z, mm/s	3	6	9	16	20
w_x, mm/s	0.4	0.6	0.9	3.8	4.4
w_y, mm/s	0.2	0.35	0.8	3.8	5
w, mm/s	3.03	6.04	9.08	16.88	21.08

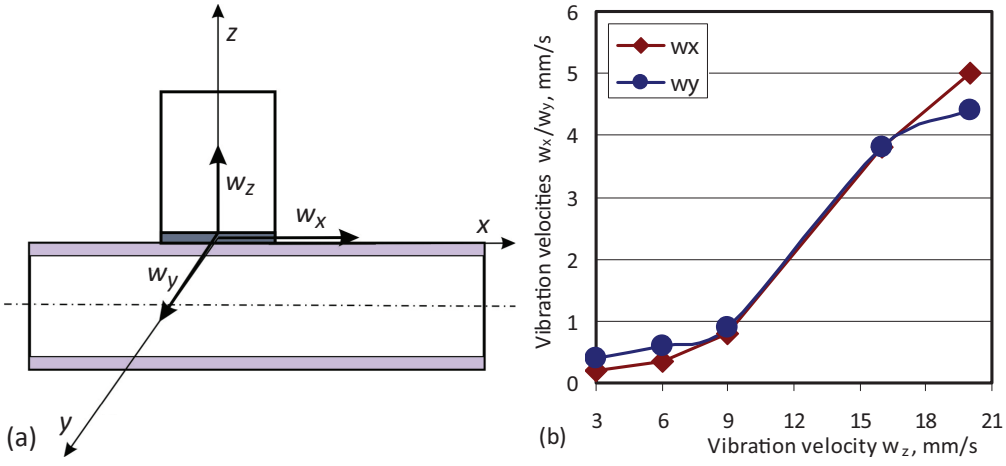

Fig. 3.10. Vibration measurements: (a) directions of measured velocity components, and (b) relationship between measured velocity components

3.4. Results and Discussion

3.4.1. Abrasive wear testing

In the first experiment, the one with the constant normal load, the abrasive wear of coatings was determined at five different sliding times (sliding distances), i.e. at 137, 274, 411, 548 and 685 s. The corresponding mass losses are presented in **Table 3.6**.

Obtained results of the mass losses are also shown as a function of sliding distance, in the form of the comparative wear curves. Wear rate (W) in mg/m is calculated by fitting the wear curves (it is the slope of wear curve), assuming that the steady-state wear was from the beginning of the tests (which is common thing for the abrasive wear). The wear curves for coatings UTP DUR 350 and EH 550 are shown in **Fig. 3.11**, for coatings LNM 420FM and Fluxofil 58 in **Fig. 3.12**, and for coating Wearshield 70 in **Fig. 3.13**.

The lowest wear rate of 4.81×10^{-2} mg/m is observed for coating Wearshield 70. The increase of wear resistance for this coating was approximately 12.8 times in comparison to coating EH 550 which shows the highest wear rate of 6.16×10^{-1} mg/m. Presence of running-in process was noticed for coating LNM 420FM. Nevertheless, abrasive wear process is stable for all deposited coatings, which can be seen from the R^2 (R-squared) value, since generally all R-squared shows acceptable goodness of fit ($R^2 = 1$ is a perfect fit).

Comparison of different hardfaced coatings were analysed by comparing its relative wear resistance values. The relative wear resistance is calculated

Table 3.6. Abrasive wear of tested coatings (experiment I)

Coating designation	Sliding time, s				
	137	274	411	548	685
	Sliding distance, m				
	43.0	86.1	129.1	172.2	215.2
	Mass loss, mg				
UTP DUR 350	25	38	55	95	120
EH 550	30	58	80	108	128
LNM 420FM	35	64	85	95	115
Fluxofil 58	25	40	52	65	75
Wearshield 70	4	5	6	8	10

as a ratio of reference specimen wear rate and wear rate of the analysed specimen, where the specimen with the lowest hardness (coating UTP DUR 350) was taken as a reference specimen (relative wear resistance of this specimen is always equal 1). Calculated relative wear resistances are presented in **Fig. 3.14**.

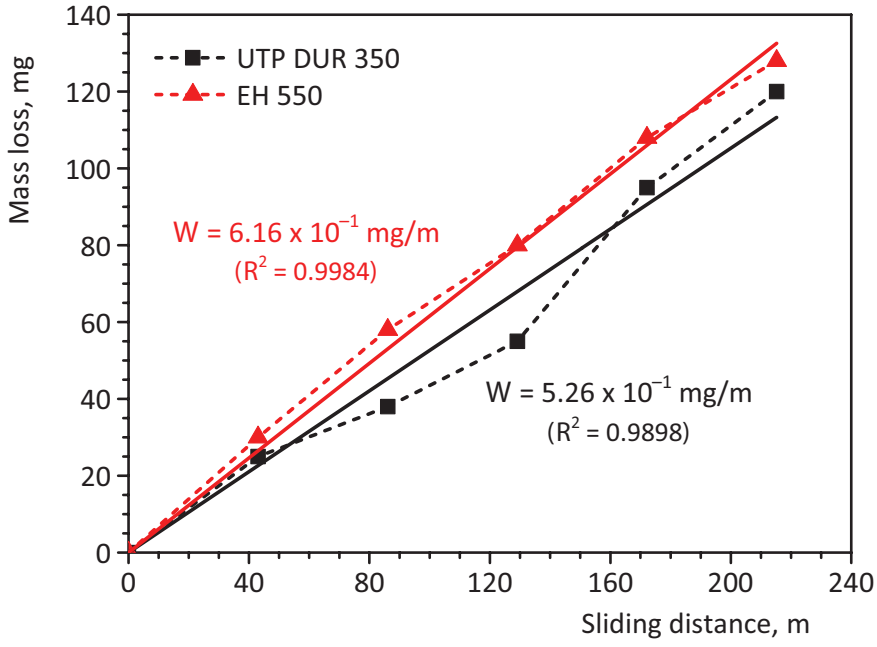

Fig. 3.11. Mass loss vs. sliding distance for coatings UTP DUR 350 and EH 550

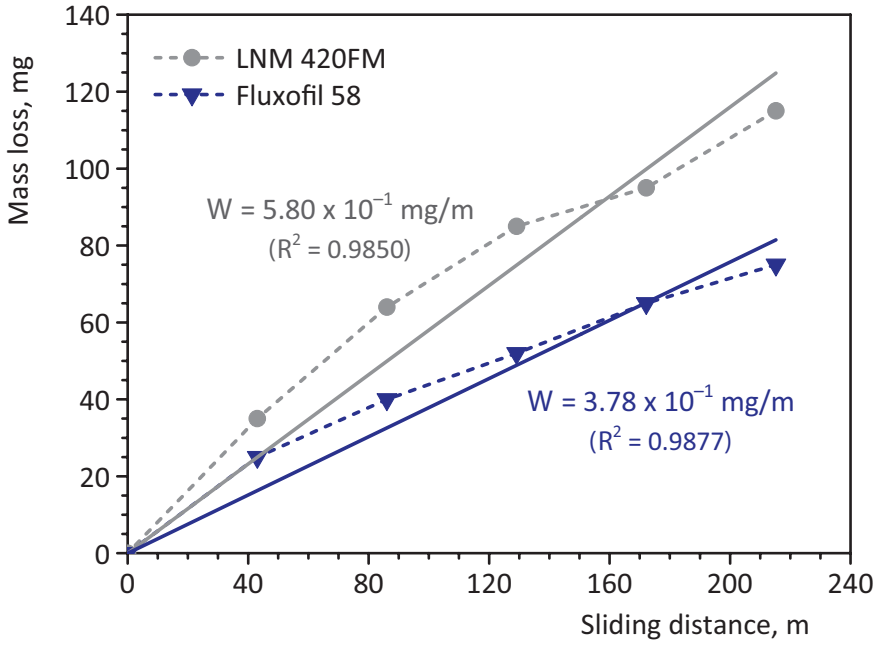

Fig. 3.12. Mass loss vs. sliding distance for coatings LNM 420FM and Fluxofil 58

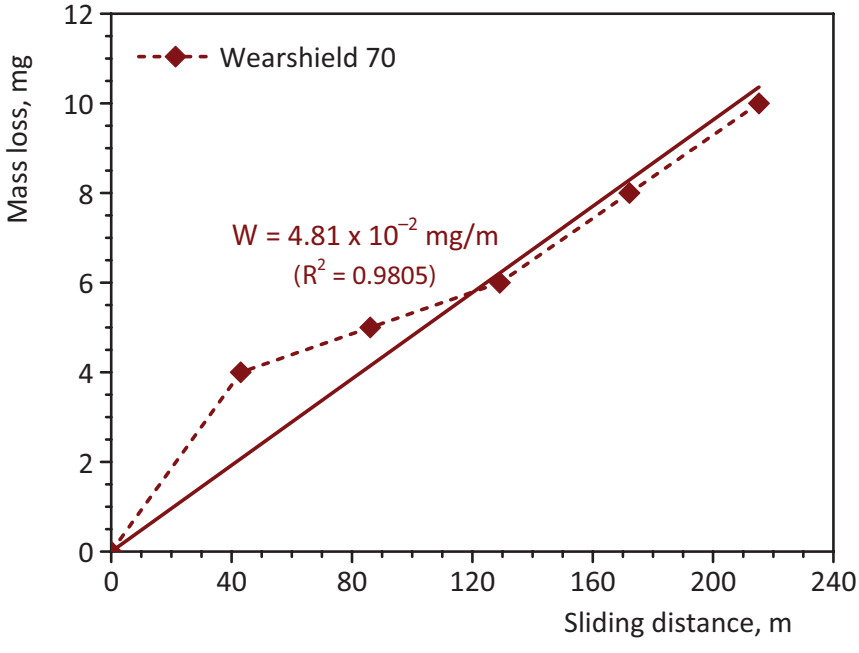

Fig. 3.13. Mass loss vs. sliding distance for coating Wearshield 70

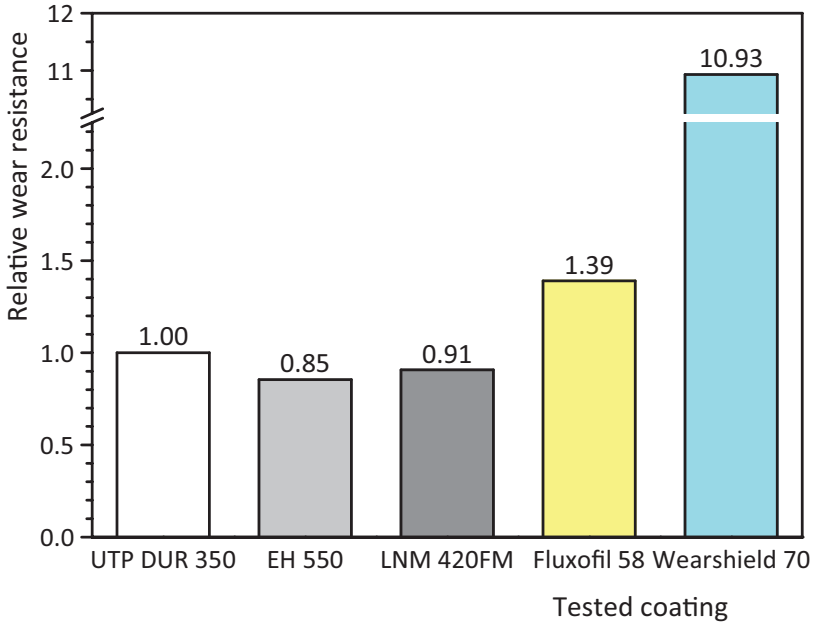

Fig. 3.14. Comparative values of relative wear resistance of tested coatings

First three coatings (UTP DUR 350, EH 550 and LNM 420FM) showed similar abrasive wear resistance. Coatings EH 550 and LNM 420FM have Cr carbides in their microstructure, which increased their hardness, but the distance between them was relatively high (they are distributed on the spherical grain boundaries), so their reinforcing effect was small. Coating Fluxofil 58 had martensite structure with elongated grains. In addition, this coating also had Cr carbides which were well distributed and together with elongated and randomly oriented grains provided somewhat higher abrasive wear resistance. The highest abrasive wear resistance of coating Wearshield 70 (one order of magnitude higher than other coatings) is most probably due to the presence W-Mo carbides [18] and particularly due to the presence of the small, well distributed Nb carbides [19].

The relationship between obtained abrasive wear values and hardness (**Table 3.4**) of tested coatings is shown in **Fig. 3.15**. It could be noticed that the hardest coating (Wearshield 70) shows highest wear resistance as well, but from the other coatings results, it is obvious that relationship between the abrasive wear and hardness values of any kind did not exist. This could be seen from the R^2 (R-squared) value, since it was very low (R^2 = 0.16), no matter that the number of values for the statistical analysis could not be statistically significant.

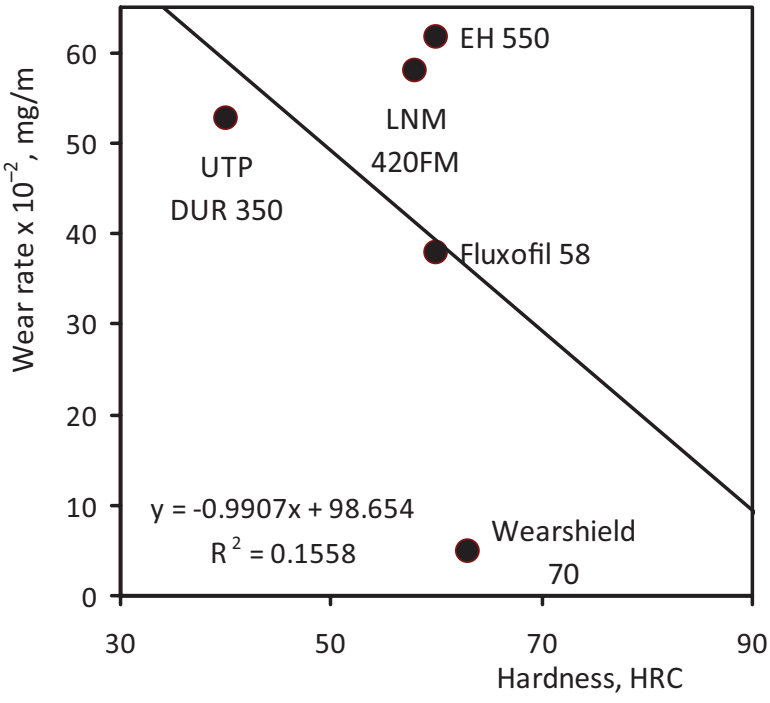

Fig. 3.15. Abrasive wear rate vs. hardness of tested coatings

The relationship shown in **Fig. 3.15** confirms the fact that the use of hardness as a parameter for predicting the abrasive wear behaviour of materials must be done with caution. For instance wear mechanisms of hardfacing coatings represent a more complex form of wear processes due to their inhomogeneous structure. For pure metal and single phase material, wear is generally inversely proportional to the hardness. However, for the multiphase alloy, the microstructure also contributes a significant effect on the wear of the material [20, 21]. The results of other studies have also shown that abrasion wear resistance of quenched and tempered steels has much weaker dependency on the bulk hardness [22].

In the second experiment, with variable normal loads, the abrasive wear of coatings was determined at four different specific loads, i.e. at 4.55, 8.10, 12.54 and 17.43 N/cm^2. The corresponding mass losses are presented in **Table 3.7**.

Corresponding wear rates of the coatings, for different specific loads, were calculated from the obtained results of the mass loss shown in **Table 3.7** and calculated sliding distance of 24.51 m. Wear rates are presented in **Fig. 3.16** (coatings UTP DUR 350, EH 550 and LNM 420FM) and **Fig. 3.17**

Table 3.7. Abrasive wear of tested coatings (experiment II)

Coating designation	Normal load, N			
	8.04	14.32	22.16	30.79
	Specific normal load, N/cm^2			
	4.55	8.10	12.54	17.43
	Mass loss, mg			
UTP DUR 350	70	80	110	140
EH 550	80	130	190	260
LNM 420FM	94	110	180	240
Fluxofil 58	10	8	6	8
Wearshield 70	7	3	2	2

(coatings Fluxofil 58 and Wearshield 70). This wear rates are total wear rates, since it were calculated from the total mass losses.

First three coatings (UTP DUR 350, EH 550 and LNM 420FM) follow the expected behavior of materials, i.e., with the increase of specific load, the wear rate also increases. This increase is almost linear, which suggest that

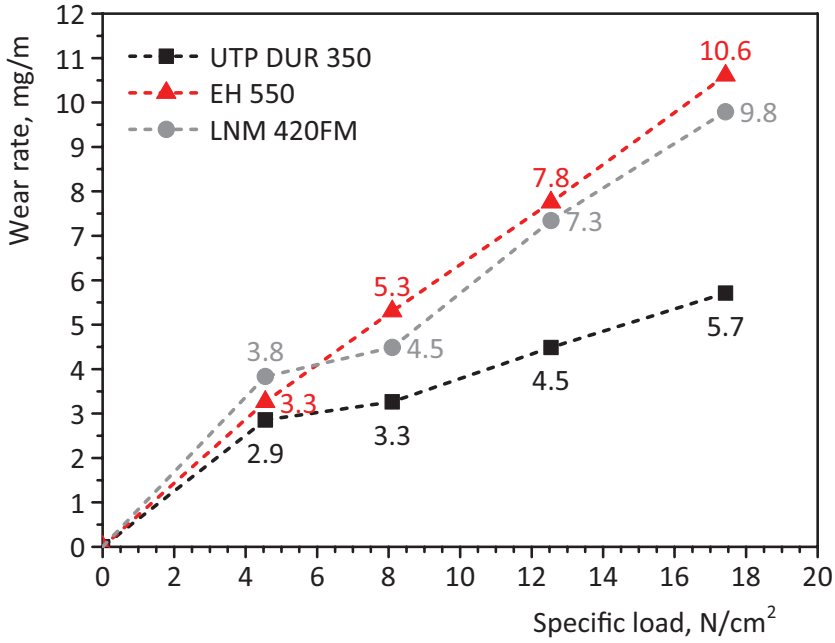

Fig. 3.16. Abrasive wear rates at different specific loads for coatings UTP DUR 350, EH 550 and LNM 420FM

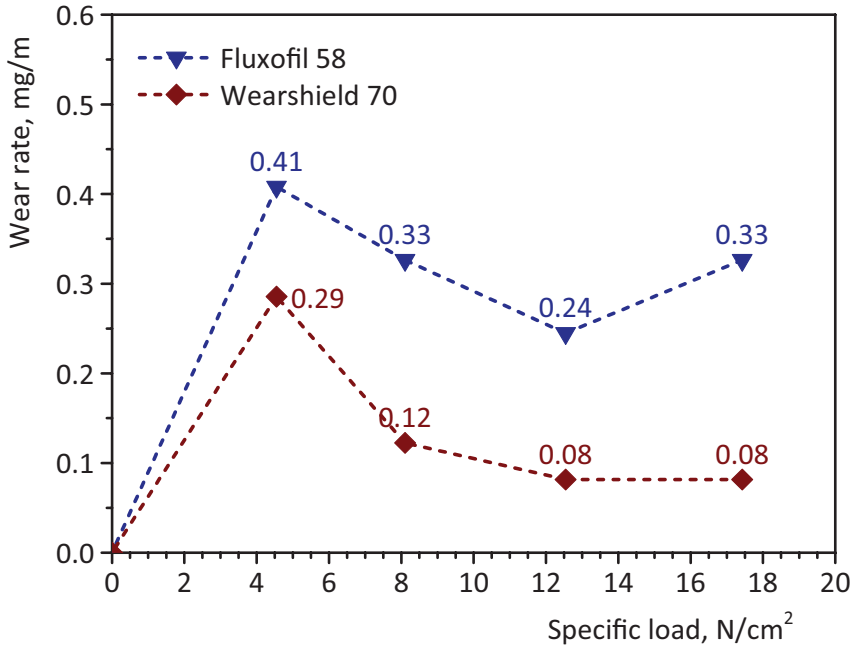

Fig. 3.17. Abrasive wear rates at different specific loads for coatings Fluxofil 58 and Wearshield 70

there was no the transition of the wear regime [23]. However, values for coatings Fluxofil 58 and Wearshield 70 deviate from this trend, and uncommon behavior is noticed, i.e., with the increase of specific load, the wear rate decreases. This is, most probably, because the wear values for coatings were small as well as the sliding distance, so the deviations of the results are possible (especially for heterogeneous materials and dry sliding conditions). In addition, there was only one test performed for each specific load.

In order to except the influence of normal load and to compare the abrasive wear results with the results from the literature, wear factor (specific wear rate) were also calculated and shown in **Table 3.8**. Specific wear rate is a parameter that is used for comparison of the materials with different hardness. It is also used when the wear of harder material in contact is analyzed [24], since well-known Archard equation takes hardness of the softer contact surface. Specific wear rate in mg/Nm is calculated as a ratio of wear rate and normal load.

By presuming that the approximate density of all coatings is 7.5 g/cm^3, it is easy to calculate the wear factor in mm^3/Nm and compare it with the results from the literature. Calculated wear factor values are ranged from 6.6 $\times 10^{-4}$ to 4.9 $\times 10^{-2}$ mm^3/Nm. These values correspond to the literature data

Table 3.8. Specific abrasive wear of tested coatings (experiment II)

Coating designation	Specific normal load, N/cm^2				Average specific wear*, mg/Nm
	4.55	8.10	12.54	17.43	
	Specific wear, mg/Nm				
UTP DUR 350	3.55×10^{-1}	2.28×10^{-1}	2.02×10^{-1}	1.85×10^{-1}	2.43×10^{-1}
EH 550	4.06×10^{-1}	3.70×10^{-1}	3.50×10^{-1}	3.44×10^{-1}	3.68×10^{-1}
LNM 420FM	4.77×10^{-1}	3.13×10^{-1}	3.31×10^{-1}	3.18×10^{-1}	3.60×10^{-1}
Fluxofil 58	5.07×10^{-2}	2.28×10^{-2}	1.10×10^{-2}	1.06×10^{-2}	1.48×10^{-2}
Wearshield 70	3.55×10^{-2}	8.55×10^{-3}	3.68×10^{-3}	2.65×10^{-3}	4.96×10^{-3}

*For coatings Fluxofil 58 and Wearshield 70 the average value was calculated without the value for 4.55 N/cm^2 load.

for metallic materials in sliding contact (under unlubricated condition, and for abrasive wear, the interval is from 10^{-5} to 10^{-1} mm^3/Nm) [25]. First three coatings (UTP DUR 350, EH 550 and LNM 420FM) have similar wear factor values, while the last two coatings (Fluxofil 58 and Wearshield 70) show one or two order of magnitude lower values, indicating good abrasive wear resistance of these two coatings. Wear factor is a very useful engineering tool, since it is approximately equal for certain load intervals. Knowing the value of wear factor for given working conditions (load and sliding distance), wear value could be relatively easily determined.

3.4.2. Vibro-abrasive wear testing

The vibro-abrasive wear of coatings was determined at six different vibration velocities, i.e., at 0; 3.03; 6.04; 9.08; 16.88, and 21.08 mm/s. The corresponding mass losses are presented in **Table 3.9**.

Corresponding wear rates of the coatings, for different vibration velocities, were calculated from the obtained results of the mass loss shown in **Table 3.9** and calculated sliding distance of 49.01 m. Wear rates are presented in **Fig. 3.18** (coatings UTP DUR 350 and EH 550), **Fig. 3.19** (coatings LNM 420FM and Fluxofil 58) and **Fig. 3.20** (coating Wearshield 70). This wear rates are total wear rates, since it were calculated from the total mass losses.

The obtained experimental results show that the presence of normal vibration load, after some value of vibration velocity, increase the abrasive wear rate (**Figs. 3.18** and **3.19**). The exception is coating Wearshield 70 for which increase of vibration velocity above some value has opposite effect (**Fig. 3.20**). This coating also showed approximately one order of magnitude

Table 3.9. Vibro-abrasive wear of tested coatings

Coating designation	Vibration velocity (w), mm/s					
	0	3.03	6.04	9.08	16.88	21.08
	Mass loss, mg					
UTP DUR 350	36	24	21	68	79	76
EH 550	28	20	13	43	40	30
LNM 420FM	22	23	24	34	53	60
Fluxofil 58	25	7	24	40	52	58
Wearshield 70	6	3	6	8	4	3

lower wear rate in comparison to other coatings. For all coatings three distinct regions can be noticed in the relationships wear rate vs. vibration velocity (adaptation, transition, and nearly stationary region).

In the first (adaptation) region ($0 < w < 6$ mm/s), the wear rates generally decrease with the increase of vibration velocity, region was wider for coatings UTP DUR 350, EH 550 and LNM 420FM, and continue up to w = 6 mm/s,

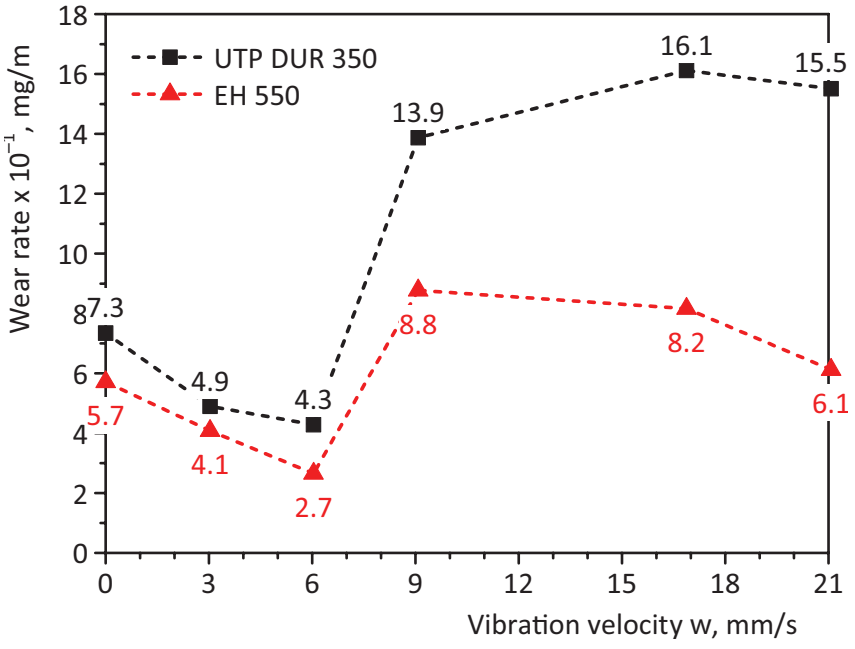

Fig. 3.18. Vibro-abrasive wear rates at different vibration velocities for coatings UTP DUR 350 and EH 550

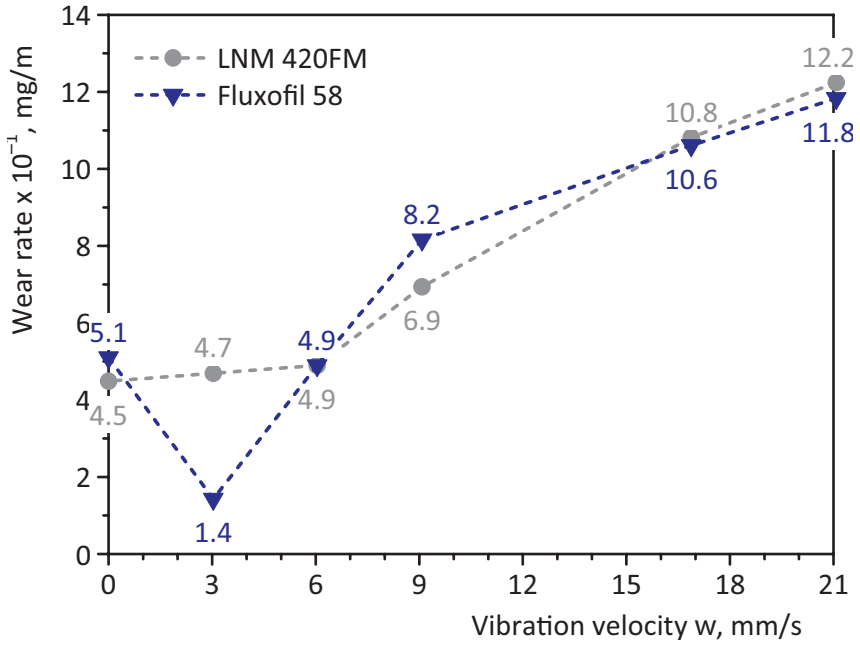

Fig. 3.19. Vibro-abrasive wear rates at different vibration velocities for coatings LNM 420FM and Fluxofil 58

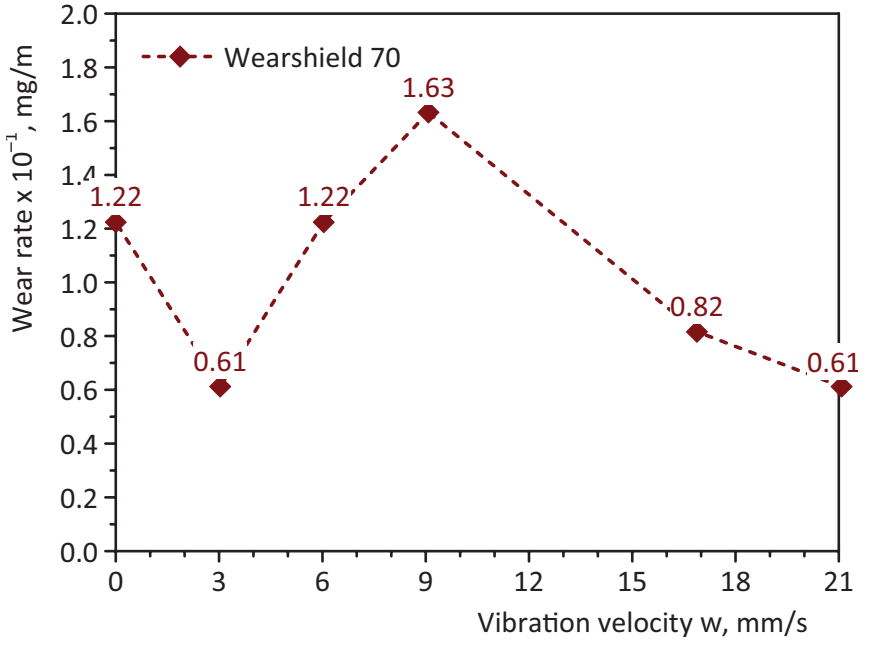

Fig. 3.20. Vibro-abrasive wear rates at different vibration velocities for coating Wearshield 70

while for coatings Fluxofil 58 and Wearshield 70 it was narrower (up to w = 3 mm/s). This decrease of wear rate can be explained with the increase of the real contact area due to the small vibrations and smoothing of the contact surface. At these vibration velocities asperities adopt to each other making the surface roughness lower. As a consequence, contact specific loads become lower so the wear rates decrease.

In the second (transition) region ($6 < w < 9$ mm/s), sudden increase of the wear rate occurs for all coatings. This region started at lower vibration velocities for coatings Fluxofil 58 and Wearshield 70, i.e. after w = 3 mm/s, since the first (adaptation) region for these two coatings was narrower. This sudden increase of wear rate can be explained with the intensifying of fatigue failure processes, since the vibration velocities are higher. Fatigue processes resulting from the micro-impacts and the micro-cutting by the abrasive particles are the basic wear mechanisms in tribosystems with high vibrations.

In the third (nearly stationary) region ($9 < w < 21$ mm/s), all coatings show apparent tendency to stabilise the wear rate and become independent of further vibration velocity increase. This is just the assumption that the further increase of vibration would not have some significant influence. Anyway, it is most probably that in this region a balance between two influential parameters is reached: increase of wear due to intensifying of fatigue failure processes, and decrease of wear due to case-hardening and/or appearance of damping effects of some of the phases in the coatings during the process of contact interaction.

In order to perceive the influence of vibrations, a wear rate without vibration is compared with the wear rate at higher vibrations for each coating (**Table 3.10**). Higher vibrations wear rate was obtained by averaging the last

Table 3.10. Approximate influence of the vibration velocity on abrasive wear

Coating designation	Vibration velocity (w), mm/s				Wear rate decrease/ increase
	w = 0 mm/s		w > 16 mm/s		
	Wear rate × 10^{-1}, mg/m	Relative wear resistance	Wear rate × 10^{-1}, mg/m	Relative wear resistance	
UTP DUR 350	7.35	1	15.81	1	2.15
EH 550	5.71	1.29	7.14	2.21	1.25
LNM 420FM	4.49	1.64	11.53	1.37	2.57
Fluxofil 58	5.10	1.44	11.22	1.41	2.20
Wearshield 70	1.22	6.00	0.71	22.14	0.58

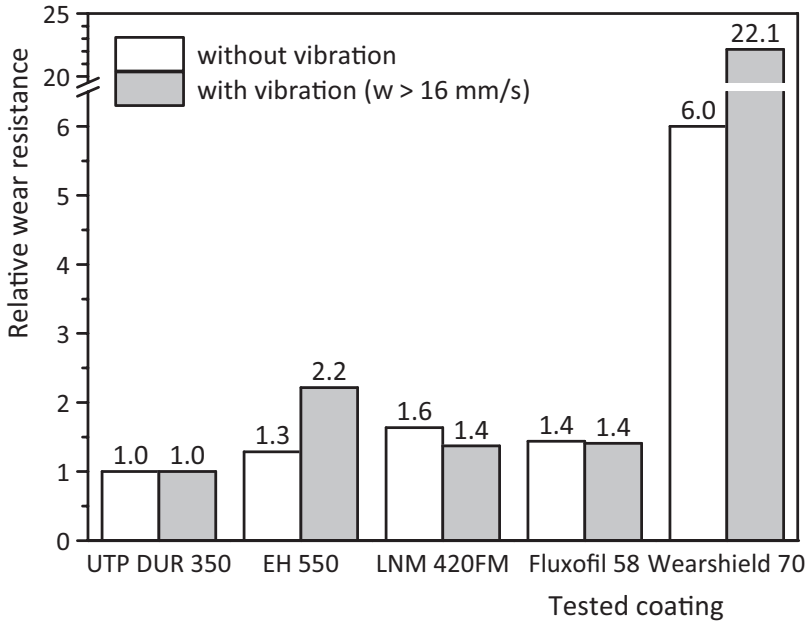

Fig. 3.21. Comparative values of relative wear resistance of tested coatings without and with vibrations at velocities higher than 16 mm/s)

two values of wear rate, i.e. at w = 16.9 mm/s and w = 21.1 mm/s. It can be noticed that the wear rate increased with the presence of high vibration velocities for all coatings, except for coating Wearshield 70. For this coating presence of vibrations had beneficiary effect. This is primarily due to the microstructure and ductility of this coating. Its microstructure consists of small, well distributed Nb carbides embedded in relatively soft matrix, which prevented movement of the dislocation and increased hardness, shear strength and ductility. Therefore the cracks grow and propagation is reduced and dumping effect is increased, resulting in decrease of the abrasive wear rate in presence of vibrations.

In **Table 3.10**, values of the relative wear resistance are also presented, in order to compare obtained hardfaced coatings. There are two relative wear resistance values for each coating, i.e., without and with vibrations at velocities higher than 16 mm/s. Both relative wear resistances presented in **Table 3.10** are calculated as a ratio of reference specimen wear rate and wear rate of the analysed specimen, where the specimen with the lowest hardness (coating UTP DUR 350) was taken as a reference specimen (relative wear resistance of this specimen is always equal 1). These values are also presented in the form of diagram in **Fig. 3.21**. The sequence of coatings by its wear resistance is similar in both cases, i.e. without and with vibration.

3.5. Conclusions

Properties of the hardfaced coatings depend on many parameters, and for every specific application and working conditions, there is one optimal value. Optimisation of the deposition parameters it this case study was directed toward minimization of the mechanical treatment (machining) of the obtained coatings.

Hardfacing is mainly applied for the repair of equipment used in road construction, agricultural and mining industry, i.e., equipment exposed to heavy-duty operating conditions under impact loads, with dominant abrasive, vibro-abrasive and corrosive wear. Tribological properties (abrasive and vibro-abrasive wear) of five different hardfaced Fe based coatings (UTP DUR 350, EH 550, LNM 420FM, Fluxofil 58 and Wearshield 70) were investigated, with the aim to compare coatings among themselves, as well as, to investigate and analyse influences of normal load and vibration velocity on wear resistance of these coatings.

First three coatings (UTP DUR 350, EH 550 and LNM 420FM) showed similar abrasive wear resistance, no matter that coatings EH 550 and LNM 420FM had and Cr carbides in their microstructure, and showed higher hardness. Distances between these carbides were relatively high, so their reinforcing effect was small. On the other hand, Cr carbides in the microstructure of coating Fluxofil 58 had better distribution and together with elongated and randomly oriented grains provided higher abrasive wear resistance of this coating. Coating Wearshield 70 showed the highest abrasive wear resistance, i.e., approximately one order of magnitude higher than other coatings. This is most probably due to the presence W-Mo carbides and particularly due to the presence of the small, well distributed Nb carbides.

It was confirmed that the use of hardness as a parameter for predicting the abrasive wear behaviour of materials is not the best choice, since the wear mechanisms of hardfacing coatings represent a more complex form of wear processes due to their inhomogeneous structure. It was noticed that the hardest coating (Wearshield 70) shows the highest wear resistance as well, but from the other coatings results, it is obvious that relationship between the abrasive wear and hardness values of any kind did not exist.

For all coatings, the values of abrasive wear factor are calculated and could be used for practical engineering calculations. Under dry sliding abrasive wear conditions, the following values could be accepted: UTP DUR 350 (2.43×10^{-1} mg/Nm); EH 550 (3.68×10^{-1}); LNM 420FM (3.60×10^{-1}); Fluxofil 58 (5.07×10^{-2} for lower loads and 1.48×10^{-2} for higher loads); Wearshield 70 (3.55×10^{-2} for lower loads and 4.96×10^{-3} for higher loads).

Abrasive wear with presence of normal vibration load (vibro-abrasion) showed strong dependence on vibration velocity. Depending on vibration velocity value, three regions could be distinguished for all coatings: (I) adaptation, (II) transition, and (III) nearly stationary region. In the adaptation region, the wear rates generally decrease with the increase of vibration velocity, which can be explained with the increase of the real contact area due to the small vibrations and smoothing of the contact surface. As a consequence, contact specific loads become lower so the wear rates decrease. In the transition region, sudden increase of the wear rate occurs for all coatings, which can be explained with the intensifying of fatigue failure processes, since the vibration velocities are higher. In the nearly stationary region, all coatings show apparent tendency to stabilise the wear rate and become independent of further vibration velocity increase. This is most probably due to the reached balance between two influential parameters: increase of wear due to intensifying of fatigue failure processes, and decrease of wear due to case-hardening and/or appearance of damping effects of some of the phases in the coatings.

Presence of vibration mainly showed negative effect on wear resistance. The exception is coating Wearshield 70 for which increase of vibration velocity above some value has beneficiary effect. This coating also showed approximately one order of magnitude lower wear rate in comparison to other coatings. Microstructure of this coating consists of small, well distributed Nb carbides embedded in relatively soft matrix, which prevented movement of the dislocation and increased hardness, shear strength and ductility. Therefore the cracks grow and propagation is reduced and dumping effect is increased, resulting in decrease of the abrasive wear rate in presence of vibrations.

References to Chapter 3

[1] **Davis, J. R.** Hardfacing, weld cladding, and dissimilar metal joining. – In: *ASM Handbook*, *Volume 6, Welding, Brazing, and Soldering*, ASM International, Metals Park, 1993, pp. 789-829.

[2] www.voestalpine.com/welding

[3] http://www.lincolnelectric.com

[4] http://www.oerlikon.com

[5] **Gualco, A., H. G. Svoboda, E. S. Surian, Luis A. de Vedia.** Effect of welding procedure on wear behavior of a modified martensitic tool steel hardfacing deposit. – *Materials and Design*, 31(9), 2010, pp. 4165-4173.

[6] **Mellor, B. G.** Welding surface treatment methods for protection against wear. – In: B. G. Mellor (Ed.), *Surface Coatings for Protection against Wear*. Cambridge: Woodhead Publishing, 2006, pp. 302-376.

[7] **Монов, А., М. Кандева.** Многокритериално изследване на композитни покрития при електродъгово равнинно наваряване. (Multi study of composite coatings in plane arc welding). – *Tribological Journal BULTRIB*, Vol. 2, 2012, 228-241.

[8] **Tonchev, N., M. Kandeva, N. Hristov.** Методика за определяне параметрите на качеството на композитни покрития при наваряване на ротационни повърхнини (Methodology for determining the quality parameters of the composite coating on surface of rotation welding). – *Proceedings of 8th International Congress "Machines, Technologies, Materials" (MTM 2011)*, Varna (Bulgaria), 19-21.09.2011, Vol. 1: Technologies, pp. 141-145.

[9] **Христов**, **Н. Д.** *Повишаване качеството на наварения метал чрез нанасяне на слоеве със специални свойства в условията на електродъгово наваряване* (*Improving the Quality of Weld Metal by Applying Layers with Special Properties in Terms of Arc Welding*). PhD Thesis. Висше транспортно училище „Тодор Каблешков", Sofia, 2011.

[10] **Tonchev, N., R. Lazarova, M. Kandeva, N. Hristov.** Металографски и механични изследвания на наварени слоеве със специфични свойства (Metallographic and mechanical investigations of fettled layers with specific properties). – *Journal of Fundamental Sciences and Applications*, Vol. 15, 2009, pp. 289-296.

[11] **Rac, A.** *Osnovi tribologije* (*Fundamentals of Tribology*). Belgrade: Mašinski fakultet Univerziteta u Beogradu, 1991.

[12] **Крагельский, И. В., В. В. Алисин (Eds.).** *Трение, изнашивание и смазка, кн. 2* (*Friction, Wear and Lubrication, Vol. 2*). Москва: Машиностроение, 1978.

[13] **Канарчук, В. Е.** *Адаптация материалов к динамическим воздействиям* (*Adaptation of Materials to Dynamic Impacts*). Киев: Наукова думка, 1986.

[14] **Блехман, И. И., Л. И. Блехман, В. Б. Васильков, К. С. Иванов, К. С. Якимова.** Об износе оборудования в условиях вибрации и ударных нагрузок (Wear and tear of machine parts affected by vibration and percussive impacts). – Вестник научно-технического развития, No 11, 2012, pp. 3-14.

[15] **Kandeva, M., T. Grozdanova, D. Karastoyanov, B. Ivanova, K. Jakimovska, A. Vencl.** Abrasive wear under vibrations of the spheroidal graphite cast iron microalloyed by tin. – *Journal of the Balkan Tribological Association*, Vol. 22, 2016, No 2. (In Press).

[16] **Kandeva, M., T. Grozdanova.** Effect of vibration velocity on the wear under conditions of abrasive friction. – *Proceedings of 14th International Conference on Tribology – SERBIATRIB '15*, Belgrade (Serbia), 13-15.05.2015, pp. 272-278.

[17] ISO 10816-1: *Mechanical Vibration – Evaluation of Machine Vibration by Measurements on Non-Rotating Parts – Part 1: General Guidelines*, 1995.

[18] **Furillo, F. T.** W-Mo carbides for hard-facing applications. – *Wear*, Vol. 60, 1980, No 1, pp. 183-204.

[19] **Wang, Q., X. Li.** Effects of Nb, V, and W on microstructure and abrasion resistance of Fe-Cr-C hardfacing alloys. – *Welding Journal*, Vol. 89, 2010, No 7, pp. 133s-139s.

[20] **Kumar, S., D. P. Mondal, H. K. Khaira, A. K. Jha.** Improvement in high stress abrasive wear property of steel by hardfacing. – *Journal of Materials Engineering and Performance*, Vol. 8, 1999, No 6, pp. 711-715.
[21] **Buchanan, V. E., P. H. Shipway, D. G. McCartney.** Microstructure and abrasive wear behaviour of shielded metal arc welding hardfacings used in the sugarcane industry. – *Wear*, Vol. 263, 2007, No 1-6, pp. 99-110.
[22] **Sundararajan, G.** The differential effect of the hardness of metallic materials on their erosion and abrasion resistance. – *Wear*, Vol. 162-164, Part B, 1993, pp. 773-781.
[23] **Vencl, A.** Tribological behavior of ferrous-based APS coatings under dry sliding conditions. – *Journal of Thermal Spray Technology*, Vol. 24, 2015, No 4, pp. 671-682.
[24] **Verbeek, H. J.** Tribological systems and wear factors. – Wear, Vol. 56, 1979, No 1, pp. 81-92.
[25] **Kato, K. K. Adachi.** Wear Mechanisms. – In: B. Bhushan (Ed.), *Modern Tribology Handbook*, CRC Press, Boca Raton, 2001, Chapter 7.

Chapter 4

HIGH VELOCITY OXYGEN FUEL (HVOF) SUPERALLOY COATINGS

4.1. Introduction

High velocity oxygen fuel (HVOF) spraying process belongs to the category of processes in which flame (combustion) energy is used as a source of thermal energy, and to the subcategory with high velocities of particles. This process uses a mixture of gaseous or liquid fuel and oxygen, which is fed into a combustion chamber, where they are ignited and combusted continuously. The coating material is in the powder form (typically size: 5-45 μm) [1], and it is fed axially through the gun into the chamber (for gas fuels) or radially after the chamber. Powder is generally transported using nitrogen or argon as a carrier gas (**Fig. 4.1**).

The combustion of the oxygen-fuel mixture produces a high temperature and high pressure in the chamber (approx. 5.5 bar for gas fuel and 5.5-8.3 bar for kerosene). This high pressure, produced in the combustion chamber, and the use of a converging-diverging expansion nozzle, which is usually located down-stream of the chamber, leads to the very high particle velocity (up to 600 m/sec for gas fuel and up to 700 m/s for kerosene). The pressure in the combustion chamber and the particle speed can be even higher with the newly developed equipment. The powder particles melt or partially melt in the combustion chamber and during the flight through the nozzle. The flame temperature varies in the range of 2500-3200 °C, depending on the fuel, the

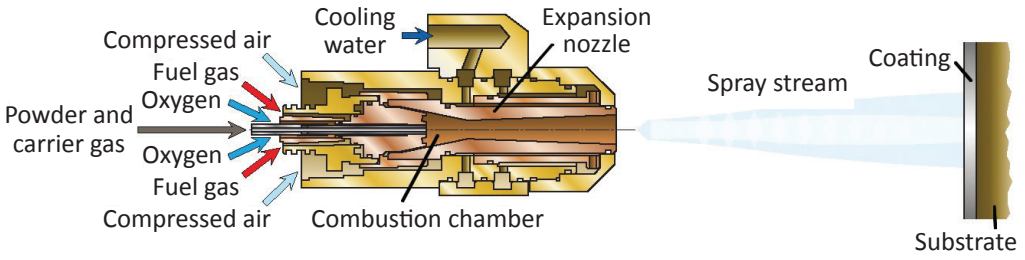

Fig. 4.1. Schematic drawing of the high velocity oxygen fuel spraying (HVOF) process with gas-fuel gun [2] (Reproduced by permission of Oerlikon Metco)

fuel gas/oxygen ratio and the gas pressure [3]. The combustion chamber, nozzle and barrel are intensively cooled by water.

The principle is somehow similar to that of the D-gun (detonation gun spraying). The difference is that in D-gun spraying the fuel burning is not continuous, i.e., it explodes with controlled detonation, and detonation wave accelerates the powder. The fuels in HVOF process can be gases (hydrogen, methane, propane, propylene, acetylene, natural gas, etc.) or liquids (kerosene, etc.) [1]. Typical deposition rates with gas fuel are: 4-8 kg/h (for metals) and 2-4 kg/h (for ceramics). With kerosene some 50 % increase of the deposition rate can be achieved. Noise level for gas fuel is approximately 125 dB, and 133 dB for kerosene.

Since coating is built up from flattened, fast solidified droplets the velocity plays an important role for the obtained density of the lamella structured coating. Temperature of the flame has a strong effect on the suitable materials to be sprayed. Ceramic coatings are mainly manufactured by using

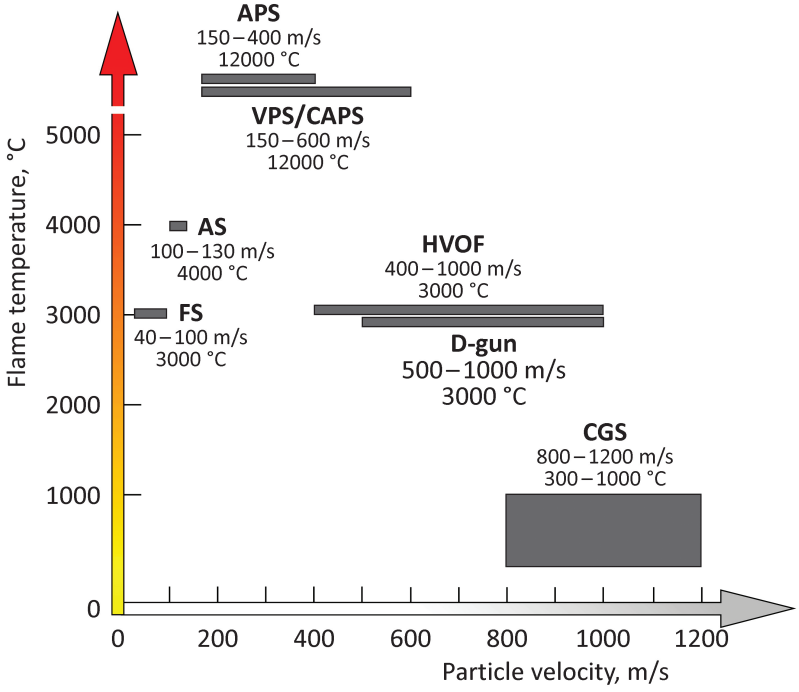

Fig. 4.2. Typical flame temperature and particle velocity operation ranges for various thermal spraying processes (FS – flame spraying; D-gun – detonation gun spraying; HVOF – high velocity oxygen fuel spraying; CGS – cold gas spraying; AS – electric arc wire spraying; APS – atmospheric plasma spraying; VPS – vacuum plasma spraying (VPS); CAPS – controlled atmosphere plasma spraying) [3]

atmospheric plasma spray method, while temperature sensitive materials, such as cermets, are more preferably sprayed by methods with a lower flame temperature [3]. Comparison of the various thermal spraying processes by the typical operation ranges of flame temperature and particles velocity is shown in **Fig. 4.2**.

As a result of the high kinetic energy transferred to the particles through the HVOF process, the coating material generally does not need to be fully melted (no need for very high temperatures), so it undergoes only slight metallurgical changes as a result of the spray process, e.g. minimal formation of mixed carbides. Additional key advantages would be: low oxide content (particles spend less time within the flame and flame temperature is lower); high density and low porosity (< 1 %) with fine, homogeneous structures; excellent adhesion (bond strength as high as 90 MPa); absence of high compressive stress, which may results in very thick coatings. HVOF process is widely used to produce cermet and metal coatings, but it has also been demonstrated to be able to deposit dense ceramic coatings. The most used powders are composites with carbide reinforcements and metal or alloy matrices [1].

High velocity oxygen fuel spraying (HVOF) process is one of the processes with the perspective future development. It is in the group of processes with high kinetic energy of sprayed particles, but having a relatively low temperature in which the "time of flight" is short and they impact on the substrate without being molten. Together with HVOF spraying, in this group are: high velocity air fuel (HVAF) spraying, D-gun, Super D-gun, Sonarc, and cold gas spraying (CGS). These techniques are adapted to spray materials of relatively low melting point, which: modify their chemical composition at spraying, such as, carbides which decarburize; melt inadequately, forming the phases less interesting from the point of view of future application, such as, "multi-oxides" (e.g. yttrium barium copper oxide – YBCO) [1].

This chapter considers solutions for the improvement of the wear resistance of equipment used in road construction, agricultural, mining and other industries [4-6], which are exposed to heavy-duty operating conditions, under the high temperatures and pressures in abrasive, erosive and corrosive environment. Some of the tested coatings are already implemented in exploitation conditions in mines of the "Maritsa Iztok-3" power plant in Bulgaria. This case study presents results of the research, carried out in two stages. The first stage considers optimization of the deposition parameters for various superalloy coatings, based on the analysis of hardness, porosity and roughness characteristics. It was done through the selection of the three deposition parameters: fuel/oxygen ratio, particles velocity and spraying distance [7-8].

In the second stage, wear resistance of the obtained coatings, produced under optimal technological regime, were investigated and analysed. The idea of the researches was to compare different coatings according their wear resistance under conditions of abrasive wear [9-11], and under conditions of erosive wear [12]. In addition, influence of preheating on abrasive wear and influence of preheating, different substrate and some deposition parameters on erosive wear was also investigated.

4.2. Optimisation of the deposition parameters

4.2.1. Materials

The substrate material for all coatings was a low-carbon steel, with chemical composition shown in **Table 4.1**. Hardness of the substrate was between 193.6 and 219.5 HV.

Table 4.1. Chemical composition (wt. %) of the coated material (low-carbon steel substrate)

Element	C	Si	Mn	Ni	P	S	Cr	Fe
Percentage	0.15	0.21	0.8	0.30	0.011	0.025	0.30	Balance

Six different commercial powder coating materials (502P, 602P, F382F, 6P50W, SX 199 and WC-12Co) have been used in experiments. Their chemical compositions, taken from the manufacturer and some physical and mechanical properties are shown in **Tables 4.2** to **4.7**. The powders were produced by the agglomeration process with a sintering stage, and the average size of the powder particles was 45 ± 2.5 μm.

The basic interactions between the components of the powders presented in **Tables 4.2** to **4.7** could be briefly described as [7-8]: (**a**) at high temperatures chromium (Cr) combines with carbon (C), silicon (Si) and boron (B) creating metalloids; with carbon it forms hard chrome carbide (Cr_3C_2), which does not dissolve in acids; presence of impurities makes chromium brittle; (**b**) at high temperatures boron (B) combines with iron (Fe) and nickel (Ni) forming borides; with carbon (C) it forms boron carbide (B_4C) of very high hardness; (**c**) nickel (Ni) in the composition of superalloy coatings exhibits ferromagnetic properties; in the presence of oxygen and high temperatures it reacts with oxygen and forms hard nickel oxide (NiO); (**d**) cobalt (Co) and iron (Fe), like nickel, show ferromagnetic properties in the composition of superalloy coatings; (**e**) molybdenum (Mo) with iron (Fe) for an alloy, and at high

Table 4.2. Properties of the powder 502P

Chemical composition, wt. %	Melting point, °C	Mohs hardness
Cr: 13.94	1907	8.5
Si: 3.65	1414	7
B: 2.52	2076	9.5
Fe: 4.19	1538	4
Co: 0.03	1495	5
C: 0.59	3550	–
Ni: Balance	1455	4
Surface temperature during the deposition at 120 mm distance: 275 °C		
Coating adhesion: 38-41 MPa		

Table 4.3. Properties of the powder 602P

Chemical composition, wt. %	Melting point, °C	Mohs hardness
Cr: 13.2	1907	8.5
Si: 3.98	1414	7
B: 2.79	2076	9.5
Fe: 4.6	1538	4
Co: 0.03	1495	5
C: 0.63	3550	–
Ni: Balance	1455	4
Surface temperature during the deposition at 120 mm distance: 263 °C		
Coating adhesion: 42-43 MPa		

Table 4.4. Properties of the powder F382F

Chemical composition, wt. %	Melting point, °C	Mohs hardness
Cr: 17.3	1907	8.5
Mo: 2.2	2623	5.5
C: 0.019	3550	–
Si: 0.9	1414	7
S: 0.009	115.2	2
P: 0.02	44.1	–
Mn: < 0.3	1246	6
Fe: Balance	1538	4
Surface temperature during the deposition at 120 mm distance: 266 °C		
Coating adhesion: 42-43 MPa		

Table 4.5. Properties of the powder 6P50W

Chemical composition, wt. %	Melting point, °C	Mohs hardness
Cr: 13.15	1907	8.5
Si: 4.28	1414	7
B: 2.87	2076	9.5
Fe: 0.04	1538	4
Ni: 29.6	1455	4
Co: 0.04	1495	5
C: 0.58	3550	–
W: Balance	3422	7.5
Surface temperature during the deposition at 120 mm distance: 145 °C		
Coating adhesion: 44-47 MPa		

Table 4.6. Properties of the powder SX 199

Chemical composition, wt. %	Melting point, °C	Mohs hardness
Cr: 21	1907	8.5
WC–Cr_3C_2–Ni: 6.1	3370	9
C: 5.8	3550	–
W: Balance	3422	7.5
Surface temperature during the deposition at 120 mm distance: 115 °C		
Coating adhesion: 51-54 MPa		

Table 4.7. Properties of the powder WC-12Co

Chemical composition, wt. %	Melting point, °C	Mohs hardness
Co: 12	1495	5
C: 5.4	3550	–
Fe: < 0.1	1538	4
Ni: < 0.1	1455	4
W: Balance	3422	7.5
Surface temperature during the deposition at 120 mm distance: 95 °C		
Coating adhesion: 63-69 MPa		

temperatures it reacts with oxygen and form molybdenum trioxide (MoO_3); (**f**) at high temperatures tungsten (W) with carbon forms very hard tungsten carbide (WC); cobalt (Co) acts as a binder with the tungsten matrix.

4.2.2. Experimental details

Characteristics of the thermal spray coatings (metallography, hardness and tensile bond strength) were accepted as a standard one. These characteristics are mutually connected and are dependent on many parameters. Generally these parameters could be divided into two groups: substrate preparation parameters and spray deposition parameters.

Substrate preparation parameters affect most of all bond strength between substrate and coatings. They include: surface roughness and cleanliness, substrate temperature, presence of the absorb moisture and gases and presence of entrapped particles used for surface roughening. Parameters that are important in choosing the abrasive for surface roughening are: type, size, shape, purity and hardness. Impact pressure and angle are also important. Inadequate surface cleanliness and presence of entrapped abrasive particles decrease the bond strength, so they should be avoided. Presence of the absorb moisture and gases can increase the porosity of coating, i.e. any foreign matter, on or just below the surface of the base material, which tends to evolve gas during deposition can cause bubbles. Substrate temperature can be important for presence of cracks, i.e. during cooling, if the expansion coefficient (and hence the contraction) of the substrate material is appreciably less than that of the coating, stresses build up and the coating may crack [13].

HVOF spraying is a very complex process, which has a great number of parameters affecting the coating formation and hence coating properties. The most commonly controlled parameters are: nozzle geometry, spraying distance, powder feed rate, fuel/oxygen ratio and gas flow density. In the spray process, the powder particles experience very high speed combined with fast heating up to its melting point or above. This high temperature may cause evaporation of the powder or some components of it, dissolution, and phase transformations [3]. Powder feed rate and spray distance are responsible for the amount of unmelted particles and precipitates. If the feed rate is too big or the spray distance is too short the powder particles do not melt completely which results in a high amount of unmelted particles. Presence of the unmelted particles and precipitates decrease the coating characteristics. Porosity shows similar effect. Presence of the oxides has dual effect, positive and negative, depending on the type of oxide and some other properties [13,14].

High velocity oxygen fuel spraying (HVOF) process, with GMA 6GII powder spray gun and propane (C_3H_8) fuel, was utilized in the experiment. Before

the spraying process, surface of the substrate was cleaned and roughened. Cleaning of the substrate surface from moisture, oxides and other contaminants was done by preheating of the substrate and subsequent treating with solvent. The surface of the substrate was roughened and activated by abrasive grit blasting, according to the requirements of ISO 11126. The chemical composition (wt. %) of the abrasive particles was: SiO_2 (> 41%), AlO (8.3-15.5%), MgO (3.2-10%), CaO (4-7%) and MnO (0.4-1.2%). The particle-size distribution was as follows: 3.15-1.4 mm (9.32%); 1.63-0.5 mm (16.4%); 1.4-1.0 mm (15.8%); 1.0-0.63 mm (39.6%); 0.5-0.315 mm (9.32%); 0.315-0.16 mm (9.32%); particles of size below 0.15 mm (balance). The parameters of the abrasive grit blasting were: inlet pressure: 0.4 MPa; operation pressure in the nozzle: 0.4 MPa; nozzle diameter: 7 mm; distance between nozzle and surface: 30 mm; impact angle: 90°.

All six coatings have been deposited under three technological deposition regimes (R1, R2 and R3), with different spray deposition parameters. Parameters used in each of the regime are shown in **Table 4.8**. Specimens were fixed on cylindrical support which rotates with rotational speed of 1.5 rpm. Three parameters that were varied were: fuel/oxygen ratio, particles velocity and spraying distance.

Spray deposition parameters were optimized according to the microstructure (porosity), hardness and roughness of the obtained coatings. Measurements of surface hardness (HRC) were performed on surfaces of the samples by using the Rockwell portable hardness tester. Each sample is deposited with various thicknesses (50, 100, 150, 200, 250, 300 and 350 μm) and hardness is measured. The roughness of the coatings was examined with mechanical profilometer, according to the ISO 4287 and ISO 4288. Surface roughness of the coatings samples is presented through the arithmetic mean deviation of

Table 4.8. Spray deposition parameters

Parameter	Value		
	R1 regime	R2 regime	R3 regime
Fuel/oxygen (C_3H_8/O_2) ratio	45/100	55/100	55/100
Particle velocity, m/s	700	1000	1000
Spraying distance, mm	80	120	160
Impact angle, °	90	90	90
Air pressure, MPa	0.5	0.5	0.5
Nitrogen pressure, MPa	0.4	0.4	0.4
Powder feed rate, g/min	22	22	22

the assessed profile (*Ra*). Measurement was performed in at least five points on the surface of coatings and the average value is presented.

4.2.3. Results and Discussion

Surface hardness of the obtained coatings was determined for various thicknesses, for each of the three technological deposition regimes (R1, R2 and R3). The corresponding hardnesses are presented in **Table 4.9**. In addition, differences between the highest and lowest value of hardness (increase of hardness), for each coating and each regime, was calculated and presented in **Table 4.9**.

In order to visually perceive the results shown in **Table 4.9**, six diagrams (for each coating) are presented (**Figs. 4.3** to **4.8**), showing the influence of technological deposition regime on the hardness distribution along the coating thickness. Hardness of all coatings decrease from surface toward the sub-

Table 4.9. Hardness distribution along the thickness of tested coatings

Coating designation	Regime	Hardness HRC							Increase of hardness
		Coating thickness, µm							
		50	100	150	200	250	300	350	
502P	R1	52	54	55	55	55	55	55	3.0
	R2	54	55	57	58	58.5	59	60	6.0
	R3	49	49	50	50	51.5	52	53	4.0
602P	R1	58.2	58.6	59	59.4	60.2	60.4	60.6	2.4
	R2	58.4	59.1	59.9	60.7	60.9	61	62	3.6
	R3	57.8	58.4	58.9	60	60.1	60.2	60.4	2.6
F382F	R1	15.5	16.5	17	18	19	20	20	4.5
	R2	18	20	23	24.5	25.5	26	26	8.0
	R3	19.5	21.5	24	24.8	25	25	25.1	5.6
6P50W	R1	52.3	53.9	55.5	57.5	57.8	58	58.3	6.0
	R2	58	59.7	59.9	60.3	60.7	61.8	62	4.0
	R3	56.5	57.5	58.8	59.4	60.3	61.4	61.6	5.1
SX 199	R1	57	63	65	66	67	68	68	11.0
	R2	66	68	69	69	70	71	72	6.0
	R3	55	56	58	60	61	61	61	6.0
WC–12Co	R1	68.35	68.35	68.4	68.45	68.48	68.5	68.5	0.2
	R2	68.6	68.65	68.7	68.8	68.9	70	70	1.4
	R3	67.3	67.5	67.9	68.3	68.4	68.5	68.5	1.2

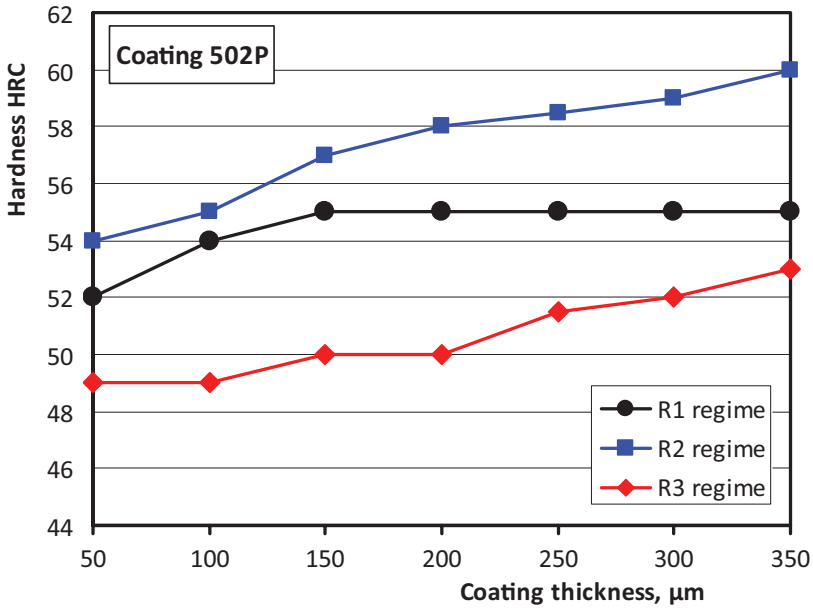

Fig. 4.3. Hardness distributions along the thickness of 502P coating

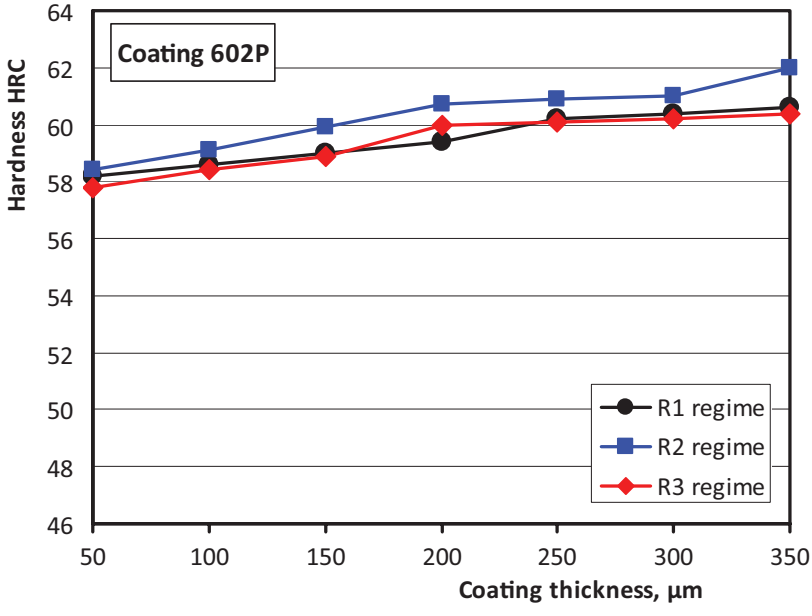

Fig. 4.4. Hardness distributions along the thickness of 602P coating

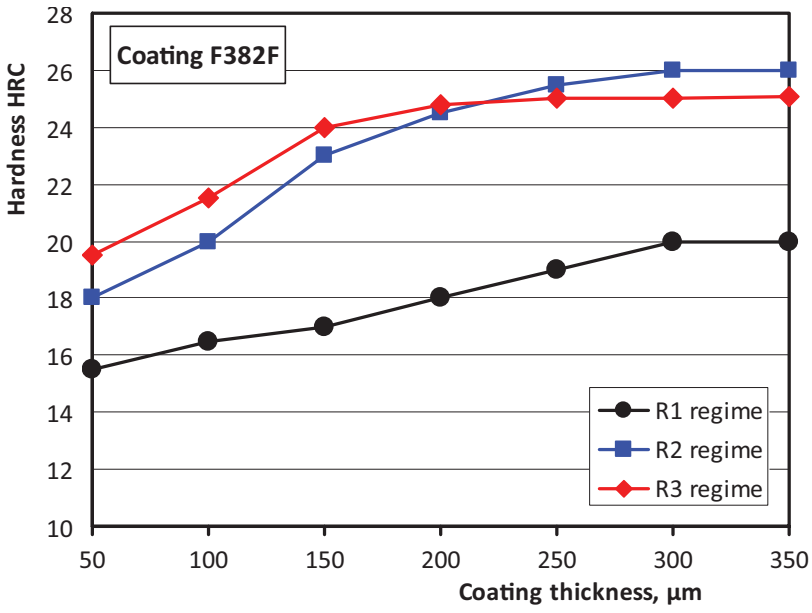

Fig. 4.5. Hardness distributions along the thickness of F382F coating

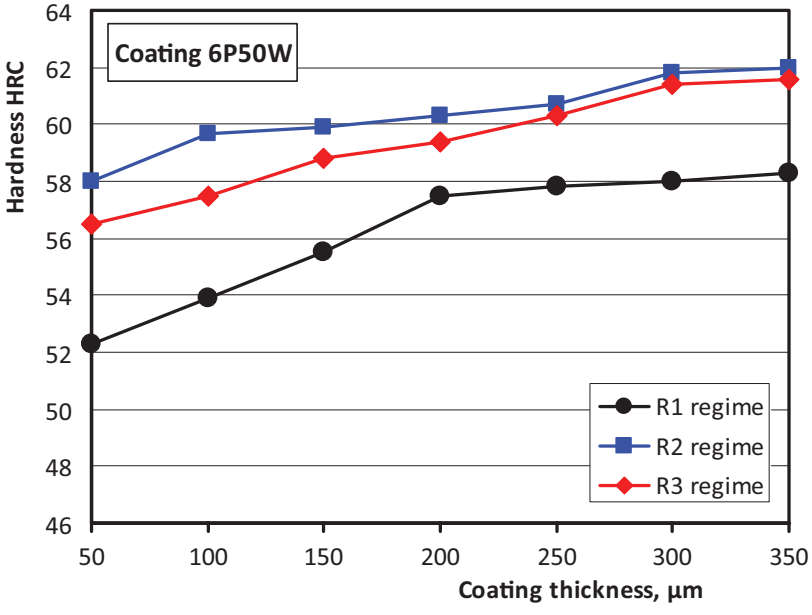

Fig. 4.6. Hardness distributions along the thickness of 6P50W coating

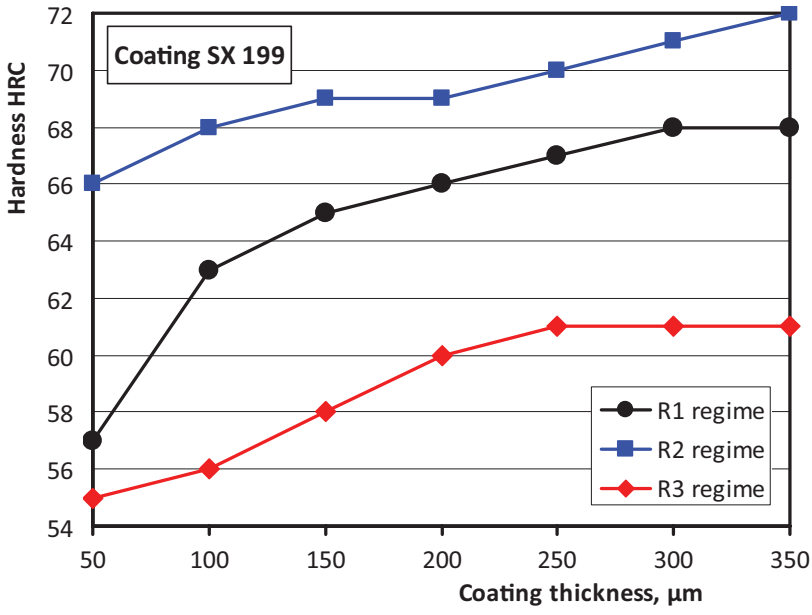

Fig. 4.7. Hardness distributions along the thickness of SX 199 coating

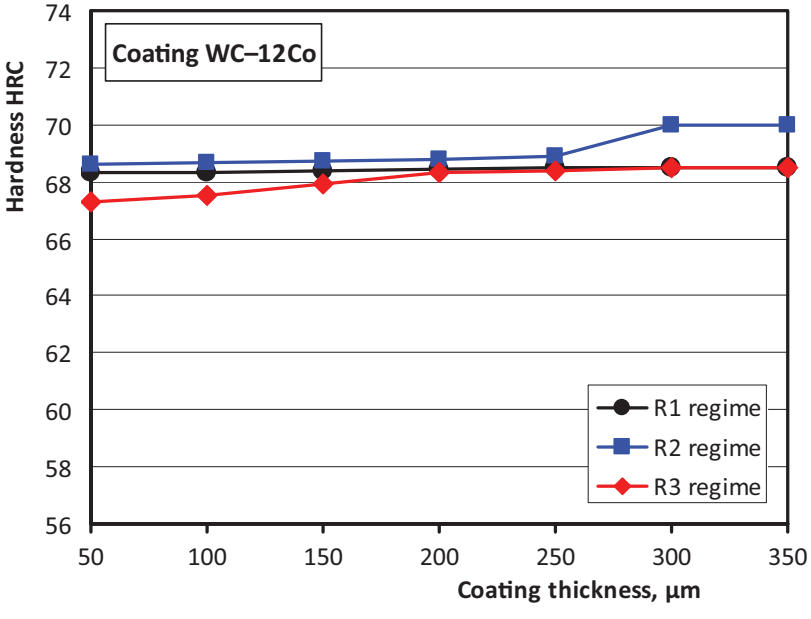

Fig. 4.8. Hardness distributions along the thickness of WC–12Co coating

Table 4.10. Porosity and surface roughness of tested coatings for three deposition regimes

Coating designation	Porosity, %			Surface roughness (*Ra*), μm		
	Regime			Regime		
	R1	R2	R3	R1	R2	R3
502P	3.7	2.5	4.7	12	7	6.5
602P	3.4	1.45	4.3	10	10	10
F382F	3.7	2	4.3	10	10	10
6P50W	3.25	1.55	3.8	9	7	9
SX 199	3.55	2.3	4.55	9	6	8
WC–12Co	3.3	1.4	4.3	13	10	12

strate, i.e., all coatings, in all regimes, showed the highest value of hardness on the surface (for thickness of 350 μm). Comparison of different technological deposition regimes showed that, for all coatings, the highest hardness is obtained for the R2 regime. The increase of hardness (difference between the hardness at surface and at 50 μm thickness) was also the highest for R2 regime in most of the cases (**Table 4.9**). This regime (fuel/oxygen ratio, particle velocity, spraying distance) could be accepted as optimal for tested coatings. Comparison of different coatings showed that the highest hardness had coatings SX 199 (72 HRC) and WC–12Co (70 HRC). Coatings 502P, 602P and 6P50W showed slightly lower hardness of 60, 62 and 62 HRC, respectively, while the lowest hardness was obtained for coating F382F (26 HRC).

Porosity of the obtained coatings was determined for each of the three technological deposition regimes (R1, R2 and R3). The corresponding values are presented in **Table 4.10**. In addition, surface roughness of the coatings was also measured and presented, through the arithmetic mean deviation of the assessed profile (*Ra*), in **Table 4.10**. The investigated coatings have relatively high hardness, and if the hardnesses of solids in contact are not the same, the more important is the roughness of the harder material, because asperities of the harder surface plough the surface of the softer body [15].

In order to visually perceive the results shown in **Table 4.10**, two diagrams are presented, showing the influence of deposition regime on porosity (**Fig. 4.9**) and on surface roughness (**Fig. 4.10**).

Surface roughnesses did not differ too much between the same coating and different deposition regime, nor between different coatings. Values of the arithmetic mean deviation of the assessed profile (*Ra*) from 6 to 13 μm were obtained for all coatings and all regimes. These values are relatively high when high tolerances of machine parts are require, so the subsequent

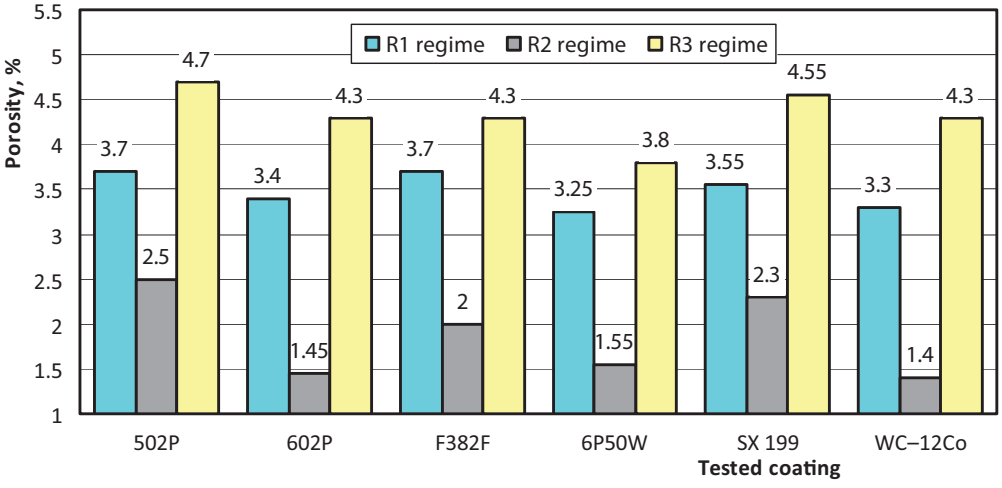

Fig. 4.9. Influence of the deposition regime (R1, R2 and R3) on porosity of tested coatings

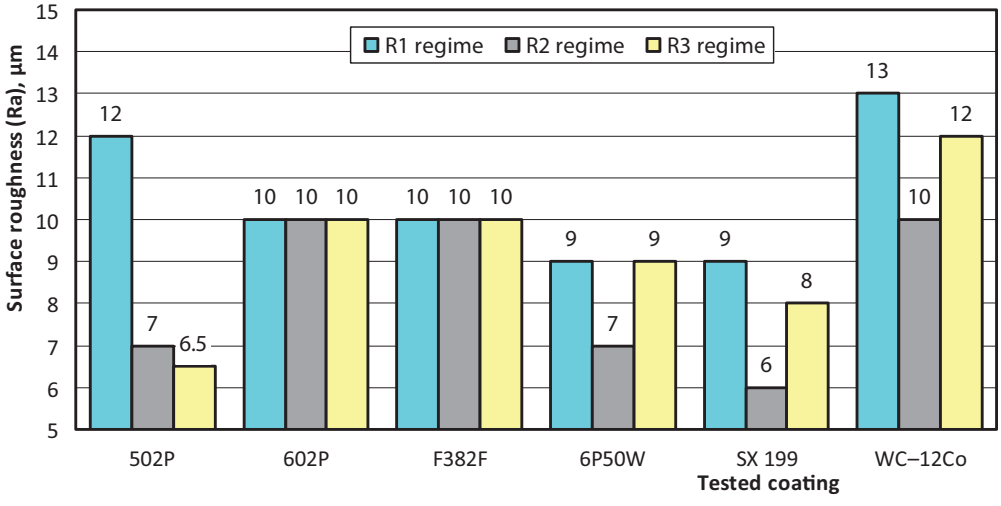

Fig. 4.10. Influence of the deposition regime (R1, R2 and R3) on surface roughness of tested coatings

machining is necessary. Nevertheless, R2 deposition regime generally obtained the lowest roughness values, for all tested coatings.

Values of porosity were similar between different coatings deposited with same regime. Generally, the porosity values are low for thermal spray coatings, but not for HVOF coatings, since HVOF process is the technique that produces

the densest coatings among all of the thermal spraying techniques. Typical values of porosity in HVOF coatings are less than 1-2% [1, 2], and some coatings can have porosity lower than 0.5% [2, 16]. Porosity is very important in some coatings, e.g. corrosion resistance coatings, where the value of porosity lower than 1% is considered as suitable for protecting the substrate material against corrosion [3]. Pores and defects in coatings create paths for corrosive fluids or aggressive chemicals to attack the substrate material. This local damage can quickly lead to critical component failure. Porosity can also affect the performance of the coated part in cyclic fatigue conditions where such defects can become stress concentrators which initiate mechanical failures.

Porosity and hardness of coating are often in good correlation. In general, increase of porosity results in decrease of coating hardness. In many cases, however, the hardness is not a simple function of density, but a function of a number of factors, including oxide or carbide content and elemental segregation. Therefore, anomalies in the correlation between hardness and density may occur [16]. Correlation between porosity and hardness of tested coatings deposited at different regimes is shown in **Fig. 4.11**. It could be noticed that, except for coatings F382F and 6P50W, this correlation is good, since the R^2 (R-squared) values are high (R^2 = 1 is a perfect fit).

The lowest porosity values are obtained for the R2 deposition regime, for all coatings. This regime had higher particles velocity and higher fuel/oxygen ratio than R1 regime, which induced higher energy of the particles and higher density of the coatings. It also had lower spraying distance than R3 regime, which means lower retention of particles in the flame and lower amount of oxides and unmelted (solidified) particles, so the porosity values are lower [17]. Coatings 602P, 6P50W and WC–12Co had porosity lower than 2%, i.e. 1.45, 1.55 and 1.4%, respectively. Other three coatings had slightly higher porosity values, i.e. 502P (2.5%), F382F (2%) and SX 199 (2.3%).

4.3. Abrasive wear testing

4.3.1. Materials and deposition conditions

The substrate material for all coatings was a medium-carbon steel, with chemical composition shown in **Table 4.11**. Hardness of the substrate was between 198.4 and 220.5 HV.

Table 4.11. Chemical composition (wt. %) of the coated material (medium-carbon steel substrate)

Element	C	Si	Mn	Ni	P	S	Cr	Fe
Percentage	0.4	0.20	0.55	0.30	0.45	0.045	0.30	Balance

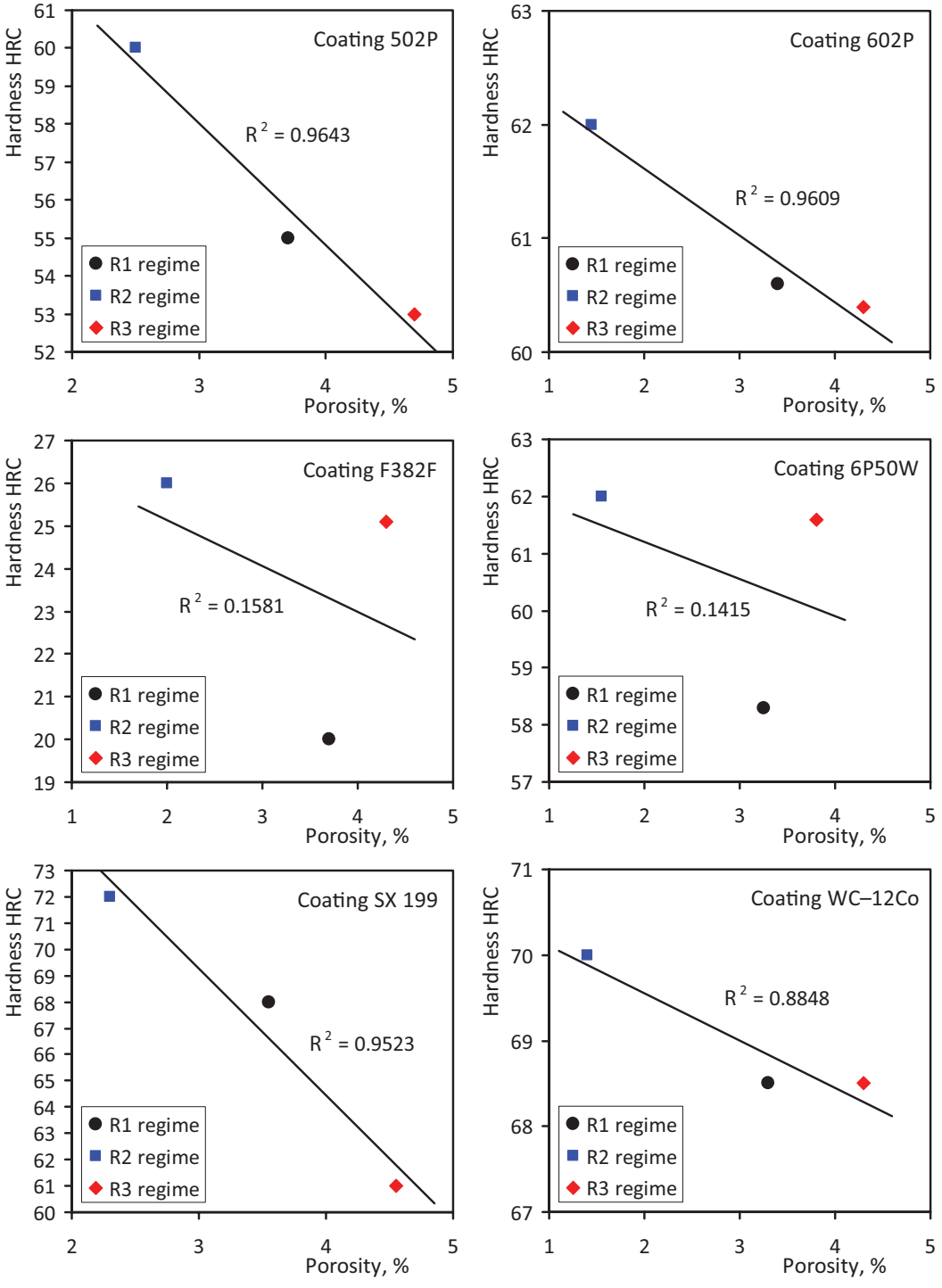

Fig. 4.11. Porosity vs. hardness for tested coatings at different deposition regimes (R1, R2 and R3)

Ten different coatings, obtained by deposition of various powder coating materials (Ni-, W-, Ni+W-, Cr_2O_3-, and Al_2O_3-based), have been used in experiments. Coatings designations and corresponding powder chemical compositions, taken from the manufacturer, are shown in **Table 4.12**. The powders were produced by the agglomeration process with a sintering stage, and the average size of the powder particles was 45 ± 2.5 μm (502P, 602P, and WC–12Co) and 35 ± 2.5 μm (80M60, 6P50W, SX 199, Cr_2O_3, Al_2O_3–$3TiO_2$ and Al_2O_3–$40TiO_2$). Samples 4 and 9 were deposited on surface preheated to 650 °C (PHS). Powders WC–12Co, 602P–6P50W–(WC–12Co), Al_2O_3–$3TiO_2$and Al_2O_3–$40TiO_2$ are mixtures of two or three powders.

Table 4.12. Coating designation and appropriate powder chemical composition (wt. %)

Sample	Coating designation	Powder chemical composition, wt. %
1	502P	Cr: 13.94; Si: 3.65; B: 2.52; Fe: 4.19; Co: 0.03; C: 0.59; Ni: Balance
2	602P	Cr: 13.2; Si: 3.98; B: 2.79; Fe: 4.6; Co: 0.03; C: 0.63; Ni: Balance
3	80M60	Cr: 14.2; Si: 4.37; C: 0.6; B: 2.9; Fe: 4.54; Cu: 2.36; Mo: 2.51; Co: 0.01; Ni: Balance
4	80M60: PHS*	
5	6P50W	Cr: 13.15; Si: 4.28; B: 2.87; Fe: 0.04; Ni: 29.6; Co: 0.04; C: 0.58; W: Balance
6	SX 199	Cr: 21; WC–Cr_3C_2–Ni: 6.1; C: 5.8; W: Balance
7	WC–12Co	Co: 12; C: 5.4; Fe: < 0.1; Ni: < 0.1; W: Balance
8	602P–6P50W–(WC–12Co)	Mixture ratio (1:1:1)
9	602P–6P50W–(WC–12Co): PHS*	
10	Cr_2O_3	Al_2O_3 < 0.03; SiO_2 < 0.07; Fe_2O_3 < 0.02; CaO < 0.03; MgO < 0.01; TiO_2 < 0.02; Cr_2O_3: Balance
11	Al_2O_3–$3TiO_2$	Mixture ratio (97:3) TiO_2: 2.25; SiO_2 < 0.014; Fe_2O_3 < 0.01; Cao < 0.01; MgO < 0.014; Al_2O_3: Balance
12	Al_2O_3–$40TiO_2$	Mixture ratio (60:40) TiO_2: 38.25; SiO_2 < 0.014; Fe_2O_3 < 0.01; Cao < 0.01; MgO < 0.014; Al_2O_3: Balance

*These coatings were deposited on preheated surface.

High velocity oxygen fuel spraying (HVOF) process, with GMA 6GII powder spray gun and propane (C_3H_8) fuel, was utilized in the experiment. Before the spraying process, surface of the substrate was cleaned and roughened. Cleaning of the substrate was done by preheating of the substrate and subsequent treating with solvent. The surface of the substrate was roughened and activated by abrasive grit blasting (SiO_2 particles with average size of 1 mm). The coatings are deposited on prismatic plates having the dimensions of 80 × 20 × 7 mm. The target coating thickness was 350 µm for coatings. The optimal deposition parameters, obtained in the fist stage of the research (R2 deposition regime), were applied for all coatings (**Table 4.8**).

4.3.2. Microstructure, thickness, roughness and hardness characteristics

Microstructural characterizations of coatings were performed on the cross-section of the samples by means of optical microscopy. Microstuctures of some typical coating samples are shown in **Fig. 4.12**.

Coatings thickness was measured in ten points on each coating surface, and the average values are shown in **Table 4.13**. The roughness of the coatings was examined with mechanical profilometer. Measurement was performed in at least five points on the surface of coatings and the average roughness, presented through the arithmetic mean deviation of the assessed

Table 4.13. As-deposited thickness, porosity, roughness and hardness of tested coatings

Sample	Coating designation	Thickness, µm	Porosity, %	Roughness (*Ra*), µm	Hardness HRC
1	502P	360	2.5	7	60
2	602P	350	1.45	10	62
3	80M60	340	3	10	62
4	80M60: PHS	350	1.8	8	60
5	6P50W	380	1.55	7	65
6	SX 199	325	2.3	6	64
7	WC–12Co	330	1.4	10	70
8	602P–6P50W–(WC–12Co)	360	1.5	8	68
9	602P–6P50W–(WC–12Co): PHS	380	1.1	6	70
10	Cr_2O_3	350	3	12	58
11	Al_2O_3–3TiO_2	330	2	7	64
12	Al_2O_3–40TiO_2	340	2.8	8	58

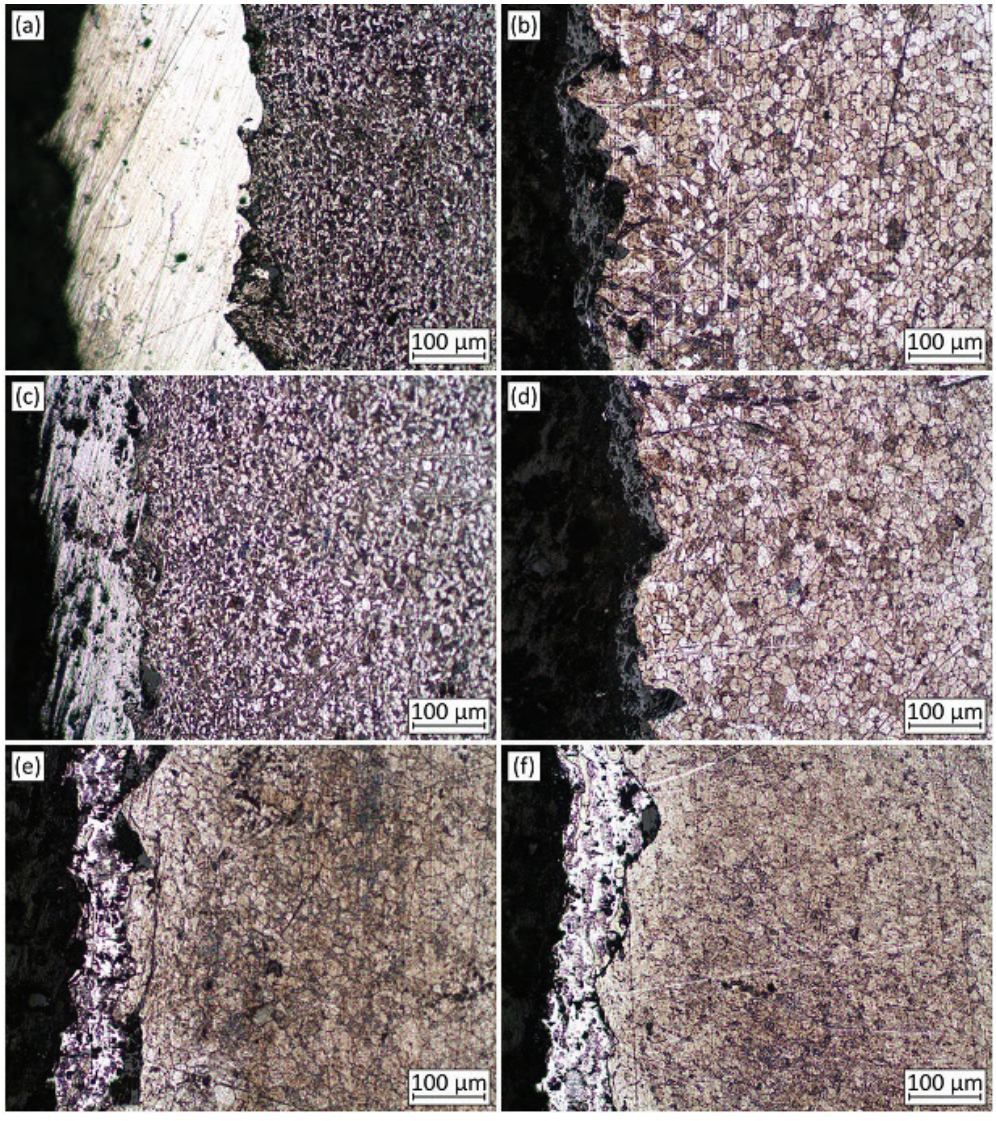

Fig. 4.12. Microstructure properties of some of the tested coatings:
(a) coating 602P, (b) coating 80M60: PHS, (c) coating WC–12Co, (d) coating 6P50W–602P–(WC–12Co), (e) coating Al_2O_3–3TiO_2, and (f) coating Al_2O_3–40TiO_2

profile (*Ra*), are presented in **Table 4.13**. Measurements of surface hardness (HRC) were carried out using Rockwell hardness tester. At least three measurements were made for each sample in order to eliminate possible segregation effects and to obtain a representative value of the material hardness. The results are shown in **Table 4.13**.

4.3.3. Experimental details

Abrasive wear tests were carried out on pin-on-disc tribometer in accordance with appropriate standard procedure [18], in the ambient air at room temperature. A schematic diagram of pin-on-disc tribometer is presented in **Fig. 4.13**. Samples for abrasive wear testing, having diameter of 15.3 mm, were cut from as-deposited samples. They are ground and polished to thickness of 310 µm, and roughness of Ra = 2.5 µm.

A cylindrical specimen (pin) with deposited coating (1) is fixed in a holder (2) of the loading box (3). A central normal load (F_n) is given through a leverage system in the loading box. The end of a pin (1), which was not rotating about its axis, is positioned perpendicular to the impregnated corundum abrasive paper (4) with grain size of 201 µm (P80 grit). The abrasive paper is fastened to, and supported by a flat horizontal rotating disc (5). The disc, driven by AC motor (6), rotates with given constant rotational speed (n) about its vertical axis. The tribometer allows sliding velocity variation by changing disc rotational speed and/or by changing the distance between rotational axis of disc and axis of sample (R).

Abrasive wear is calculated as a mass loss, i.e., as a difference between the initial mass of the sample and its mass after given number of abrasion cycles (N), counted by the counter (pos. 7 in **Fig. 4.13**). The abrasive wear is presented and analysed through the mass wear rates. Before and after testing, the coated disc was degreased and cleaned, and its mass is measured by the electronic balance with accuracy of 0.1 mg. Normal load of 471 g (4.62 N) was constant for all tests and coatings. Taking into account the assumed contact area (sample cross-sec-

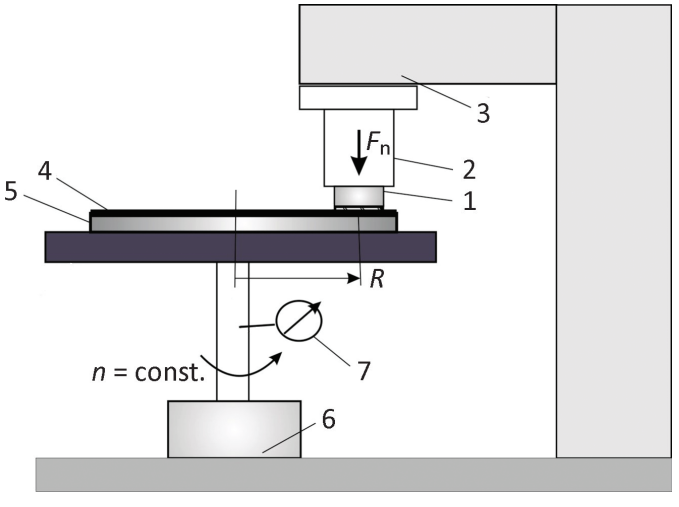

Fig. 4.13. Schematic diagram of abrasive wear testing on pin-on-disc tribometer

tion area) of approximately 1.84 cm^2 (diameter of the cylindrical test specimens was 15.3 mm), the specific load was 2.51 N/cm^2. The rotational speed of disc (*n*) was constant, i.e. *n* = 40 rpm, and the distance between rotational axis of disc and axis of sample (*R*) was 37 mm. Thus, the sliding velocity of the pin is 0.155 m/s. The sliding distance (*s*) is calculated from the following equation:

$$s = 2R\pi \cdot \mathrm{N}, \tag{4.1}$$

where *R* is the distance between rotational axis of disc and axis of sample, and N is the number of abrasion cycles.

4.3.4. Results and Discussion

Abrasive wear of the coatings was determined at various number of cycles, i.e. at N = 500, 1000, 1500, 2000 and 2500, and corresponding mass losses are presented in **Table 4.14**. Obtained results of the mass loss (**Table 4.14**) are also shown as a function of sliding distance, in the form of the comparative wear curves. The wear curves for coatings 502P and 602P are shown in **Fig. 4.14**, for coatings 80M60 and 80M60: PHS in **Fig. 4.15**, for coatings 6P50W

Table 4.14. Abrasive wear of tested coatings

Sample	Coating designation	Number of cycles (N)				
		500	1000	1500	2000	2500
		Sliding distance, m				
		116.2	232.5	348.7	465.0	581.2
		Mass loss, mg				
1	502P	8.6	18.1	25.6	30.2	31.3
2	602P	4.5	5.9	7.2	7.9	8.8
3	80M60	7.2	8.8	10.5	12.2	13.5
4	80M60: PHS	2.0	3.3	4.7	5.1	6.7
5	6P50W	1.8	2.2	2.8	3.0	3.2
6	SX 199	5.0	6.5	8.0	8.9	10.5
7	WC–12Co	0.5	0.8	0.9	1.2	1.4
8	602P–6P50W–(WC–12Co)	3.2	4.7	5.2	5.6	6.3
9	602P–6P50W–(WC–12Co): PHS	18.0	18.8	20	22.6	25.8
10	Cr_2O_3	17.5	25.4	35.1	40.8	44.6
11	Al_2O_3–3TiO_2	44.4	86.2	109.4	126.5	160.9
12	Al_2O_3–40TiO_2	14.7	21.8	29.8	36.4	38.3

and SX 199 in **Fig. 4.16**, for coatings WC–12Co and 602P–6P50W–(WC–12Co) in **Fig. 4.17**, for coatings 602P–6P50W–(WC–12Co): PHS and Cr_2O_3 in **Fig. 4.18** and for coatings Al_2O_3–3TiO_2 and Al_2O_3–40TiO_2 in **Fig. 4.19**.

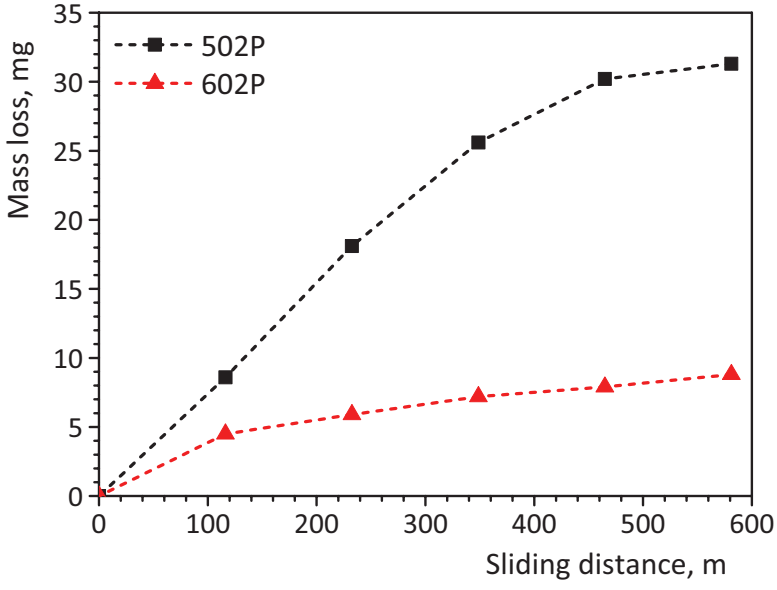

Fig. 4.14. Mass loss vs. sliding distance for coatings 502P and 602P

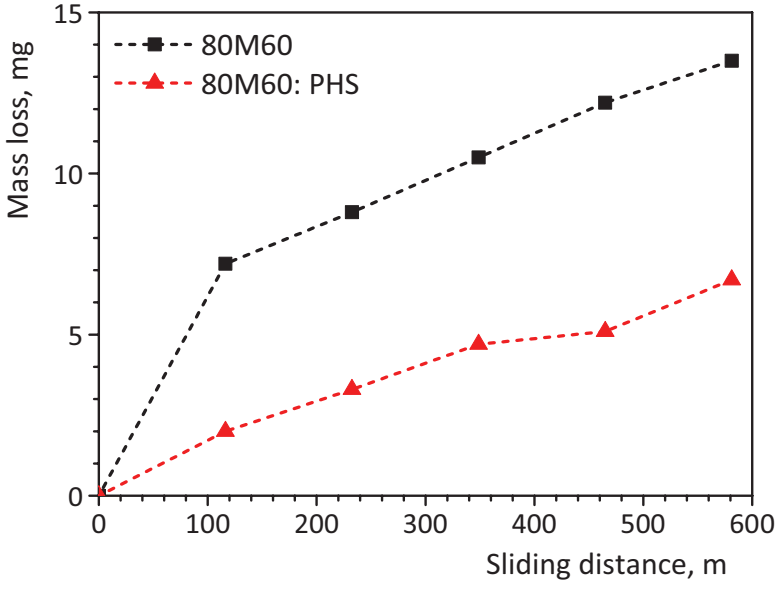

Fig. 4.15. Mass loss vs. sliding distance for coatings 80M60 and 80M60: PHS

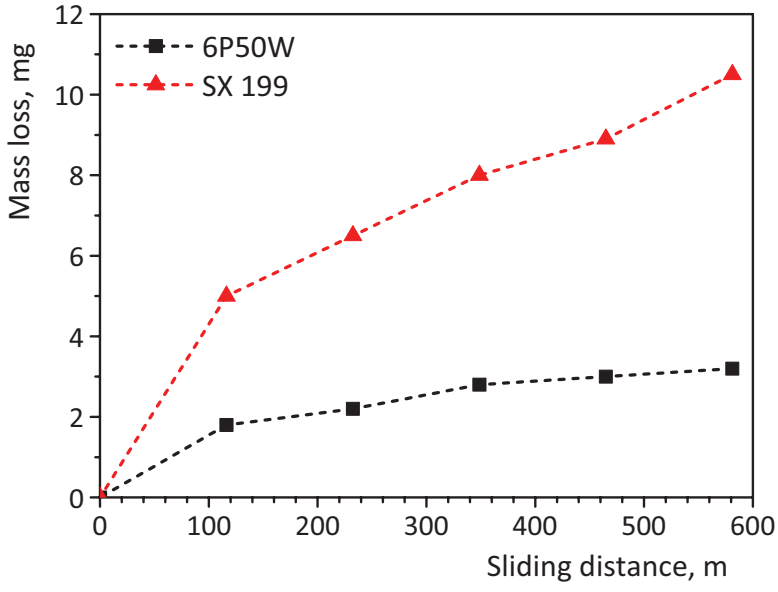

Fig. 4.16. Mass loss vs. sliding distance for coatings 6P50W and SX 199

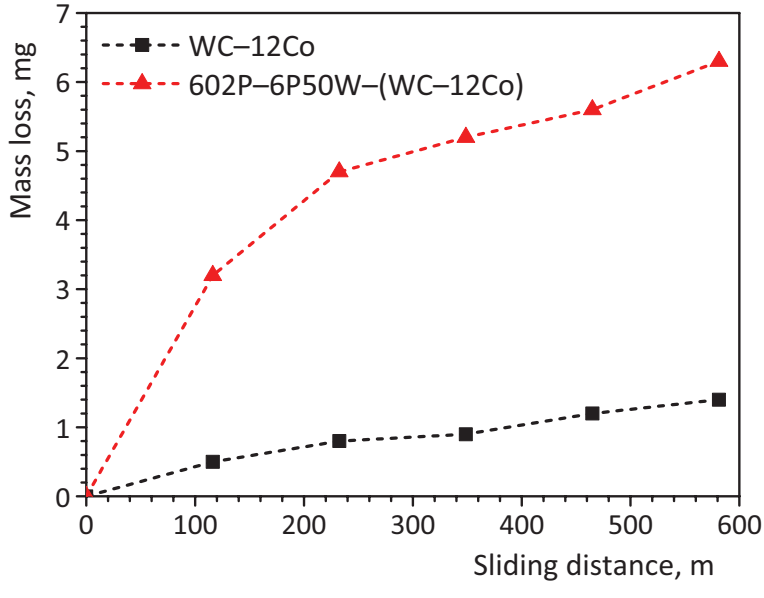

Fig. 4.17. Mass loss vs. sliding distance for coatings WC–12Co and 602P–6P50W–(WC–12Co)

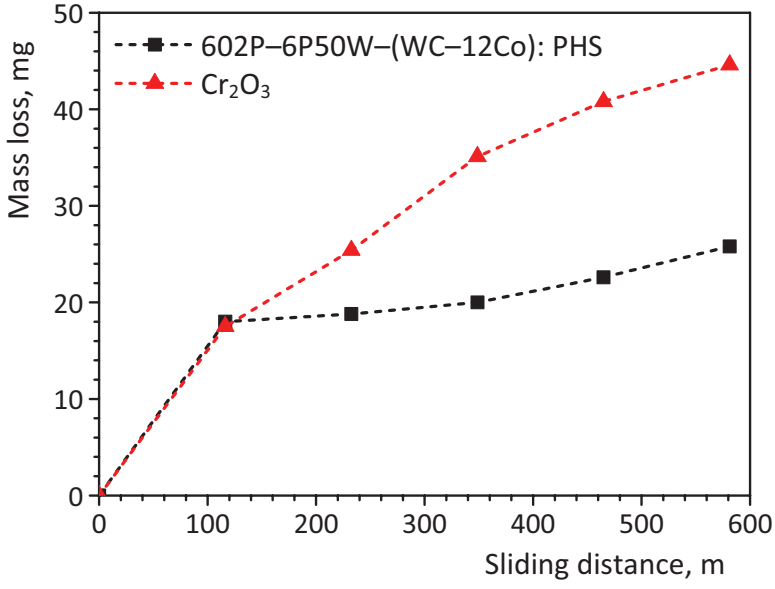

Fig. 4.18. Mass loss vs. sliding distance for coatings 602P–6P50W–(WC–12Co): PHS and Cr_2O_3

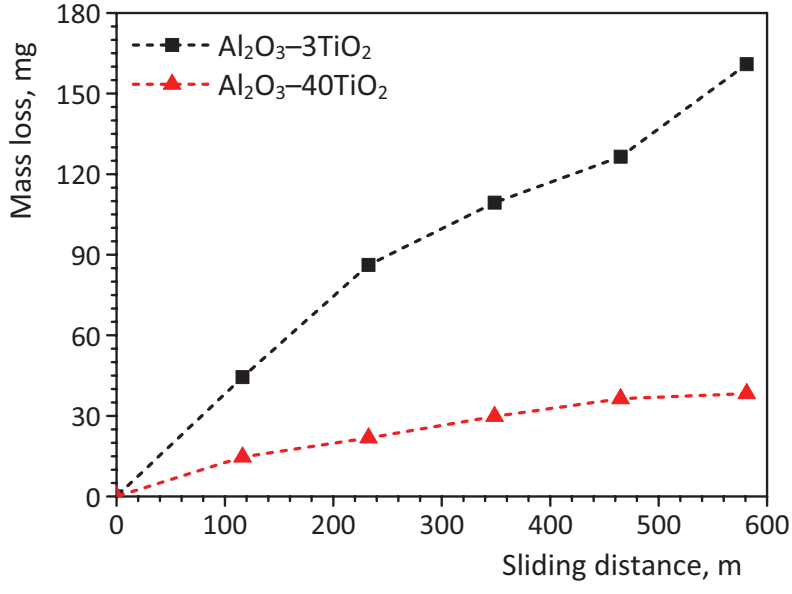

Fig. 4.19. Mass loss vs. sliding distance for coatings Al_2O_3–$3TiO_2$ and Al_2O_3–$40TiO_2$

Presence of running-in process was noticed for all coatings. Duration of running-in phase was different for different coatings, but for most of them it ends after 200 m. After this phase the change of mass loss with sliding distance is more or less linear. Since the steady-state wear did not occur from the beginning of the tests and all coatings show running-in phase which cannot be ignored, in this case study, wear rates were not calculated by fitting the wear curves (it is the slope of wear curve). Wear rate, in mg/m, is calculated as a total wear rate, i.e., as a ratio of total mass loss (for N = 2500) and corresponding sliding distance (*s* = 581.2 m). Comparison of different HVOF coatings were analysed by comparing its calculated wear rate values, which are presented in **Figs. 4.20** and **4.21**.

The lowest abrasive wear rate of all coatings of 0.24×10^{-2} mg/m showed coating WC–12Co. Wear rate of this coating was more than 100 times lower comparing to the Al_2O_3–$3TiO_2$ coating wear rate of 27.68×10^{-2} mg/m. Good abrasive wear resistance of WC–12Co coating is not a surprise since the thermal sprayed coatings based on tungsten carbide are the most durable materials in terms of wear resistance. Although they are not suitable for high temperature applications, they can be applied in many areas of industry due to the combination of very hard carbides and tough matrix. The good wettability of carbides WC in Co matrix contributes to the high cohesive strength of WC–Co cermets [19]. These coatings are the most important thermal-sprayed coatings that are used against abrasion [20]. A systematic study by Barbezat et al. [21] indicated that under dry sand/rubber wheel abrasion test coating WC–12Co exhibited lower abrasion rate than WC–17Co coating. Schubert et al. [19] also reported that, under dry sand/rubber wheel abrasion test, between three variants of WC–Co coatings (with the Co content of 12, 17 and 25 %), the WC–12Co coating had the lowest wear rate.

In the WC–Co coatings produced with the HVOF technique, porosity is caused by the gas produced during the process. The liberation of carbon through the decarburization reactions results in two possibilities: oxidation of the carbon according to $2C + O_2 \rightarrow 2CO$ (gas) or diffusion of carbon into the matrix material [22]. Compared to other spraying techniques, HVOF spraying is one of the best methods for depositing conventional WC-Co cermets, because the higher velocities and lower temperatures experienced by the powder result in less decomposition of WC during spraying process [23]. Therefore, coatings with higher amount of retained WC and lower porosity are expected. Porosity of WC–12Co coating of 1.4 % (**Table 4.13**) was among lowest, compare to the other tested coatings, so it is reasonable to presume that the decarburization of WC during deposition was minimized, providing good abrasive wear resistance.

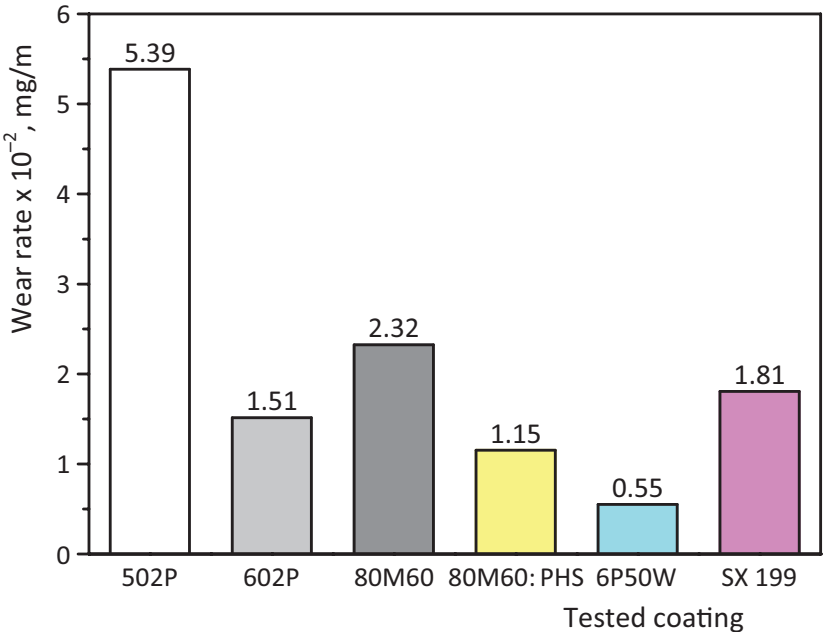

Fig. 4.20. Comparative abrasive wear rate values for coatings 502P, 602P, 80M60, 80M60: PHS, 6P50W and SX 199

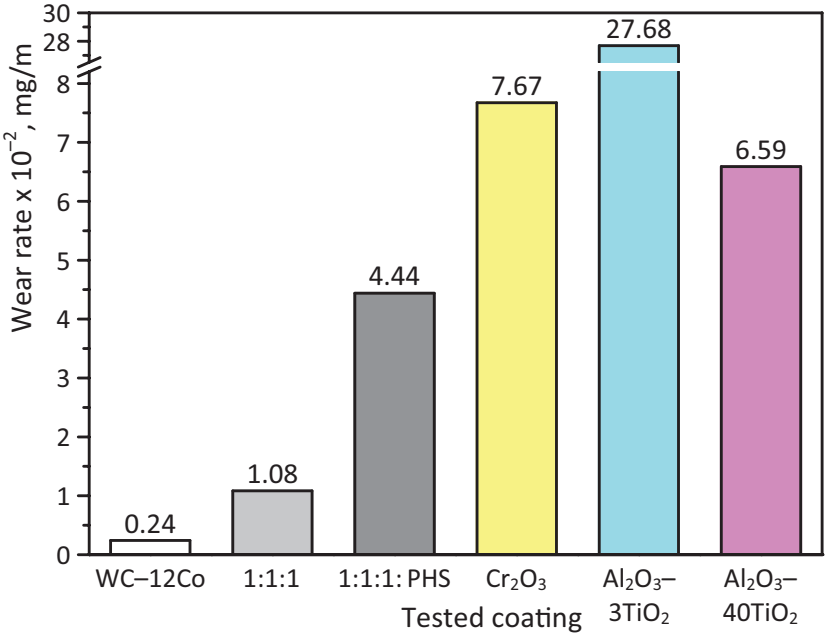

Fig. 4.21. Comparative abrasive wear rate values for coatings WC–12Co, 602P–6P50W–(WC–12Co), 602P–6P50W–(WC–12Co): PHS, Cr_2O_3, Al_2O_3–3TiO_2 and Al_2O_3–40TiO_2; 1:1:1 = 602P–6P50W–(WC–12Co)

Preheating of the substrate showed double-nature effect. In case of 80M60 coating deposited on preheated substrate, 2 times lower abrasive wear rate is obtained, while in case of 602P–6P50W–(WC–12Co) coating preheating of the substrate increased abrasive wear rate by more than 4 times. For the analysis of this phenomenon appropriate microstructure analysis and other coating characteristics are necessary.

The relationship between obtained abrasive wear values and hardness (**Table 4.13**) of tested coatings is shown in **Fig. 4.22**. It could be noticed that the hardest coating (WC–12Co) shows highest abrasive wear resistance as well, but from the other coatings results, it is obvious that relationship between the abrasive wear and hardness values of any kind did not exist. This could be seen from the R^2 (R-squared) value, since it was extremely low (R^2 = 0.02). According to Liu et al. [24], the abrasive wear resistance of thermal spray coating can be related, not only to hardness, but also to indentation toughness of the coating. In addition, Barbezat et al. [21] concluded that coatings with a homogeneous microstructure give better abrasion resistance. Therefore, hardness cannot be the only parameter for predicting the abrasive wear resistance of materials, which is confirmed by the results presented in **Fig. 4.22**.

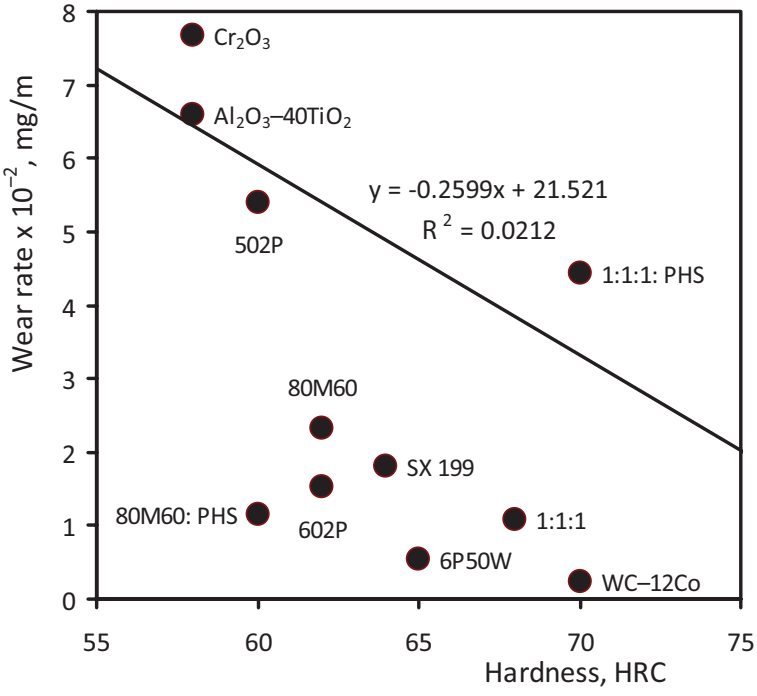

Fig. 4.22. Abrasive wear rate vs. hardness of tested coatings (value for coating Al_2O_3–3TiO_2 is not shown); 1:1:1 = 602P–6P50W–(WC–12Co)

4.4. Erosive wear testing

4.4.1. Materials and deposition condition

Two substrate materials were used. First substrate material was a low-carbon steel, with chemical composition shown in **Table 4.15**. Hardness of this substrate was between 193.6 and 219.5 HV. One of the coatings (coating 80M60) was also deposited on the Al-Cu wrought alloy EN AW-2017A (second substrate). Chemical composition of this substrate is shown in **Table 4.16**.

Ten different coatings, obtained by deposition of various powder coating materials (Ni-, W-, Ni+W-, Cr_2O_3-, and Al_2O_3-based), have been used in experiments. Coatings designations and corresponding powder chemical compositions, taken from the manufacturer, are shown in **Table 4.17**. The powders were produced by the agglomeration process with a sintering stage, and the average size of the powder particles was 45 ± 2.5 μm (602P and WC–12Co) and 35 ± 2.5 μm (80M60, 6P50W, Cr_2O_3, Al_2O_3–3TiO_2 and Al_2O_3–40TiO_2). Samples 2 and 4 were deposited on surface preheated to 650 °C (PHS), and sample 3 was deposited on different substrate than the rest of the coatings. Samples 9 and 10 were deposited with different spraying distance than the rest of the coatings. Powders 602P–6P50W–(WC–12Co), Al_2O_3–3TiO_2 and Al_2O_3–40TiO_2 are mixtures of three or two powders.

High velocity oxygen fuel spraying (HVOF) process, with GMA 6GII powder spray gun and propane (C_3H_8) fuel, was utilized in the experiment. Before the spraying process, surface of the substrate was cleaned and roughened. Cleaning of the substrate was done by preheating of the substrate and subsequent treating with solvent. The surface of the substrate was roughened and activated by abrasive grit blasting (SiO_2 particles with average size of 1 mm). The coatings are deposited on prismatic plates having the dimensions of 80 × 20 × 7 mm. The optimal deposition parameters, obtained in the fist stage of the research (R2 deposition regime, **Table 4.8**), were applied for all

Table 4.15. Chemical composition (wt. %) of the coated material 1 (low-carbon steel substrate)

Element	C	Si	Mn	Ni	P	S	Cr	Fe
Percentage	0.15	0.21	0.8	0.30	0.011	0.025	0.30	Balance

Table 4.16. Chemical composition (wt. %) of the coated material 2 (Al-Cu alloy substrate)

Element	Si	Fe	Cu	Mn	Mg	Cr	Zn	Zr + Ti	Al
Percentage	0.654	0.19	4.38	0.79	0.82	0.013	0.14	0.05	Balance

Table 4.17. Coating designation, substrate and appropriate powder chemical composition (wt. %)

Sample	Coating designation	Substrate	Chemical composition, wt. %
1	80M60	Low-carbon steel	Cr: 14.2; Si: 4.37; C: 0.6; B: 2.9; Fe: 4.54; Cu: 2.36; Mo: 2.51; Co: 0.01; Ni: Balance
2	80M60: PHS*		
3	80M60: Al	Al-Cu alloy	
4	602P–6P50W–(WC–12Co)	Low-carbon steel	Mixture ratio (1:1:1)
5	602P–6P50W–(WC–12Co): PHS*		
6	Cr_2O_3		Al_2O_3 < 0.03; SiO_2 < 0.07; Fe_2O_3 < 0.02; CaO < 0.03; MgO < 0.01; TiO_2 < 0.02; Cr_2O_3: Balance
7	Al_2O_3–3TiO_2		Mixture ratio (97:3) TiO_2: 2.25; SiO_2 < 0.014; Fe_2O_3 < 0.01; Cao < 0.01; MgO < 0.014; Al_2O_3: Balance
8	Al_2O_3–40TiO_2: 120**		Mixture ratio (60:40) TiO_2: 38.25; SiO_2 < 0.014; Fe_2O_3 < 0.01; Cao < 0.01; MgO < 0.014; Al_2O_3: Balance
9	Al_2O_3–40TiO_2: 100**		
10	Al_2O_3–40TiO_2: 80**		

*These coatings were deposited on preheated surface.
** Different spraying distance.

coatings, except for coating samples 9 and 10. Parameters for these two coatings were slightly changed, since the spraying distance was 100 and 80 mm for Al_2O_3–40TiO_2: 100 and Al_2O_3–40TiO_2: 80 coating, respectively.

4.4.2. Thickness and hardness characteristics

Coatings thickness was measured in ten points on each coating surface, and the average values are shown in **Table 4.18**. Measurements of surface hardness (HRC) were carried out using Rockwell hardness tester. At least three measurements were made for each sample in order to eliminate possible segregation effects and to obtain a representative value of the material hardness. The results are shown in **Table 4.18**.

Table 4.18. As-deposited thickness and hardness of tested coatings

Sample	Coating designation	Thickness, μm	Hardness HRC
1	80M60	695	60 – 62
2	80M60: PHS	510	66 – 68
3	80M60: Al	450	54 – 56
4	602P–6P50W–(WC–12Co)	520	65 – 66
5	602P–6P50W–(WC–12Co): PHS	490	62 – 64
6	Cr_2O_3	200	62 – 64
7	Al_2O_3–3TiO_2	250	38 – 40
8	Al_2O_3–40TiO_2: 120	380	50 – 52
9	Al_2O_3–40TiO_2: 100	240	52 – 54
10	Al_2O_3–40TiO_2: 80	320	56 – 58

4.4.3. Experimental details

Erosive wear tests were carried out on jet nozzle type erosion equipment (**Fig. 4.23**) in the ambient air, at room temperature. This testing utilizes repeated gas-entrained solid particle impingement erosion, and involves a small nozzle delivering a stream of gas containing solid particles which impacts the surface of a test specimen.

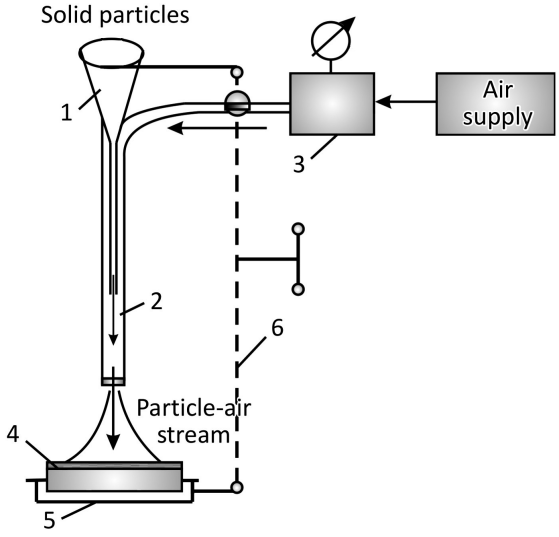

Fig. 4.23. Schematic diagram of erosive wear testing

Table 4.19. Parameters used in the erosive wear testing

Test parameter	Value
Solid particles material	Silicon dioxide (SiO_2)
Maximum size of the particles	350 μm
Air stream pressure	0.1 MPa
Particles flow	136.7 g/min
Particles impact angle	90°
Distance between the sample and the nozzle	10 mm
Duration of the test	6 minutes

Solid particles are poured from the reservoir (1) by freefalling to the nozzle tube (2). Length of the nozzle is 25 mm, diameter is 8 mm, and exit diameter is 6 mm. Before the tests, solid particles material was sieved through a set of sieves and dried in an oven for removal of moisture from the particles. The air stream is provided by the compressed air at controlled pressure, purified from particles and moisture (3). Air stream also enters the nozzle tube (2), where the formation of two-phase (particle-air) working stream takes place. The test sample (4) is fixed in a holder (5) attached to the reversing mechanism (6). Samples for erosive wear testing, having the dimensions of 20 × 20 × 7 mm, were cut from as-deposited samples. Surface of the samples were additionally machined (grinded or polished) before the testing. With reversing mechanism (6), two working parameters are controlled: (a) distance of the sample from the nozzle and (b) impact angle of the particles. Parameters used in the erosive wear testing (solid particles material, maximum size of the particles, air stream pressure, particles flow, particles impact angle, distance between the sample and the nozzle and duration of the test) were the same for all tested coatings (**Table 4.19**).

In order to achieve a higher confidence level in evaluating test results, three replicate tests were run for all materials. The arithmetic mean value of these three measurements is taken as a result. Erosive wear is calculated as a mass loss, i.e., as a difference between the initial mass of the sample and its mass after the end of test. Before and after testing, the coated sample was degreased and cleaned, and its mass is measured by the electronic balance with accuracy of 0.1 mg. Wear rate is given in mg/min as the mass loss of the sample material divided by the duration of the test.

4.4.4. Results and Discussion

Experimental results for mass loss and calculated wear rate for all tested materials are given in **Table 4.20**.

Table 4.20. Erosive wear of tested coatings

Sample	Coating designation	Mass loss, mg	Wear rate, mg/min
1	80M60	14.84	2.47
2	80M60: PHS	1.32	0.22
3	80M60: Al	20.02	3.34
4	602P–6P50W–(WC–12Co)	4.18	0.70
5	602P–6P50W–(WC–12Co): PHS	6.62	1.10
6	Cr_2O_3	7.62	1.27
7	Al_2O_3–3TiO_2	3.35	0.56
8	Al_2O_3–40TiO_2: 120	22.49	3.75
9	Al_2O_3–40TiO_2: 100	8.86	1.48
10	Al_2O_3–40TiO_2: 80	1.42	0.24

For easier comparison of different HVOF coatings, calculated erosive wear rates (**Table 4.20**) are also presented in the diagrams form in **Figs. 4.24** and **4.25**.

The lowest erosive wear rate of all coatings of 2.20×10^{-1} mg/min showed coating 80M60: PHS. Wear rate of this coating was approximately 17 times lower comparing to the Al_2O_3–40TiO_2: 120 coating wear rate of 37.48×10^{-1} mg/min. The microstructure analysis of coating 80M60: PHS shows absences of micro cracks, oxides and non-metal inclusions. Although the oxides could be very hard, they are brittle and unsuitable for erosive wear conditions. Structure of the formed metalloids is homogeneous, providing high cohesive strength of the coating. On the other hand, the same coating deposited on low-carbon steel substrate without preheating (coating 80M60) shows more than 10 times higher erosive wear rate. The microstructure analysis of this coating shows lower homogeneity, different grain size distribution and presence of oxide inclusions, which lead to decrease of plasticity and impact strength of coating. The erosive wear rate of coating 80M60 was even higher when it was deposited on Al-Cu alloy substrate without preheating (coating 80M60: Al). All this suggest that erosive wear rate of coating 80M60 depend very much on optimal deposition parameters (substrate preheating) and/or substrate material, since the erosive wear rate of this coating can be as low as 2.20×10^{-1} mg/min or up to 33.37×10^{-1} mg/min, depending on only this two parameter.

In contrast to coating 80M60, preheating of the low-carbon steel substrate increased the erosive wear rate of coating 602P–6P50W–(WC–12Co), which data were: without preheating 6.97×10^{-1} mg/min and with

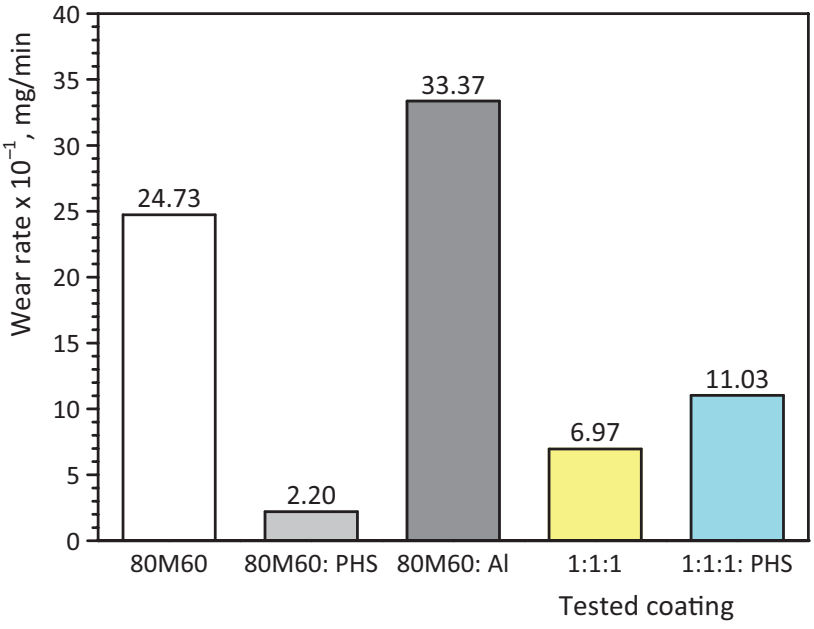

Fig. 4.24. Comparative erosive wear rate values for coatings 80M60, 80M60: PHS, 80M60: Al, 602P–6P50W–(WC–12Co) and 602P–6P50W–(WC–12Co): PHS; 1:1:1 = 602P–6P50W–(WC–12Co)

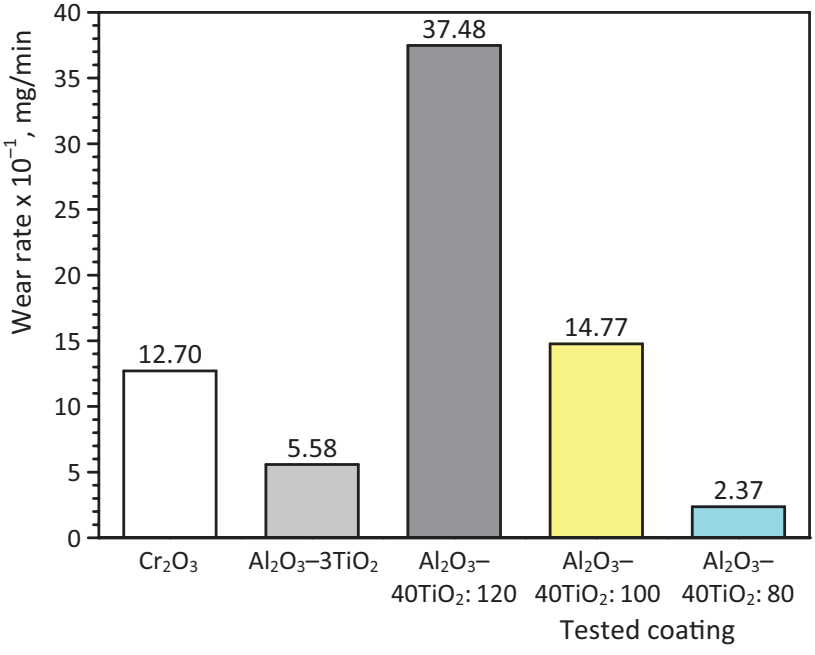

Fig. 4.25. Comparative erosive wear rate values for coatings Cr_2O_3, Al_2O_3–$3TiO_2$, Al_2O_3–$40TiO_2$: 120, Al_2O_3–$40TiO_2$: 100 and Al_2O_3–$40TiO_2$: 80

preheating 11.03 × 10^{-1} mg/min, i.e. 1.58 times higher. This means that, as in case of abrasive wear, preheating of the substrate showed double-nature effect.

The highest erosive wear rate of all coatings of 37.48 × 10^{-1} mg/min showed coating Al_2O_3–40TiO_2: 120 (spraying distance of 120 mm. Simultaneously, the same coating deposited with different spraying distance of 80 mm (Al_2O_3–40TiO_2: 80) showed second lowest erosive wear rate of all coatings of 2.37 × 10^{-1} mg/min. The erosive wear rate of the same coating deposited with spraying distance of 100 mm (Al_2O_3–40TiO_2: 100) was between these two coatings. This clearly suggests that the decrease of erosive wear rate for this coating is obtained by decreasing the spraying distance from 120 to 100 and to 80 mm. The differences between the same coatings Al_2O_3–40TiO_2 deposited with different spraying distance are related to the amount of oxides formed in the coating during deposition process. Although it is not measured, it is obvious that with smaller spraying distance the amount of oxides will be lower due to the shorter retention of powder particles in the HVOF flame. It is also evident that higher amount of formed oxides had negative influence on erosive wear resistance.

The relationship between obtained erosive wear values and hardness (**Table 4.18**) of tested coatings is shown in **Fig. 4.26**. It could be noticed that

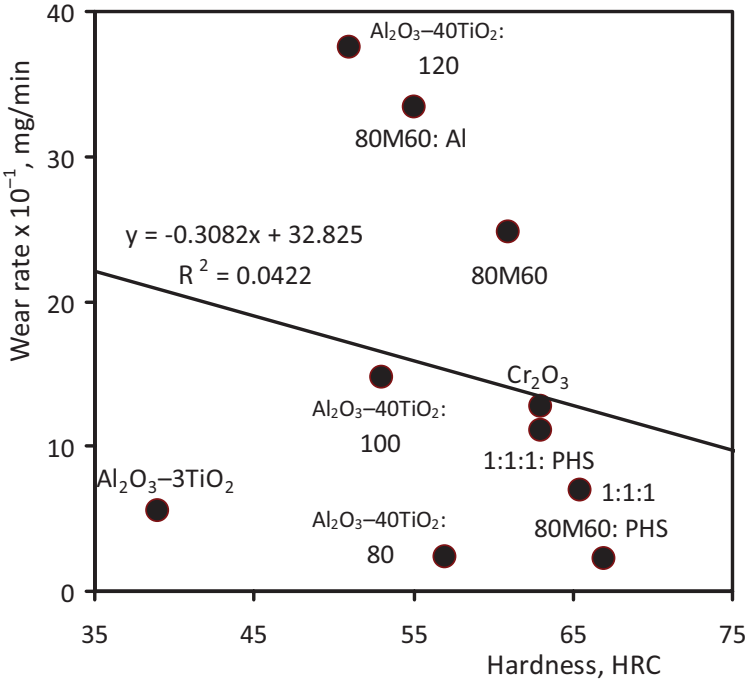

Fig. 4.26. Erosive wear rate vs. hardness of tested coatings; 1:1:1 = 602P–6P50W–(WC–12Co)

the hardest coating (80M60: PHS) shows highest erosive wear resistance as well, but from the other coatings results, it is obvious that relationship between the erosive wear and hardness values of any kind did not exist. This could be seen from the R^2 (R-squared) value, since it was extremely low (R^2 = 0.04). Since the similar relationship was obtained in abrasive wear testing (**Fig. 4.22**) it is confirmed that hardness is definitely not the appropriate parameter for predicting the abrasive or erosive wear resistance of tested HVOF coatings.

4.5. Conclusions

High velocity oxygen fuel (HVOF) spraying is a very complex process, which has a great number of parameters affecting the coating formation and hence coating properties. The amount of the fuel and oxygen in the process, spray distance and the powder feed rate are the most influential parameters. Amount of fuel and oxygen determine the flame temperature and particles velocity and the spray distance influence the amount of oxides in the coatings. Powder feed rate and spray distance are responsible for the amount of unmelted particles and precipitates. Optimisation of the deposition parameters it this case study was performed by varying three parameters, i.e., fuel/oxygen ratio, particles velocity and spraying distance. Optimisation was analysed through microstructure (porosity), hardness and roughness of the obtained coatings, and deposition regime R2 was accepted as optimal for tested coatings.

Investigated HVOF coatings were intend to be used as improvement of the wear resistance of equipment used in road construction, agricultural, mining and other industries, i.e., equipment exposed to heavy-duty operating conditions, under the high temperatures and pressures in abrasive, erosive and corrosive environment. Tribological properties (abrasive and erosive wear) of various superalloy coatings were investigated, with the aim to compare coatings among themselves, as well as, to investigate and analyze influences of substrate preheating, different substrate and spraying distance on wear resistance of these coatings.

The lowest abrasive wear rate of all coatings showed tungsten-based coating (WC–12Co), with the wear rate of more than 100 times lower comparing to the Al_2O_3–$3TiO_2$ coating. The WC–12Co coating is a combination of very hard carbides and tough matrix, and good wettability of carbides WC in Co matrix contributes to the high cohesive strength of WC–Co cermets. Porosity of this coating of 1.4% was among lowest, compare to the other tested coatings, so most probably the decarburization of WC during deposition was minimal. This provided high density and good abrasive wear resistance.

The lowest erosive wear rate of all coatings showed nickel-based coating deposited on preheated substrate (80M60: PHS), with the wear rate of approximately 17 times lower comparing to the Al_2O_3–$40TiO_2$: 120 coating. The microstructure analysis of 80M60: PHS coating shows absences of micro cracks, oxides and non-metal inclusions. Although the oxides could be very hard, they are brittle and unsuitable for erosive wear conditions. Structure of the formed metalloids is homogeneous, providing high cohesive strength of the coating.

Preheating of the substrate in both, abrasive and erosive wear testing, showed double-nature effect. In case of 80M60 coating, deposition on preheated substrate lower the abrasive and erosive wear rate, while in case of 602P–6P50W–(WC–12Co) coating, preheating of the substrate increased abrasive and erosive wear rate. Influence of different substrate (low-carbon steel and Al-Cu alloy) on erosive wear resistance is shown through the 80M60 and 80M60: Al coatings, where the coating deposited on Al-Cu alloy (80M60: Al) showed lower erosive wear resistance. Different spraying distances (120, 100 and 80 mm) were applied during deposition of Al_2O_3–$40TiO_2$ coating, in order to investigate their influence on erosive wear resistance of obtained coatings. It was shown that the increase of erosive wear resistance is obtained by decreasing the spraying distance. This is related to the amount of oxides, which had negative influence, formed in the coating during deposition process. Lower spraying distance induce lower amount of oxides due to the shorter retention of powder particles in the HVOF flame.

The relationship between obtained abrasive/erosive wear values and hardness showed that the hardest coatings (WC–12Co in abrasive wear testing and 80M60: PHS in erosive wear testing) showed highest abrasive/erosive wear resistance as well, but from the other coatings results, it is obvious that relationship between the abrasive/erosive wear and hardness values of any kind did not exist. Therefore, it is confirmed that hardness is definitely not the appropriate parameter for predicting the abrasive or erosive wear resistance of tested HVOF coatings.

References to Chapter 4

[1] **Pawlowski, L.** *The Science and Engineering of Thermal Spray Coatings*. Chichester: John Wiley & Sons, 2008.

[2] --. *High Velocity Oxy-Fuel (HVOF) Solutions*. Brochure. Oerlikon Metco. Winterthur. 2015. (http://www.oerlikon.com/metco).

[3] **Oksa, M., E. Turunen, T. Suhonen, T. Varis, S.-P. Hannula.** Optimization and characterization of high velocity oxy-fuel sprayed coatings: Techniques, materials and applications. – *Coatings*, Vol. 1, 2011, No 1, pp. 17-52.

[4] **Пейчев, И.** Приложения на високоскоростни технологични (HVOF и плазма) процеси за нанасяне на износоустойчиви покрития. Защита от корозия и ерозия при електроцентрали (Application of high-speed technological processes (HVOF and plasma) for the laying of wear-resistant coatings. Protection of corrosion and erosion in electric power plants). – *Tribological Journal BULTRIB*, Vol. 1, 2010, pp. 101-107.

[5] **Пейчев, И.** Триботехнологични изисквания към термично депонираните покрития за подобряване ресурса на детайли и съоръжения в индустрията (Trbotechnological requirements to thermal cladded coatings aiming improvement of details and equipment resource in industry). – *Proceedings of XXVI International Scientific Conference "65 Years Faculty of Machine Technology"*, Sozopol (Bulgaria), 13-16.09.2010, pp. 561-564.

[6] **Пейчев, И.** Развитие, състояние и иновации на термично депонираните покрития в България (Development, state and innovation by thermal cladded coatings in Bulgaria). – *Proceedings of XXVI International Scientific Conference "65 Years Faculty of Machine Technology"*, Sozopol (Bulgaria), 13-16.09.2010, pp. 565-571.

[7] **Peichev, I., M. Kandeva, E. Assenova, V. Pojidaeva.** About the deposition of superalloys by means of supersonic HVOF process. Proceedings of *12th International Conference on Tribology – SERBIATRIB '11*, Kragujevac (Serbia), 11-13.05.2011, pp. 91-97.

[8] **Пейчев, И., М. Кандева.** Характеризиране на композитни покрития, нанесени чрез газотермична свръхзвукова струя (HVOF-процес) при различни технологични режими (Characterizing of composite coatings deposited through gas-thermal super sound stream (HVOF-process) at different technological regimes). – *Tribological Journal BULTRIB*, Vol. 2, 2012, pp. 187-197.

[9] **Кандева, М., И. Пейчев, А. Димитрова.** Износване на композитни покрития, нанесени чрез газотермична свръхзвукова струя (HVOF-процес) (Wear of composite coatings deposited through gas-thermal super sound stream (HVOF-process)). – *Tribological Journal BULTRIB*, Vol. 2, 2012, pp. 198-212.

[10] **Kandeva, M., B. Ivanova, V. Pozhidaeva, D. Karastoyanov, J. Javorova.** Composite coatings to improve durability of the working body of the drill. – *Proceedings of 5th World Tribology Congress (WTC 2013)*, Turin (Italy), 08-13.09.2013, Paper 1251.

[11] **Kandeva, M., D. Karastoyanov, A. Vencl, I. Peichev, B. Ivanova, E. Assenova.** Wear-resistance of composite coatings deposited by gas-flame supersonic HVOF process, *Proceedings of XIV International Scientific Conference "Tribology and Reliability"*, Saint Petersburg (Russia), 17-19.09.2014, pp. 307-321

[12] **Кандева, М., И. Пейчев.** Струйно-абразивна износоустойчивост на газотермични покрития с микрочастици (Jet-abrasive wearresistance of gas-thermal powder coatings with microparticles). – *Proceedings of 9th Interna-*

tional Congress "Machines, Technologies, Materials" (MTM 2012), Varna (Bulgaria), 19-21.09.2012, Vol. 2: Section Machines, pp. 131-135.
[13] **Vencl, A.** Optimization of the deposition parameters of thick atmospheric plasma spray coatings. – *Journal of the Balkan Tribological Association*, Vol. 18, 2012, No 3, pp. 405-414.
[14] **Mrdak, M. R., A. Vencl, B. D. Nedeljkovic, M. Stanković.** Influence of plasma spraying parameters on properties of the thermal barrier coatings. – Materials Science and Technology, Vol. 29, 2013, No 5, pp. 559-567.
[15] **Ivković, B., M. Djurdjanović, D. Stamenković.** The influence of the contact surface roughness on the static friction coefficient. – *Tribology in Industry*, Vol. 22, 2000, No 3-4, pp. 41-44.
[16] **Jiang, H., M. Lau, V. L. Tellkamp, E. J. Lavernia.** Synthesis of nanostructured coatings by high-velocity oxygen-fuel thermal spraying. – In: H. Singh Nalwa (Ed.), *Handbook of Nanostructured Materials and Nanotechnology, Vol. 1: Synthesis and Processing.* San Diego: Academic Press, 2000, pp. 159-213.
[17] **Cabral-Miramontes, J. A., C. Gaona-Tiburcio, F. Almeraya-Calderón, F. H. Estupiñan-Lopez, G. K. Pedraza-Basulto, C. A. Poblano-Salas.** Parameter studies on high-velocity oxy-fuel spraying of CoNiCrAlY coatings used in the aeronautical industry. – *International Journal of Corrosion*, Vol. 2014, 2014, Article ID 703806.
[18] БДС 14289: *Метали. Метод за изпитване на абразивно износване при триене върху закрепени абразивни частици* (*Metals. Test method for abrasive wear by fixed abrasive particles*), 1977.
[19] **Schubert, J., Š. Houdková, M. Kašparová, Z. Česánek.** Effect of Co content on the properties of HVOF sprayed coatings based on tungsten carbide. – *Proceedings of 21st International Conference on Metallurgy and Materials – Metal 2012*, Brno (Czech Republic), 23-25.05.2012, pp. 1086-1091.
[20] **Wood, R. J. K. M. Roy.** Tribology of thermal-sprayed coatings. – In: M. Roy (Ed.), *Surface Engineering for Enhanced Performance against Wear*. Wien: Springer, 2013, pp. 1-43.
[21] **Barbezat, G., A. R. Nicol, A. Sickinger.** Abrasion, erosion and scuffing resistance of carbide and oxide ceramic thermal sprayed coatings for different applications. – *Wear*, Vol. 162-164, Part A, 1993, pp. 529-537.
[22] **Nerz, J., B. Kushner, A. Rotolico.** Microstructural evaluation of tungsten carbide-cobalt coatings. – *Journal of Thermal Spray Technology*, Vol. 1, 1992, No 2, pp. 147-152.
[23] **Chivavibul, P., M. Watanabe, S. Kuroda, J. Kawakita, M. Komatsu, K. Sato, J. Kitamura.** Effect of powder characteristics on properties of warm-sprayed WC-Co coatings. – *Journal of Thermal Spray Technology*, Vol. 19, 2010, No 1, pp. 81-88.
[24] **Liu, Y., T. E. Fischer, A. Dent.** Comparison of HVOF and plasma-sprayed alumina/titania coatings – Microstructure, mechanical properties and abrasion behaviour. – *Surface and Coatings Technology*, Vol. 167, 2003, No 1, pp. 68-76.